The Optical-GeV connection in Fermi Blazars

A thesis
submitted for the degree of

Doctor of Philosophy

in

The Department of Physics,

Pondicherry University,

Puducherry - 605 014, India

by

Bhoomika

Indian Institute of Astrophysics,

Bangalore - 560 034, India

July 2020

The Optical-GeV connection in Fermi Blazars

Bhoomika

Indian Institute of Astrophysics

Indian Institute of Astrophysics

Bangalore - 560 034, India

Title of the thesis	:	**The Optical-GeV connection in Fermi blazars**
Name of the author	:	**Bhoomika**
Address	:	Indian Institute of Astrophysics
		II Block, Koramangala
		Bangalore - 560 034, India
Email	:	bhoomika@iiap.res.in
Name of the supervisor	:	**Prof. C.S.Stalin**
Address	:	Indian Institute of Astrophysics
		II Block, Koramangala
		Bangalore - 560 034, India
Email	:	stalin@iiap.res.in

Declaration of Authorship

I hereby declare that the matter contained in this thesis is the result of the investigations carried out by me at the Indian Institute of Astrophysics, Bangalore, under the supervision of Prof. C. S. Stalin. This work has not been submitted for the award of any other degree, diploma, associateship, fellowship, etc. of any other university or institute.

Signed: *Bhoomika*

Date: 08 / January / 2021

Certificate

This is to certify that the thesis titled **'The Optical-GeV Connection in Fermi Blazars'** submitted to the Pondicherry University by Ms. Bhoomika for the award of the degree of Doctor of Philosophy, is based on the results of the investigations carried out by her under my supervision and guidance, at the Indian Institute of Astrophysics. This thesis has not been submitted for the award of any other degree, diploma, associateship, fellowship, etc. of any other university or institute.

Signed: _C. S. Stalin_

Date: 08 January 2021

List of Publications

1. **Bhoomika Rajput**, C. S. Stalin, Sunder Sahayanathan, Suvendu Rakshit, Amit Kumar Mondal, 'Temporal correlation between the optical and γ-ray flux variations in the blazar 3C 454.3', 2019, *Monthly Notices of the Royal Astronomical Society*, 486, 1781. *

2. **Bhoomika Rajput**, C. S. Stalin, Suvendu Rakshit, 2020, 'Long term γ-ray variability in blazars', 2020 *Astron. Astrophys.*, 634A, 80R. †

3. **Bhoomika Rajput**, C. S. Stalin, Sunder Sahayanathan, 'Correlation between optical and γ-ray flux variations in bright flat spectrum radio quasars', *Monthly Notices of the Royal Astronomical Society*, 498, 5128. ‡

4. **Bhoomika Rajput**, C. S. Stalin, Sunder Sahayanathan, 'Correlation between optical and γ-ray flux variations in BL Lacs', *in preparation* §

5. **Bhoomika Rajput**, C. S. Stalin, 'Optical flux and polarization variations in the flat spectrum radio quasar 3C 279', *in preparation* ¶

6. Vaidehi S. Paliya, **Bhoomika Rajput**, C. S. Stalin, S. B. Pandey, 'Broadband Observations of the Gamma-Ray Emitting Narrow Line Seyfert 1 Galaxy SBS 0846+513', 2016, *The Astrophysical Journal*, 819, 121.

---

*presented in Chapter 3
†presented in Chapter 5
‡presented in Chapter 3
§presented in Chapter 4
¶presented in Chapter 6

Presentations

1. Poster presentation in the *Extragalactic Relativistic Jets: Cause and Effect*, ICTS, Bangalore, India, during 12-20 October, 2015.

2. Oral presentation in the *Jet Triggering Mechanisms in Black Hole Sources* TIFR, Mumbai, India, during 20-23 January, 2016.

3. Oral presentation in the *Wide Band Spectral and Timing Studies of Cosmic $X-ray$ Sources* TIFR, Mumbai, India, during 10-13 January, 2017.

4. Poster presentation in the *Astronomical Society of India meeting 2017 (ASI:2017)*, B. M. Birla Auditorium, Jaipur, Rajasthan, India, during 6-10 March, 2017.

5. Oral presentation in the *Recent Trends in the Study of Compact Objects − Theory and Observation (RETCO − III)*, IIST, Trivandrum, Kerala, India, during 5-7 June, 2017.

6. Oral presentation in the *High Energy Emission from Active Galactic Nuclei*, University of Calicut, Kerala, India, during 28-30 November, 2017.

7. Poster presentation in the *International Fermi Symposium*, Baltimore, MD, USA, during 14-19 October, 2018.

8. Oral presentation in the *Astronomical Society of India meeting 2019 (ASI:2019)*, Christ University, Bangalore, India, during 18-22 February, 2019.

9. Poster presentation in the *Astronomical Society of India meeting 2020 (ASI:2020)*, IISER Tirupati, India, during 12-16 February, 2020.

Acknowledgements

I wish to express my sincere gratitude to all those who helped me to finish the work. My research work on my PhD could not have been done without the support of a lot of people.

I am deeply grateful to my thesis supervisor Prof. C. S. Stalin for his guidance, support and continuous encouragement. He has helped me repeatedly during my PhD tenure in scholarly, non-academic, and personal problems. He has always inspired me to do the hard work, discuss research papers time to time, be frank in research and to do the best in life. I would take the opportunity to thank my collaborator Sunder Sahayanathan for his valuable suggestions and helping me unconditionally in my research work.

I want to thank Suvendu, Priyanka, Amit, Kshama and Indrani for their help and guidance in learning astronomical tools to carry out my research work and for their scientific discussion. I would very much like to thank Prof. Ram Sagar for his presence in our group discussion and for his valuable remarks.

I would also like to thank Director IIA, Prof. Annapurni Subramanyan, Dean IIA, Prof. G. C. Anupama, all the academic and administrative staff, including the Board of Graduate Studies, for their assistance and support in creating a research friendly atmosphere for me. I am very grateful to Ashok, Anish, Fayaz and other 'Data Center' staff for their time-to-time assistance in computer and internet related matters. I would really appreciate the high performance computing facility Nova at IIA. This facility is used to most part of my research work. I would like to thank the members of my Doctoral Committee and the administration of the University of Pondicherry for their support and input during my various research phases. I thank to the IIA library team for helping me to access necessary books and journals. Many thanks to the Administrative Officer, the Personnel Officer,

Kanhaiya, Supriyo, Asish Raj and Arun Surya.

Last but not least, I would like to thank my parents, grandparents and other family members for their continuous support and blessings in pursuing my career in research. I am very grateful to my sister Pratime and my brother Yogesh for their love and affection, and for supporting me unconditionally in every wrong or right decision in my life.

Data usage

In this thesis, I have extensively used data from various ground and space based telescopes. I would like to thank all the members of the team who made the data available.

Major part of the thesis work has been done using 3FGL catalog of the *Fermi* γ-ray Space Telescope, which was launched on 11th June, 2008. *Fermi* mission is a joint venture of NASA, the United States Department of Energy, and Government agencies in France, Germany, Italy, Japan, and Sweden. *Fermi* γ-ray space telescope is the most sensitive mission in the energy range of 50 MeV to 1 TeV with a wide effective area and high resolution performance.

I have also used data from the Swift X-ray telescope(Swift-XRT), which was launched on November 20, 2004. *Swift-XRT* covers the energy range of 0.2-10 KeV. Data from the Swift Ultra-Violet Optical Telescope (Swift-UVOT) has also been used. The UVOT is an optical telescope with a diameter of 0.3 m and with a field of view of 17 arc min. It provides data in several filters that span the wavelength range of 1700 to 6500 A

Ground based data from SMARTS (Small and moderate aperture research telescope system) and Steward have also been used in the thesis. SMARTS provides data in the optical B, V, R and Infrared J and K. Yale University and Fermi GI grant NNX 12AP15 G support the SMARTS observations of LAT-monitored blazars. This thesis has also used optical photometric and polarimetric data from the Steward Observatory sponsored by NNX08AW56 G, NNX09AU10 G, and NNX12AO93 G grants from *Fermi* Guest Investigator.

Dedicated to

my family, my teachers and my friends

Abstract

Blazars are a class of active galactic nuclei (AGN) that have relativistic jets that are oriented close to the observers line of sight. They display flux variability across the entire accessible electromagnetic spectrum from low energy radio to high energy γ-rays. They are classified into BL Lacertae objects (BL Lacs) and flat spectrum radio quasars (FSRQs) based mainly on the absence or presence of broad emission lines in their optical/IR spectra. They dominate the extragalactic γ-ray sky and are also suggested to be the possible sources of astrophysical neutrinos. The recent detection of neutrinos by the IceCube collaboration has been found to be closely associated with flaring blazars. In the leptonic model of emission from blazar jets, the low energy emission is from acceleration and cooling of relativistic electrons through synchrotron emission process and the high energy emission is through inverse Compton scattering off jet relativistic electrons that produce the synchrotron emission. The seed photons for the inverse Compton process come either from inside the jet (synchrotron self-Compton or SSC), or from outside the jet (external Compton or EC). Whereas in the hadronic model of emission from blazar jets, relativistic protons also contribute to the high energy emission through the proton synchrotron emission or photo-pion production processes.

An efficient way to constrain the leptonic v/s hadronic emission from blazar jets is through modelling of the broad band spectral energy distribution of blazars. However, this is hindered by (i) the difficulty in accumulating simultaneous or near simultaneous data over a range of wavelengths and (ii) complexity of the available models in explaining the observed SED. An alternative and relatively cheap method to constrain the leptonic v/s hadronic emission in blazars is via the analysis of flux variations in the optical and γ-ray bands. In the leptonic model of emission from blazar jets, as the relativistic electrons in the jet are responsible for the optical and γ-ray emission a close

correlation between the optical and γ-ray flux variations are expected. Alternatively in the hadronic model of emission from blazar jets, as the optical emission is from electron synchrotron and the γ-ray emission might be due to proton synchrotron, a close correlation between optical and γ-ray flux variations are not expected.

In this thesis, I mainly concentrated on the question "Is leptonic model able to explain the optical and γ-ray flux variations and optical polarization behaviour in blazars?" I have followed the following approaches to address the above question (i) to constrain the leptonic scenario in blazars through correlation analysis of flux variations in the optical and γ-ray bands (ii) characterize the γ-ray variability characteristics of different categories of blazars on month like time scales and (iii) characterize the correlation between flux and polarization variations in blazars to constrain the connection between different emission regions in the jets of blazars.

To achieve the first objective, I analyzed ten years (2008 - 2018) of multiband data on a sample of five FSRQs (3C 454.3, PKS 1510-089, 3C 279, 3C 273 and CTA 102) and three BL Lac objects (AO 0235+164, OJ 287 and PKS 2155-304). In the case of FSRQs, I noticed (i) correlated optical and γ-ray flux variations, (ii) optical flare without a γ-ray counterpart and (iii) γ-ray flare without an optical counterpart. In all the three BL Lacs analyzed in this thesis, I found correlated optical and γ-ray flare. Our SED modelling of those epochs indicates that correlated optical and γ-ray flux variations are mostly driven by changes in the bulk Lorentz factor, while γ-ray flares without optical counterparts are due to an increase in the bulk Lorentz factor and/or increase in the electron energy density and optical flares without γ-ray counterparts are due to an increase in the magnetic field. Details are given in Chapter 3 and Chapter 4 of the thesis.

The second objective of characterizing the long term γ-ray flux variability characteristics of blazars is addressed by analyzing the one month binned light curves of 1120 blazars, of which 481 are FSRQs and 639 are BL Lacs. Monthly binned light curves on these sources were generated for a period of about 9 years from 2008

August to 2017 December and the variability was quantified by excess variance (F_{var}). On month like time scales, 371/481 FSRQs are variable (80%) while only about 50% (304/639) of BL Lacs are variable. FSRQs are thus found to be more variable than BL Lac objects. Large F_{var} in FSRQs is also confirmed from the analysis of ensemble structure function. Details of this are given in Chapter 5 of the thesis.

The third objective of the thesis is addressed in Chapter 6 of the thesis where I made an attempt to systematically study the optical flux and polarization variations in the flat spectrum radio quasar 3C 279. The total flux and polarization data in the optical V-band cover a period of about 10 years from 2008−2018 August. During this period the source varied in optical brightness by about 5 magnitudes. On day like timescales, I identified eleven epochs wherein statistically significant correlation between total and polarized flux exists. Of these, on five epochs total and polarized flux are correlated while on the remaining six epochs total and polarized flux are anti-correlated. The varied levels of correlation observed between optical flux and polarization degree on day like timescale point to the presence of multiple emission regions in the jet of 3C 279.

Contents

List of Figures

List of Tables

Abbreviations

AGN	**A**ctive **G**alactic Nuclei
QSO	**Q**uasi **S**tellar **O**bject
NLRG	**N**arrow **L**ine **R**adio **G**alaxy
FR I	**F**anaroff-**R**iley type I
FR II	**F**anaroff-**R**iley type II
BLRG	**B**road **L**ine **R**adio **G**alaxy
SSRQ	**S**teep **S**pectrum **R**adio **Q**uasars
BL Lac	**BL L**acertae
FSRQ	**F**lat **S**pectrum **R**adio **Q**uasars
LAT	**L**arge **A**rea **T**elescope
EGRET	**E**nergetic **G**amma-**R**ay **E**xperiment **T**elescope
CGRO	**C**ompton **G**amma-**R**ay **O**bservatory
SMARTS	**S**mall and **M**oderate **A**perture **T**elescope **S**ystem
$M_\odot$	Solar **M**ass

Chapter 1

Introduction

Active galactic nuclei (AGN) refer to objects in which the nucleus of a galaxy is active. This activity is generally manifested in the presence of broad emission lines (with typical widths in excess of 5000 km sec^{-1}) in the spectrum of these objects. The total energy emitted from a normal galaxy is the sum of the emission coming from all the stars present in that galaxy but in the case of AGN the central source of emission is more than 100 times brighter than the total emission from all the stars. They emit radiation over the entire accessible electromagnetic spectrum from low energy radio to high energy γ-rays. AGN are believed to be powered by accretion of matter onto supermassive black holes with masses greater than 10^6 $M_\odot$ situated at the centers of galaxies (Lynden-Bell 1969; Shakura and Sunyaev 1973).

AGN are highly luminous objects and their luminosity varies from 10^{40} ergsec^{-1} to 10^{48} ergsec^{-1} (Fabian 1999). The different observed properties of AGN depend mainly on the direction of orientation or random pointing rather than physical properties (Urry and Padovani 1995). AGN are broadly divided into two categories namely radio-loud and radio-quiet AGN. This classification is based on the radio-loudness parameter (R) defined as the ratio of the flux density at 5 GHz to the

Optical emission Line Properties

Type 2
(Narrow Line)

Type1
(Broad Line)

Type 0
(Unusual)

Radio Quiet :

Seyfert 2

Seyfert 1
QSO

Radio Loudness

Radio Loud :   NLRG   FR I   BLRG   Blazars   BL Lacs

FR II   SSRQ   FSRQ

FSRQ

Decrease in angle to the line of sight
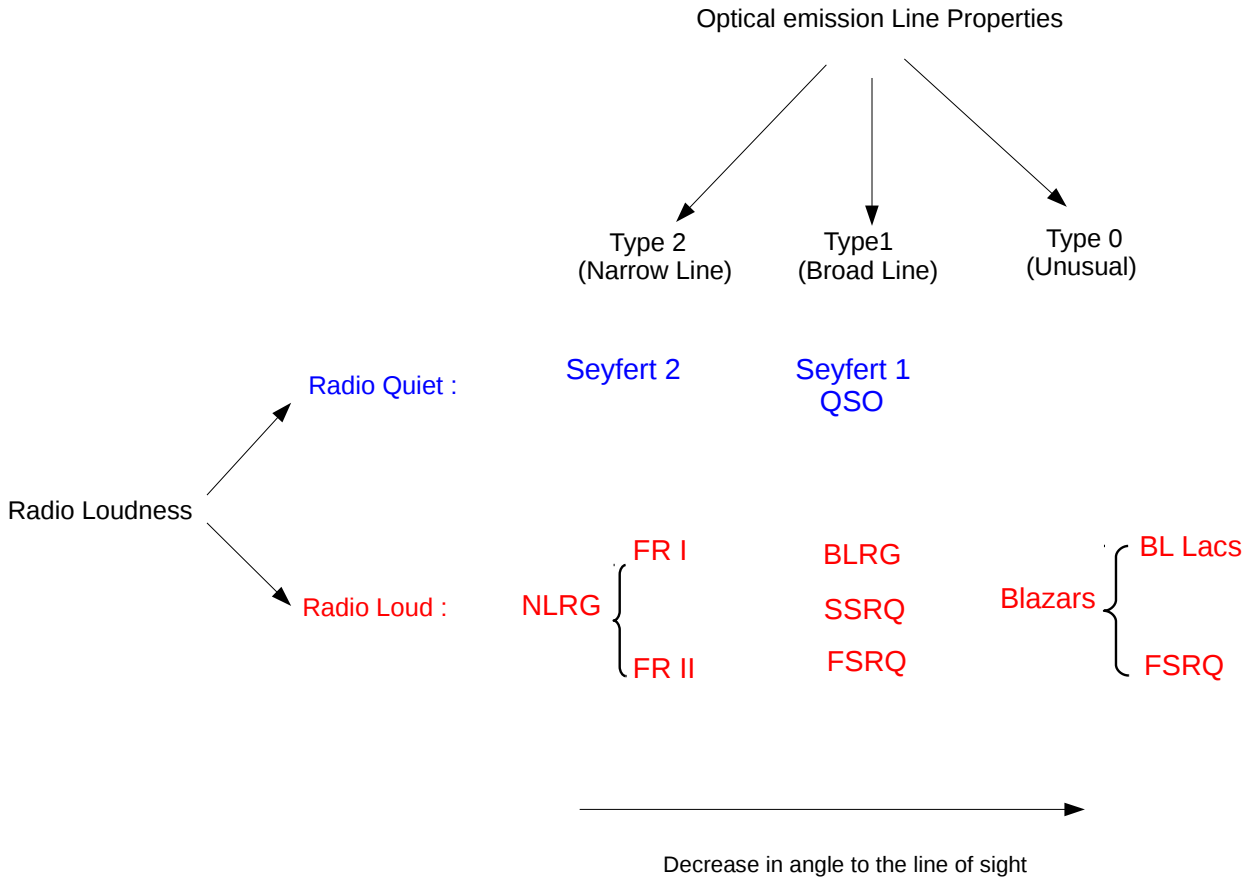
FIGURE 1.1: AGN taxonomy (Adopted from Urry and Padovani 1995)

flux density in the optical B-band (R = f_{5GHz}/f_{B-band}; Urry and Padovani 1995). Radio-loud AGN are those with R > 10 (Kellermann *et al.* 1989). Radio-loud and radio-quiet AGN are further divided into several categories which is summarized in Figure 1.1 and the unification scheme of AGN is shown in Figure 1.2.

1.1   Radio-Loud AGN

Radio-loud AGN are those with the R parameter greater than 10 (Kellermann *et al.* 1989). The radio emission from the radio-loud AGN are driven primarily by the synchrotron emission from their relativistic jets (Begelman *et al.* 1984). The
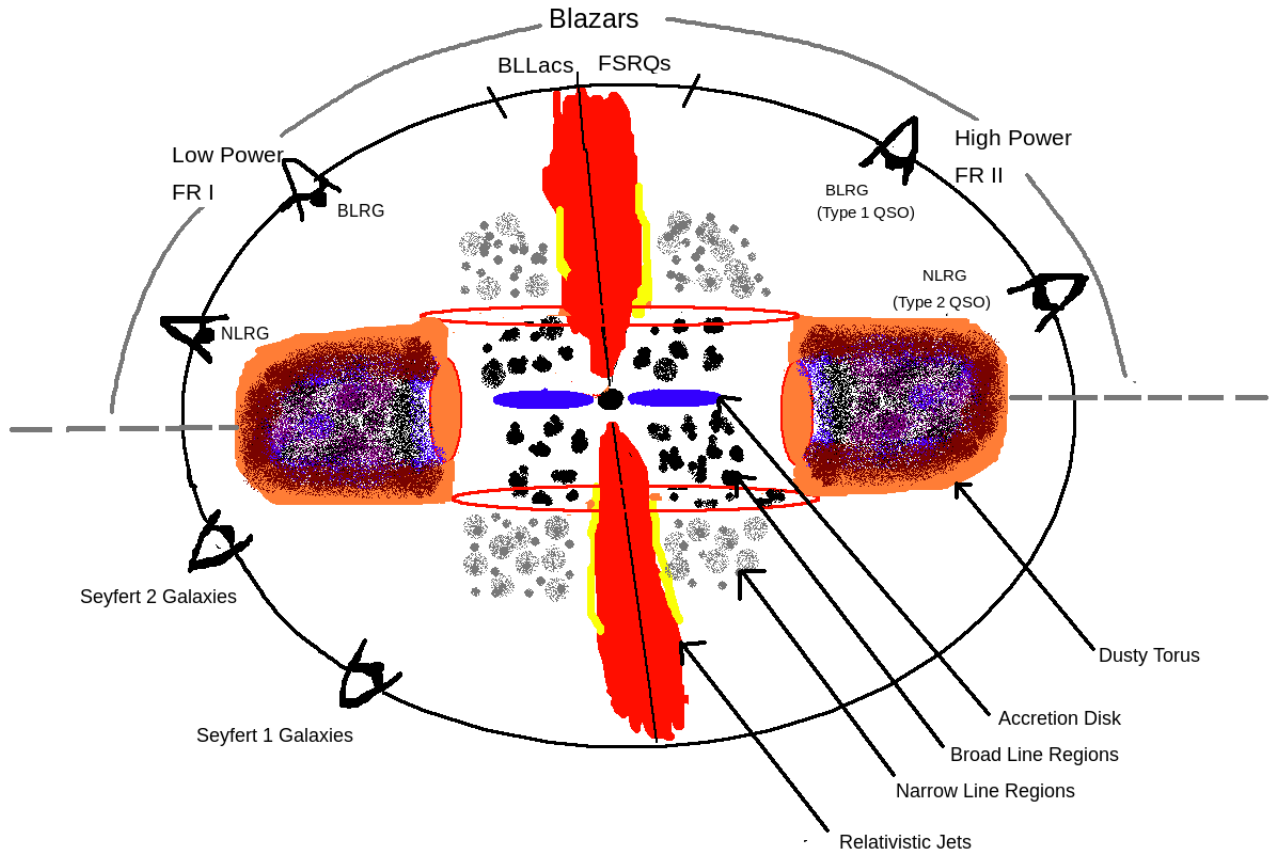
FIGURE 1.2: Unification model of AGN

bipolar jets originating from the galactic center are beamed relativistically along the jet axes and they emit radiation throughout the entire accessible electromagnetic spectrum. Radio-loud AGN include radio galaxies, quasars and blazars.

1.1.1 Blazars

Blazars are a peculiar category of AGN that have their relativistic jets pointed close to the line of sight to the observer with angle $\leq 10°$ (Antonucci 1993; Urry and Padovani 1995). Blazars are mainly hosted by elliptical galaxies. They are classified into flat spectrum radio quasars (FSRQs) and BL Lacerate objects (BL Lacs)

based on the strength of the emission lines in their optical/infrared (IR) spectrum. Both classes of objects emit radiation over the entire accessible electromagnetic spectrum from low energy radio to high energy γ-rays. As blazars are aligned close to the observer, the emission is highly Doppler boosted causing them to appear as bright sources in the extra-galactic sky. They dominate the extragalactic γ-ray sky first hinted by the Energetic Gammma-ray Experiment Telescope (EGRET) observations on board the *Compton Gamma-Ray Observatory* (CGRO; Hartman *et al.* 1999) and now made apparent by the Large Area Telescope (LAT) onboard the *Fermi* Gamma-ray space telescope (hereinafter *Fermi*; Atwood *et al.* 2009). Since the jets in blazars are aligned close to the observer, in the beaming model, the observed emission (S_{obs}) from the jet is Doppler boosted relative to what is measured in the co-moving frame of the jet (S_{int}) as $S_{obs} = S_{int}\delta^q$ (Lin *et al.* 2017) where q = $2 + \alpha$ for a stationary jet and q = $3 + \alpha$ for a jet with distinct blobs, α is the spectral index defined as $S_\nu \propto \nu^{-\alpha}$, δ is the Doppler factor given by $\delta = [\Gamma(1 - \beta cos\theta)]^{-1}$, where $\Gamma = (1 - \beta^2)^{-1/2}$ is the bulk Lorentz factor, θ is the angle between the observer's line of sight and the jet axis and $\beta = v/c$ is the jet speed. In addition to flux enhancement, the observed time scale of variability is also shortened by a factor δ^{-1}, which is relative to that of the co-moving frame. These two effects increase our chances of detecting variations in blazars over a range of time scales and amplitudes. In fact, blazars are known to show flux variations over the accessible bands of the electromagnetic spectrum on timescales ranging from month to days and minutes. Characterizing the minimum time scale of variability (t_{min}) from blazar light curves is important as it provides important constraints on the size of the emitting region in blazar jets via $R < ct_{min}\delta(1+z)^{-1}$. Flux variations on minute time scales have been observed in optical/IR and X-ray regimes (Ghosh *et al.* 2000; Pandey *et al.* 2017). Additionally, in high-energy γ-rays, flux variations as short as minutes have been observed in few sources (Albert *et al.* 2007; Aharonian *et al.* 2007; Aleksić *et al.* 2011; Arlen *et al.* 2013; Shukla *et al.* 2018; Meyer *et al.* 2019). One of the models to explain the observed flux variations in blazars is the shock-in-jet model, which was first proposed by Marscher

and Gear (1985) and recently developed further byBöttcher and Dermer (2010). Other models that explain blazar variability include jet-star interaction (Barkov *et al.* 2012) and the magnetic reconnection models (Giannios 2013).

The broad band spectra of blazars is dominated by emission from the jet with weak or absent emission lines from the broad line region (BLR). In addition to flux variations, blazars also show large optical and radio polarization as well as optical polarization variability. In the radio band they have flat spectra with the radio spectral index $(\alpha_r) < 0.5$ ($S_\nu \propto \nu^{-\alpha_r}$). Based on the location of the peak (ν_p) of the synchrotron emission in their broad-band spectral energy distribution (SED), blazars are further divided into low synchrotron peaked (LSP) blazars with $\nu_p < 10^{14}$ Hz, intermediate synchrotron peaked (ISP) blazars with $10^{14} Hz \leq \nu_p \leq 10^{15} Hz$, and high synchrotron peaked (HSP) blazars with $\nu_p > 10^{15} Hz$ (Abdo *et al.* 2010a). The majority of FSRQs belong to the LSP category, while a large fraction of HSP sources are BL Lacs. Ghisellini *et al.* (2011) proposed a more physical distinction between FSRQs and BL Lacs which is based on the luminosity of the broad line region (L_{BLR}) relative to the Eddington luminosity (L_{Edd}), where L_{Edd} $= 1.38 \times 10^{38}$ $(M_{BH}/M_\odot)$ erg sec^{-1}, and M_{BH} is the mass of the black hole.

1.1.1.1 Flat Spectrum Radio Quasars (FSRQs)

FSRQs are believed to be the beamed counterparts of the more luminous Fanaroff−Riley type II (FRII; Fanaroff and Riley 1974) radio sources. In the optical spectra they have strong emission lines with equivalent width > 5 Å. They have $L_{BLR}/L_{Edd} >$ 5×10^{-5}. The optical spectrum of the FSRQ 3C 273 is shown in Figure 1.3.
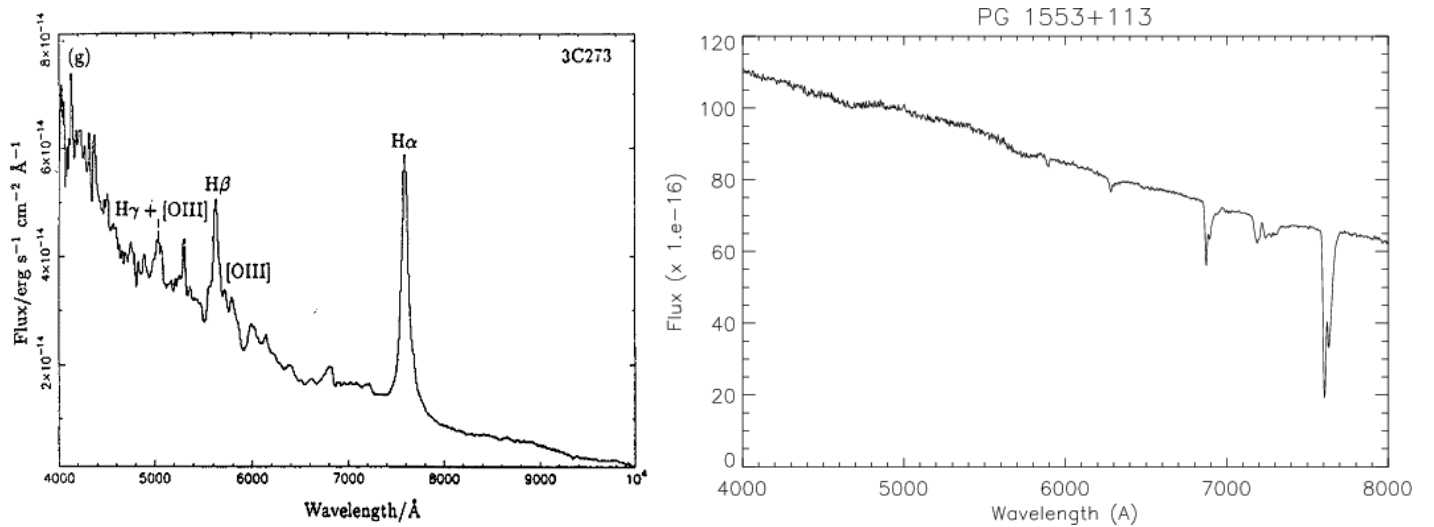
FIGURE 1.3: Left panel: The optical spectrum of the FSRQ 3C 273 (Credit : M.G.Yates et al. 1989). Right panel: The optical spectrum of the BL Lac PG 1553+113 (Credit : Treves et al. 2007)

1.1.1.2 BL Lacs

BL Lacs are the beamed counterparts of the less luminous Fanaroff−Riley type I (FR I; Fanaroff and Riley 1974) radio sources. They generally have a featureless optical spectrum and in case emission lines are present, they are very weak (equivalent width < 5 Å). They have $L_{BLR}/L_{Edd} < 5 \times 10^{-5}$. The optical spectrum of a BL Lac object PG 1553+113 is shown in the right panel of Figure 1.3.

1.2 γ-ray variability in blazars

Blazars show flux variations over the entire accessible electromagnetic spectrum over a range of time scale from days to hours to minutes. (Miller *et al.* 1989; Albert *et al.* 2007; Aleksić *et al.* 2011; Gaur *et al.* 2012b; Arlen *et al.* 2013; Pandey *et al.* 2017; Shukla *et al.* 2018; Meyer *et al.* 2019). Flux variability studies of AGN at short time scales can help to constrain the physical processes that happen close to their central regions. Relativistic jet based models are able to explain flux

variations in blazars. The shock-in-jet scenario (Marscher and Gear 1985; Blandford and Eichler 1987; Jones and Ellison 1991; Baring *et al.* 2017) and jet-in-jet scenario (Giannios and Spruit 2006; Giannios 2013; Sironi *et al.* 2015; Guo *et al.* 2016) are the most viable scenarios to explain the variability behaviour of blazars. Inhomogeneities found in the jets in shock-in-jet models cause relativistic shocks that move down in the relativistically flowing plasma. Particles get accelerated in this process. Particle acceleration in these models happens around the shock in a single region with the radius of the cross-section of around $10^{15} - 10^{16}$ cm. So the short-term variability from hour to minute timescale can not be described by this model unless the bulk Lorentz factor is very large or the size of the cross-section is very small. Also, in magnetically dominated jets, particle acceleration by shock waves in the jets may not be effective (Bell *et al.* 2018). In magnetically dominated plasma, magnetic reconnection or jet-in-jet scenario may be an efficient model to discern the short-term variability of blazars (Shukla and Mannheim 2020). This model provides the possibilities of ultrarelativistic flows of plasmoids within the reconnection region on small scale. Due to the ultrarelativistic motion of the small plasmoids, these mini-jets impart additional Doppler boosting. Therefore, without impacting the bulk motion (Γ) of the whole jets, these small-scale plasmoids help us to understand the minute-scale variability of blazars (Petropoulou *et al.* 2016; Christie *et al.* 2019; Shukla and Mannheim 2020).

Blazars have been extensively studied for flux variations at multiple wavelengths, however, the exact mechanisms that cause flux variability are not fully understood yet. Therefore, extensive observations on a large sample of blazars are needed to enhance our understanding on the flux variability characteristics of blazars. One of the bands of the electromagnetic spectrum where flux variability is less characterized is the γ-ray regime, which is attributed to the paucity of flux variability measurements over a large number of sources. But this band needs to be explored since this is the region where the peak of the high-energy hump of the broad-band SED of blazars lie.

1.3 Optical flux and Polarization variability in Blazars

The radio to optical emission of blazars is observed to be highly polarized with variations in both polarization degree and position angle. In synchrotron emission process the radiation emitted from a single charged particle is elliptically polarized. The left-handed and right-handed components of elliptical polarization will be omitted for any particle distribution and the radiation will be partially linearly polarized (Rybicki and Lightman 1986). If the power radiated per unit frequency in the parallel and perpendicular direction of the magnetic field are $P_{parallel}(\omega)$ and $P_{perpendicular}(\omega)$ then the degree of linear polarization is

$$\prod(\omega) = \frac{P_{perpendicular}(\omega) - P_{parallel}(\omega)}{P_{perpendicular}(\omega) + P_{parallel}(\omega)} \tag{1.1}$$

In synchrotron emission, with particles having a power law distribution with index p, the degree of polarization is

$$\prod = \frac{p+1}{p+\frac{7}{3}} \tag{1.2}$$

Optical flux variations in quasars are known since their discovery about six decades ago (Kinman *et al.* 1966) and subsequently optical polarization were measured for many sources (Angel and Stockman 1980). Blazars in addition to flux variations are also characterized by a high degree ($> 3\%$) of optical polarization and polarization variability. The observed polarized emission in optical as well as at other longer wavelengths from these sources is a strong evidence for the presence of synchrotron emission produced by the relativistic jets in them which is also responsible for the low energy component of their broad band SED (Stockman and Angel 1978; Mead *et al.* 1990; Impey *et al.* 1991; Lister 2001; Marscher *et al.* 2002; Massardi *et al.* 2011). Observations of polarized emission therefore provide valuable information for understanding the physics behind the jets radiation, as it

can give us inputs on the magnitude and direction of the magnetic field within relativistic jets. Changes in the observed polarization position angle could be related to changes in the direction of the magnetic field in the jet along the observer's line of sight. Moreover, as the flux variations in the optical and GeV γ-rays are connected with each other (Bonning *et al.* 2009; Chatterjee *et al.* 2013; Rajput *et al.* 2019 and references therein for no correlation between optical and γ-ray flux variations) flux and polarization variability observations at different wavelengths can provide important inputs on the connection between different emission regions in the jets of these sources. Also, observations with *Fermi* has revealed close association between the γ-ray flare and the rotation of the optical polarization position angle which again can constrain the nature of the high energy γ-ray emission process (Marscher *et al.* 2008, 2010).

Investigations on the relation between total flux and polarization degree (PD) in blazars that are available in literature, point to varied correlations. For example, on an analysis of optical flux and polarization data during the period $2013-2014$ in 3C 279, Rani *et al.* (2018) found a negative correlation between optical flux and PD. Again for 3C 279, analyzing different activity states of the source, Larionov *et al.* (2020) found different types of behaviour between total flux and PD with no preferred correlations. Rakshit *et al.* (2017) based on monitoring observations of the source OJ287 during its outburst in 2016 found positive correlation between flux and PD, negative correlation between flux and PD and no correlation between flux and PD. Hagen-Thorn *et al.* (2008) found a general tendency of negative correlation between PD and flux, with the highest degree of polarization occurring at the lowest flux levels. This is for the source BL Lac using together the data for more than 20 years. For the same source using data collected during the period 2008 to 2010, Gaur *et al.* (2014) found the V-band flux to anti-correlate with PD in one observing season, while no trend between flux and PD was observed during the second observing season. Jorstad *et al.* (2006) found positive correlation between PD and total flux in the sources $0420-014$, 3C 279, 3C 345 and OJ 287 while negative correlation was noticed in 3C 66A and BL Lac. On intra-night

timescales, in the source A0 0235+164, Hagen-Thorn *et al.* (2008) found a positive correlation between total flux and PD. For the TeV blazar 1ES 1959+650, Sorcia *et al.* (2013) using data accumulated during the period 2009 August to November found close correlation between flux and PD. Source 3C 454.3 was found to have different behaviors between optical V-band flux and PD (Rajput *et al.* 2019).

Available polarimetric observations therefore indicate that the polarization behaviours shown by blazars are complex. Coordinated polarization observations along with flux monitoring at multiple wavelengths are needed to unravel the physical processes in the jets of blazars. The complexity of polarization results we know as of today is based on limited observations on few blazars, and more sources need to be investigated to understand the relation between flux and polarization variations.

1.4   Spectral Energy Distribution in Blazars

The broad band SED in blazars is characterized by a two hump structure, one peaking at low energies in the optical/IR/X-ray region and the other one peaking at high energies in the X-ray/MeV region (Fossati *et al.* 1998; Mao *et al.* 2016). While the origin of the low energy hump of the SED is well understood, the cause of the high energy hump in the SED is highly debated. The luminosity ratio of the peak of the high energy hump to the low energy hump is defined as Compton dominance (CD). For FSRQs the CD value is > 1 and for BL Lacs the value is < 1. An example SED for a FSRQ 3C 279 is shown in Figure 1.6, while that of a BL Lac object Mrk 421 is shown in Figure 1.7.

1.5 Origin of the high energy emission in blazars

1.5.1 Leptonic scenario

In the one-zone leptonic model a population of ultrarelativistic electrons (or positrons) is injected into a spherical emission region of co-moving radius R with power-law distribution (Böttcher *et al.* 2013). This spherical emission region moves along the jet axis with the constant relativistic speed $\beta_\Gamma c$ corresponding to the bulk Lorentz factor Γ. In this model, the low energy hump in the broad band SED of a blazar is due to synchrotron emission process and the high energy emission is due to inverse Compton (IC) emission processes (Abdo *et al.* 2010c). The seed photons for the IC process can be either the synchrotron photons that are internal to the jet (synchroton self Compton or SSC; Konigl 1981; Marscher and Gear 1985; Ghisellini and Maraschi 1989) or external to the jet (external Compton or EC; Begelman *et al.* 1987). In the case of EC, the seed photons can be from the disk (Dermer and Schlickeiser 1993; Boettcher *et al.* 1997), the BLR (Sikora *et al.* 1994; Ghisellini and Madau 1996) and the torus (Błażejowski *et al.* 2000; Ghisellini and Tavecchio 2008).

1.5.1.1 Synchrotron emission

Emission from blazar jets is dominated by synchrotron process. This is due to the motion of relativistic non-thermal particles in the presence of a magnetic field. the characteristics of the emitted radiation depend on the strength of the magnetic field as well as the velocities of the charged particles. Synchrotron radiation is polarized and the magnetic field information is given by the degree and direction of polarization.

Consider a relativistic charged particle (electron) of mass m and charge e spiral

uniformly with velocity v in the magnetic field B as shown in the Figure 1.4. The frequency of the gyration (Rybicki and Lightman 1986) is then given as

$$\omega_B = \frac{eB}{\gamma m c} \qquad (1.3)$$

Where γ is the Lorentz factor. The power emitted by the relativistic particle in this process under an acceleration $a_\perp$ is:

$$P_{synchrotron} = \frac{2}{3} \frac{\gamma^2 q^2 a_\perp^2}{c^3} \qquad (1.4)$$

where $a_\perp = \omega_B \ v_\perp$

After solving this equation for an isotropic distribution of velocity, we get

$$P_{synchrotron} = \frac{4}{3} \sigma_T c \beta^2 \gamma^2 U_B \qquad (1.5)$$

Where $\sigma_T = \frac{8}{3} \ \pi \ r_\circ^2$ is the Thomson scattering cross-section and U_B is magnetic energy density and given by $\frac{B^2}{8\pi}$.

1.5.1.2 Inverse Compton process

Inverse Compton process is also a non-thermal process. In the case of blazars, the low energy photons get Compton up-scattered by the relativistic electrons present in the jet. The low energy photons gain energy in this process and gets up-scattered to high energy as shown in Figure 1.5. In the inverse Compton process, the radiated power is given as (Rybicki and Lightman 1986).

$$P_{IC} = \frac{4}{3} \sigma_T c \beta^2 \gamma^2 U_{ph} \qquad (1.6)$$

Where U_{ph} is the initial photon energy density.
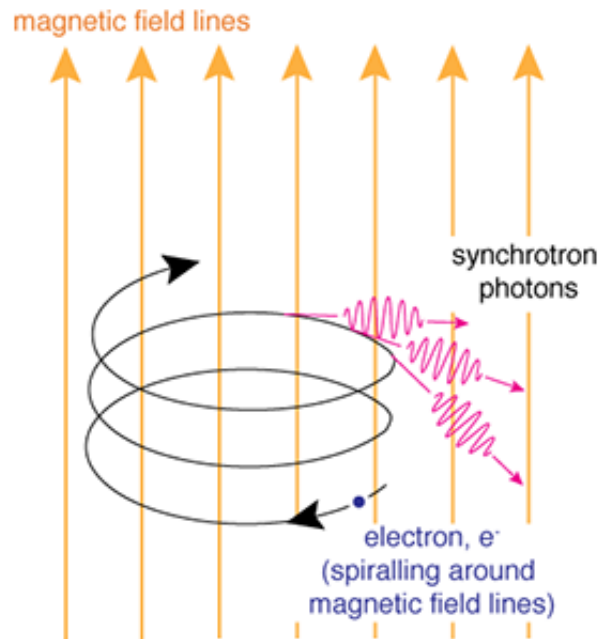
FIGURE 1.4: Spiral motion of a charged particle in the uniform magnetic field (Credit : NASA's Imagine the Universe)
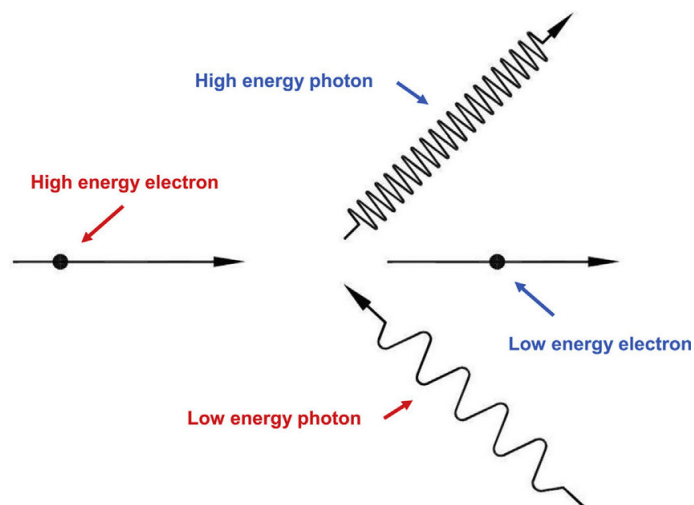
FIGURE 1.5: Schematic illustration of inverse Compton process (Credit : Michael D. Wright et al. 2015)

In the jets of blazars, the low energy photons (seed photons) can come from within the jets produced through the synchrotron emission process, known as the synchrotron-self Compton process. Seed photons from outside the jets such as the accretion disc, torus, broad-line region, etc. can also contribute to the inverse Compton process and this mechanism is referred to as the external Compton process.

1.5.2   Hadronic scenario

Protons can also significantly contribute to the high energy emission from jets in blazars. In this scenario, the γ-ray emission is due to synchroton radiation from extremely relativistic protons (Mücke *et al.* 2003) or the cascade process resulting from proton-proton or proton-photon interaction (Mannheim 1993).

1.6   Broad band SED modelling: The current scenario

Though leptonic models are found to fit the observed SED of majority of blazars, for some blazars, their SEDs are also well fit by either hadronic (Mücke *et al.* 2003; Böttcher *et al.* 2013) or lepto-hadronic models (Diltz and Böttcher 2016; Paliya *et al.* 2016). Blazars are expected to be emitters of neutrinos. These astrophysical neutrinos that are produced by hadronic process can travel unattenuated from the source to the observer. TXS 0506+056 is the first blazar associated with the detection of neutrinos by the IceCube neutrino Observatory on 22 September 2017 and this was coincident in direction and time with a γ-ray flare from TXS
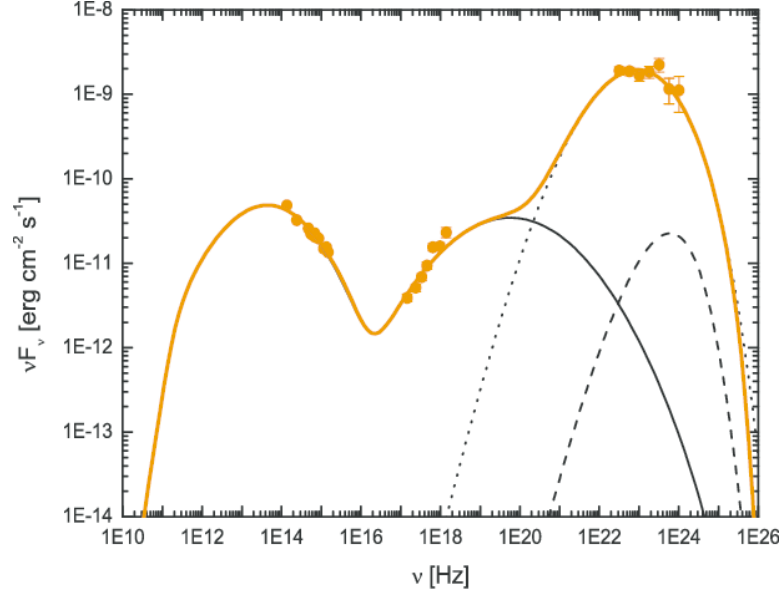
FIGURE 1.6: Spectral energy distribution of the FSRQ 3C 279. Here the black solid line refers to the synchrotron and SSC process. The black dotted and dashed lines refer to the external Compton process through dusty torus and BLR respectively. And the yellow solid line represents sum of all the components. (Credit : Yan et al. 2015)

0506+056. This gives observational evidence of hadronic emission in blazars (Ice-Cube Collaboration *et al.* 2018b). Also, recently another blazar has been found to be spatially coincident with the IceCube neutrino event IC-200107A (Paliya *et al.* 2020). Even during different brightness/flaring states of a source, a single emission model is not able to fit the broad band SED at all times. For example in the source 3C 279, while the flare during March − April 2014 is well fit by leptonic model (Paliya *et al.* 2015), the flare in 2013 December with a hard γ-ray spectrum is well described by lepto-hadronic processes (Paliya *et al.* 2016). Thus, the recent availability of multiwavelength data coupled with studies of sources at different active states indicate that we still do not have a clear understanding of the physical processes happening close to the central regions of blazars.
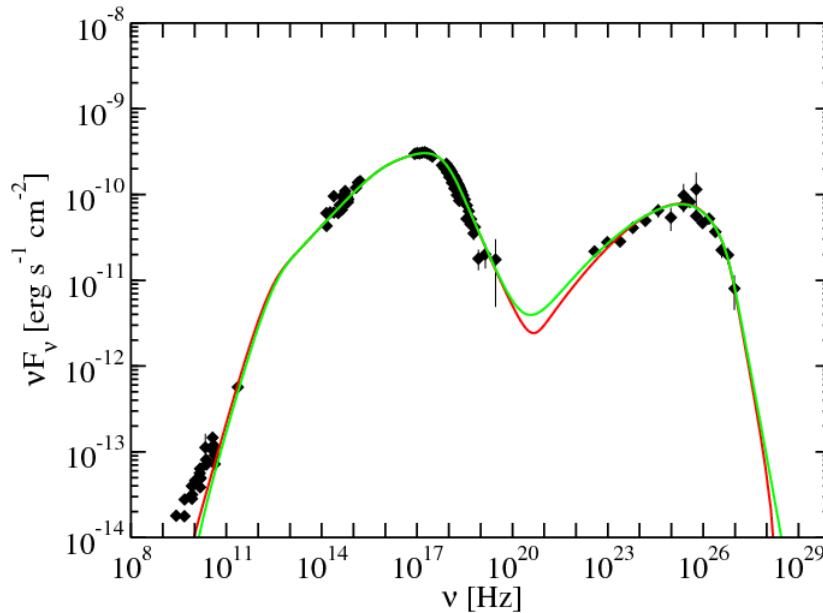
FIGURE 1.7: Spectral energy distribution of the BL Lac Mrk 421. Here red and green solid lines refer to the one-zone SSC model obtained with different minimum variability timescales of 1 day and 1 hour respectively. (Credit : Abdo et al. 2011)

1.7 Optical - GeV variability to constrain the origin of high energy emission in blazars

An alternative to the SED modeling approach to constrain the emission models in blazars is though multiband flux monitoring observations. In the leptonic scenario of emission from the jets of blazars (Böttcher 2007), a close correlation between the optical and γ-ray flux variations is expected. However, in the hadronic scenario of emission from blazars (Mücke and Protheroe 2001), optical and γ-ray flux variations may not be correlated. Thus, optical and γ-ray flux variability observations could constrain the leptonic v/s hadronic emission model of blazar jets. Recent observations made with *Fermi* (Atwood *et al.* 2009) coupled with observations in the optical and infrared wavelengths indicate that in majority of the blazars studied for flux variations, γ-ray flares are closely associated with flares detected at the optical wavelengths with or without lag (Bonning *et al.* 2009; Chatterjee *et al.* 2012; Liao *et al.* 2014; Carnerero *et al.* 2015). However the availability of good

time resolution of optical and γ-ray lightcurves has led to the identification of isolated flaring events in optical and γ-rays termed as "orphan" flares. Both orphan γ-ray flares (prominent flares in GeV band γ-rays with no corresponding flares in the optical band) and orphan optical flares (flaring events in the optical band with no counterpart in the γ-ray band) are now known in blazars. Till recently, optical flares with no corresponding γ-ray flares, are known in PKS 0208−5122 (Chatterjee *et al.* 2013) and S4 1849+67 (Cohen *et al.* 2014) and γ-ray flares with no corresponding optical flares, are known in PKS 2142−75 (Dutka *et al.* 2013), PKS 1510−089 (MacDonald *et al.* 2015) PKS 0454−234 (Cohen *et al.* 2014) and 3C 454.3 (Vercellone *et al.* 2011).

1.8   Major objectives of the thesis

Advances in observational astronomy during the last decade, has enabled one to acquire simultaneous data on blazars that covers IR, optical, ultra-violet (UV), X-ray and γ-ray energies. The availability of such observations has triggered interest in constraining the high energy emission process in blazars via SED modelling. However, this is a difficult approach as it requires near simultaneous data over various wavelengths such as optical/UV/IR, X-rays and γ-rays as well as realistic models and SED fitting tools that incorporate sophisticated minimization techniques. Results available on few sources show that observations are fit equally by leptonic as well as lepto-hardonic modes. A definitive way to constrain the leptonic v/s hadronic emission process in blazars is through the measurement of high energy polarization in blazars. But, such high energy polarization measurements do not exist currently and must await the launch of X-ray polarimetric missions such as IXPE (Weisskopf *et al.* 2016) and AMEGO (McEnery *et al.* 2019).

The number of sources that are known to be emitters of high energy γ-ray emission (100 MeV to 300 GeV) has increased significantly since the launch of *Fermi* in 2008. The availability of such a data set would enable to probe the high energy γ-ray variability characteristics of blazars. Also, *Fermi* observations has revealed close association between γ-ray flare and the rotation of the optical polarization position angle which again can constrain the nature of the high energy emission in blazars. Given the vast amount of multi-wavelength data that exists on blazars today, in this thesis work, I aim to address the following

1. How do the flux variations in the high energy GeV band relate with the flux variations in the optical band in FSRQs and BL Lacs? Can such a correlation analysis of flux variations in the optical and GeV band constrain the leptonic scenario in blazars?

2. Are there any differences in the long term γ-ray flux variability characteristics between FSRQs and BL Lacs?

3. What is the association between γ-ray and optical flux variations with optical polarization variations?

The above will be addressed in the following chapters.

Chapter 2

Observations, sample selection and data reduction

The number of blazars that are known to be emitters of γ-rays has increased manifold since the launch of *Fermi* in the year 2008. The recently released 4LAC catalog (Abdollahi *et al.* 2020) contains around 3000 blazars of which 681 are FSRQs and 1102 are BL Lacs. However, during the start of the thesis the *Fermi* catalog of AGN that was available is the 3LAC catalog which contains 481 FSRQs and 639 BL Lacs. Ground based optical (in B, V and R-bands) and IR (J and K bands) observations of few *Fermi* detected blazars were carried out by the Small and Moderate Apetrure Telescope System (SMARTS[*]; Bonning *et al.* 2012). Similarly optical V-band and spectro-polarimetric observations on few *Fermi* blazars were carried out by the Steward Observatory (Smith *et al.* 2009). Observations provided by *Fermi*, SMARTS and Steward Observatory form the main data that was used to address the objectives of this thesis.

---

[*]http://www.astro.yale.edu/smarts/glast/home.php

2.1 Sample Selection

2.1.1 Optical - GeV connection

To investigate the correlations between optical and GeV flux variations in blazars, I first selected all sources that are classified as FSRQs and BL Lacs in the third catalog of AGN detected by LAT onboard *Fermi* (3LAC; Ackermann *et al.* 2015a). For the selected sources I then looked into their one day binned γ-ray light curves and selected those sources that have at least one flare with the γ-ray flux exceeding 10^{-6} photons cm^{-2} s^{-1}. This leads us to a sample of 84 FSRQs and 21 BL Lacs. For the 84 FSRQs and 21 BL Lacs, I also looked in the archives of SMARTS for the availability of optical and IR data overlapping the γ-ray data. Of the 84 FSRQs, optical and IR data in SMARTS is available for 40 sources. Of these 40, three sources namely 3C 454.3, PKS 1510−089 and 3C 279 have the largest number of data points in the optical and IR bands with the total exceeding 500. To these three, I added two more sources namely 3C 273 and CTA 102 due to their high γ-ray activity states (Ciprini 2016; Bastieri 2009). Thus, in FSRQs I considered five sources for study of correlations between optical and γ-ray flux variations. Similarly for BL Lacs, out of the 21 sources with at least on γ-ray flare exceeding 10^{-6} photons cm^{-2} s^{-1}, six sources, namely AO 0235+164, PKS 0301−243, PKS 0426−380, PKS 0537−441, OJ 287 and PKS 2155−304 have optical and IR data in the SMARTS archives. Of these I selected only three sources namely AO 0235+164, OJ 287 and PKS 2155-304 as they are the ones with the maximum number of points in the optical and IR bands put together. Thus for analysis of the correlation between optical and γ-ray flux variations I selected a total of 8 sources, of which five are FSRQs and three are BL Lacs. The details of these sources are given in Table 2.1.

TABLE 2.1: Details of the objects analysed in this thesis. The γ-ray flux in the 100 MeV - 300 GeV band is in units of 10^{-7} ph cm^{-2} s^{-1} and Γ is the γ-ray photon index in the 100 MeV $-$ 300 GeV band.

Type	Name	3FGL name	α_{2000}	δ_{2000}	z	Γ	γ-ray flux
FSRQ	3C 273	3FGL J1229.1+0202	12:29:06.70	+02:03:09	0.158	2.661	6.73
FSRQ	3C 279	3FGL J1256.1$-$0547	12:56:11.17	$-$05:47:22	0.536	2.343	8.79
FSRQ	PKS 1510$-$089	3FGL J1512.8$-$0906	15:12:50.53	$-$09:06:00	0.360	2.364	9.13
FSRQ	CTA 102	3FGL J2232.5+1143	22:32:36.41	+11:43:51	1.037	2.520	13.70
FSRQ	3C 454.3	3FGL J2254.0+1608	22:53:57.7	+16:08:54	0.859	2.35	24.7
BL Lac	AO 0235+164	3FGL J0238.6+1636	02:38:38.9	+16:36:59	0.940	2.06	1.41
BL Lac	OJ 287	3FGL J0854.8+2006	08:54:48.9	+20:06:31	0.306	2.12	0.99
BL Lac	PKS 2155$-$304	3FGL J2158.8-3013	21:58:52.0	$-$30:13:32	0.116	1.75	1.12

2.1.2 γ-ray flux variability

The sample of objects for analysis of γ-ray flux variability was taken from the third catalogue of AGN detected by *Fermi*-LAT (3LAC; Ackermann *et al.* 2015a). For this work I selected a total of 1120 sources detected between 100 MeV and 300 GeV with test statistic (TS) > 25. The TS is a measure of source detection significance and is defined as TS = 2log(likelihood) between models with and without the source (Mattox *et al.* 1996). Of these 1120 sources, 639 are BL Lacs and 481 are FSRQs. About 50% of the BL Lacs in my sample have no measured redshift. Excluding those objects, the BL Lacs in my sample have redshifts between 0.03 and 1.72, while the FSRQs have redshifts between 0.16 and 3.10. The distribution of the redshifts of the sample is shown in Figure 2.1. By further dividing the sources in the sample that were selected for this study and based on the position of synchrotron peak frequency in their broad-band SED, I have 599 LSPs, 232 ISPs and 289 HSPs. Also shown in Figure 2.2 and Figure 2.3 are the distributions of the γ-ray luminosity in the 1 - 100 GeV range and the γ-ray photon index. The γ-ray luminosities and the photon indices were taken from the 3LAC catalogue. FSRQs are highly luminous and have steeper photon indices in the γ-ray band

relative to BL Lacs, which is similar to what is known based on the analysis of three months of data from *Fermi* (Ghisellini and Tavecchio 2009).

2.2   Data Reduction

2.2.1   Fermi γ-ray space Telescope

The γ-ray data used in this thesis work is from the LAT instrument onboard *Fermi*. The LAT (Atwood *et al.* 2009) is an imaging, high energy γ-ray telescope, which covers the energy range 20 MeV to more than 300 GeV. The LAT is a pair-conversion telescope, which mainly operates in scanning mode and covers the entire sky once every $\sim$ 3 hr.

I analyzed 10 years γ-ray data using the *Fermi* Science Tool version v10r0p5 with appropriate selections and cuts recommended for the scientific analysis of PASS8 data [†]. The photon-like events categorized as 'evclass=128, evtype=3' with energies 0.1$\leqslant$E$\leqslant$300 GeV γ-rays within a circular region of interest (ROI) of 15° centered on the source and with zenith angle 90° were extracted. The appropriate good time intervals were then generated by using the recommended criteria "(DATA_QUAL > 0)&&(LAT_CONFIG==1)". The likely effects of cuts and selections, as well as the presence of other sources in the ROI, were incorporated by generating exposure map on the ROI and an additional annulus of 15° around it with the third LAT catalogue (3FGL - gll_psc_v16.fit; Acero *et al.* 2015). I used isotropic model, "iso_P8R2_SOURCE_V6_v06" and the Galactic diffuse emission model "gll_iem_v06" . To evaluate the significance of detection, I used the maximum-likelihood (ML) ratio test defined as TS = 2$\triangle$ log(L), where L is the likelihood function between models with and without a γ-ray point source at the

---

[†] http://fermi.gsfc.nasa.gov/ssc/data/analysis/documentation/
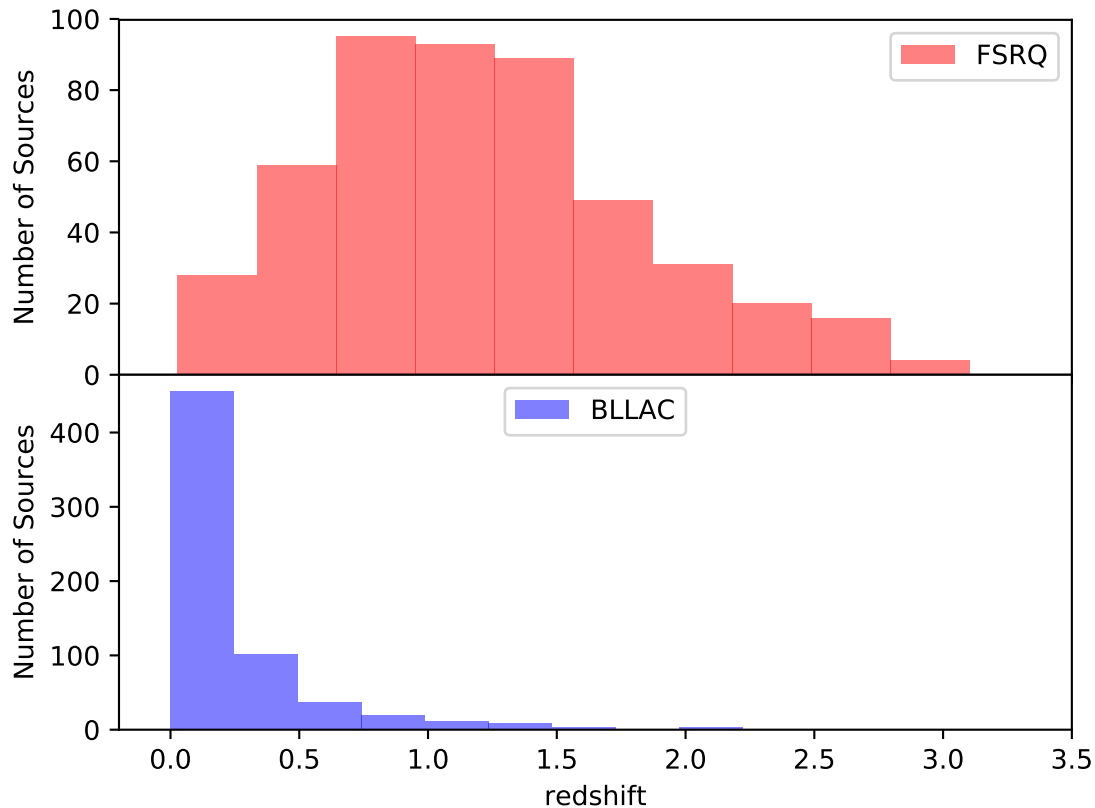
FIGURE 2.1: Distribution of redshifts for FSRQs and BL Lacs.

position of the source. I considered the source as detected if TS > 9, which corresponds to a 3σ detection (Mattox *et al.* 1996). I generated the source light curve with time binning of 1 day (for the analysis of correlation between optical and γ-ray flux variations) and 1 month (for γ-ray variability analysis). For bins with TS < 9, the source was considered undetected. All the errors associated with *Fermi*-LAT points are the 1σ statistical uncertainties.

2.2.2 Swift-XRT

Swift X-ray telescope (XRT; Burrows *et al.* 2005) is a sensitive X-ray imaging telescope designed to measure flux, spectra, lightcurves of GRBs and afterglows
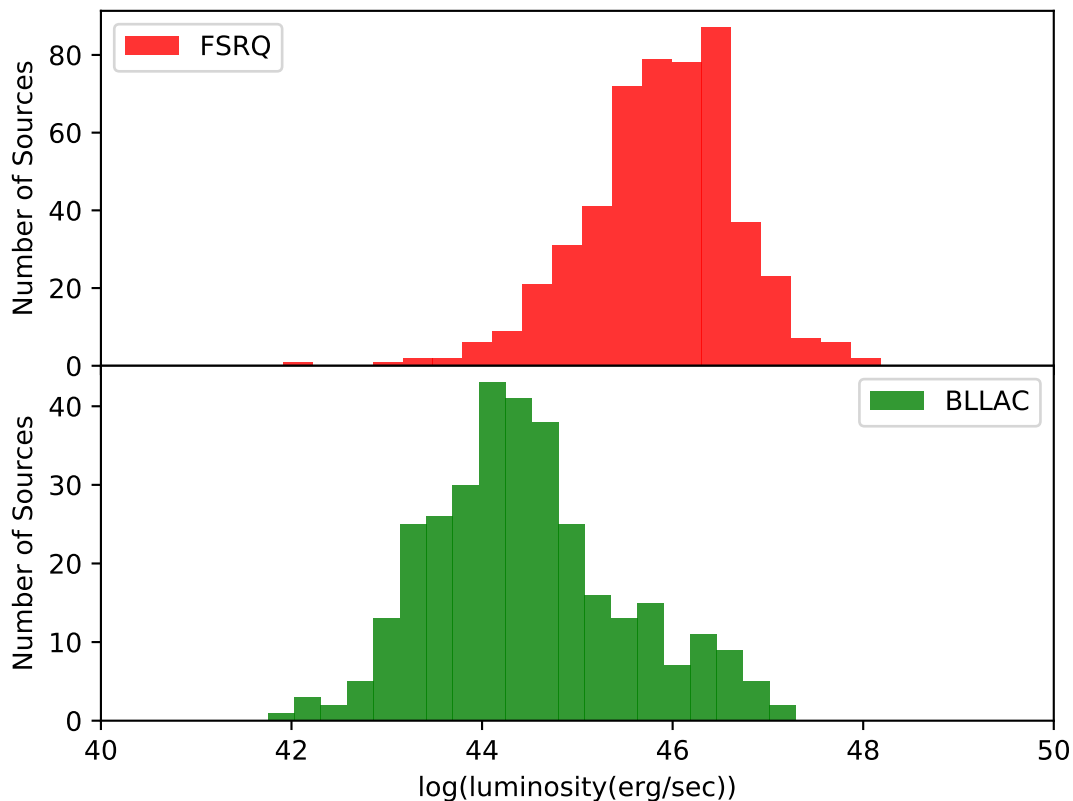
FIGURE 2.2: Distribution of γ-ray luminosities for FSRQs and BL Lacs.

across a wide dynamic range of more than 7 flux magnitude orders. The parameters of the *Swift* X-ray telescope are given in Table 2.2. For X-rays covering the energy range of $0.3 - 10$ keV, I used the data from the X-ray telescope onboard the *Swift* satellite (Gehrels *et al.* 2004) taken from the archives at HEASARC [‡]. The data collected during the period 2008 August $-$ 2018 August were analyzed with default parameter settings following the procedures given by the instrument pipeline. For light curve analysis, data collected using both window timing (WT) and photon counting (PC) modes were used. For spectral analysis for the sources 3C 454.3, PKS 1510$-$089, 3C 279, CTA 102, AO 0235+164 and OJ 287, I used the data collected only from the PC mode. While, for the source 3C 273, I used PC mode data for the quiescent state but for γ-ray flaring state I used the WT mode data

---

[‡]https://heasarc.gsfc.nasa.gov/docs/archive.html
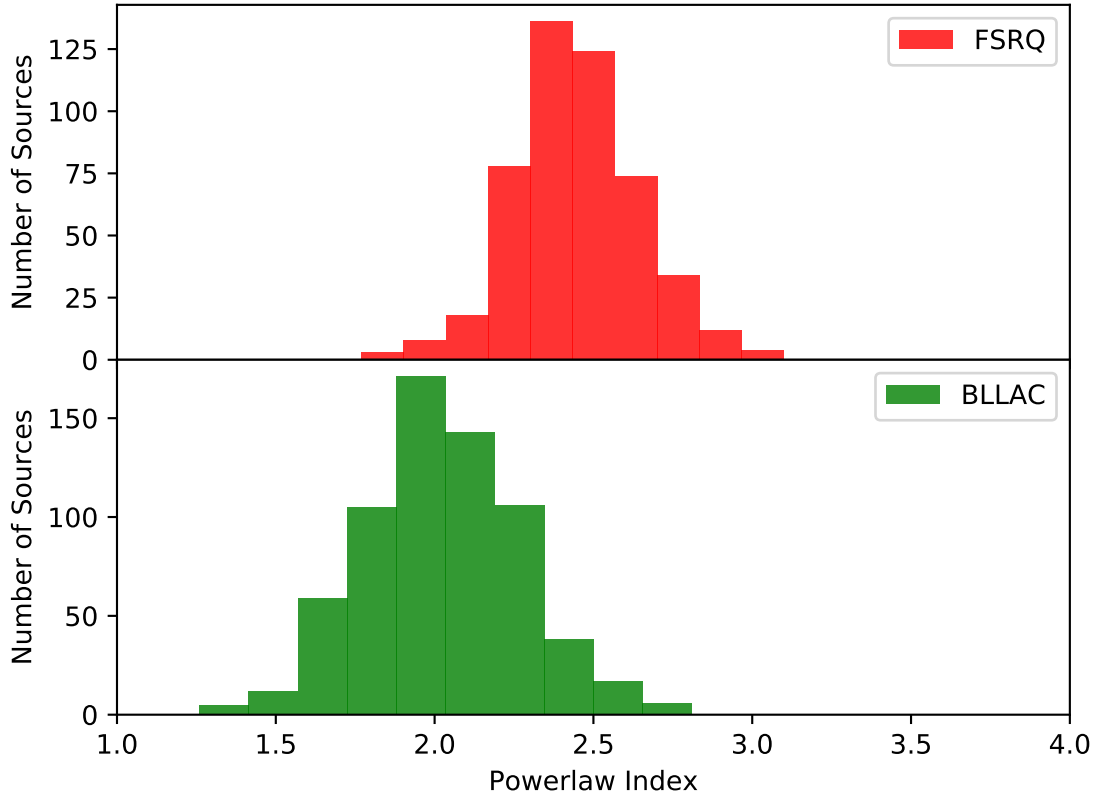
FIGURE 2.3: Distribution of photon indices for FSRQs and BL Lacs.

and for the source PKS 2155−304, I used WT mode data for the quiescent state and PC mode data for the flaring states. The WT mode data is used due to the non availability of PC mode data. The collected XRT data were processed with the `xrtpipeline` task using the latest CALDB files available with version HEASOFT-6.21. I used the standard grade selection 0−12. The calibrated and cleaned events files were summed to generate energy spectra. For PC mode, I extracted the source spectra from a circular region of radii 60″, and the background spectra were selected from the region of radii 80″ away from the source. In WT mode, for the source I used a circular region of 60″ radii while for the background I used the region between 80″ and 120″ radii centered around the source. I combined the exposure maps using `XIMAGE` and created the ancillary response files using `xrtmkarf`. I used an absorbed simple power law model with the Galactic neutral

TABLE 2.2: Characteristics of *Swift*-XRT

Field of View	23.6 × 23.6 arcmin
Energy range	0.2 − 10 keV
Effective area	135 cm^2 @ 1.5 keV
Sensitivity	2×10^{-14} erg cm^{-2} s^{-1} in 10^4 s
Detector readout modes	Photon-counting, Imaging and Timing
Position accuracy	2.5 arcseconds
Operation	Autonomous

hydrogen column density of N_H=6.5× 10^{20} cm^{-2}, 6.89× 10^{20} cm^{-2}, 2.21× 10^{20} cm^{-2}, 4.81× 10^{20} cm^{-2}, 1.68× 10^{20} cm^{-2}, 6.59× 10^{20} cm^{-2}, 2.38× 10^{20} cm^{-2} and 1.29× 10^{20} cm^{-2} (Kalberla *et al.* 2005) for the sources 3C 454.3, PKS 1510−089, 3C 279, CTA 102, 3C 273, AO 0235+164, OJ 287 and PKS 2155−304 respectively to perform the fitting within XSPEC (Arnaud 1996). Within XSPEC, I adopted χ^2 statistics and the calculated uncertainties were at the 90% confidence level.

2.2.3 UV−Optical Data

For UV and optical I used the data from the *Swift*-UV-Optical telescope (UVOT). The UVOT is co-aligned to XRT and provides both ultraviolet and optical coverage simultaneously in a 17'×17' within the 170 − 650nm wavelength range. The data was analyzed using the online tool[§]. To generate the lightcurve the magnitudes thus obtained and uncorrected for Galactic reddening were then converted to fluxes using the zero points taken from Breeveld *et al.* (2011). However corrections due to galactic absorption were applied to generate the average spectrum.

[§]https://www.ssdc.asi.it/cgi-bin/Swiftuvarchint

2.2.4 Optical−NIR Data

In addition to UVOT, optical data were also taken from SMARTS ¶ in B, V and R band as well as the from Steward Observatory ‖ in V-band. Similarly near-infrared (NIR) data in J and K bands were taken from observations carried out using the ANDICAM instrument on the SMARTS 1.3 m telescope as part of a blazar monitoring campaign, supporting the *Fermi* multiwavelength AGN science. The details of the instrument and the data reduction procedures for SMARTS observations can be found in Bonning *et al.* (2012). Similarly the details of the instrument and the reduction procedures adopted for observations carried out in the Steward Observatory can be found in Smith *et al.* (2009). The data in the optical and NIR bands taken from the Steward Observatory and SMARTS are the standard magnitudes and the data were not reduced in this thesis to get the magnitudes.

2.3 Cross-Correlation Analysis

To check for the presence of any correlation between optical and γ-ray flux variations I cross-correlated the optical and γ -ray light curves using the discrete correlation (DCF) technique of Edelson and Krolik (1988) and the interpolated cross-correlation function (ICCF) technique of Gaskell and Sparke (1986); Gaskell and Peterson (1987). Errors in both DCF and ICCF were obtained by performing a model-independent Monte Carlo simulation that involves both flux randomization and random selection of subsets (RSS) according to the procedures outlined in Peterson *et al.* (2004). In each iteration of Monte Carlo simulation, I randomly

---

¶http://www.astro.yale.edu/smarts/glast/home.php
‖http://james.as.arizona.edu/∼psmith/Fermi

first took N independent points from the parent light curve of N data points, regardless of whether any point was previously selected using RSS process. After RSS method the new light curve includes M data points. To take into account the uncertainties in the calculated flux values, the fluxes of the M data points were then altered randomly by adding the uncertainties of the calculated flux multiplied by a random Gaussian number. I estimated the CCF of the modified light curve for each Monte Carlo iteration and estimated the τ_{cent} using the points within 60 per cent of the CCF value. To get the significance cross-correlation results, this process has been repeated for 10000 iterations keeping only those CCF with a peak value > 0.5. The median of the cross-correlation centroid distribution (CCCD) is taken as a measure of the time lag. Within a confidence interval of 68% I measured uncertainties around the median value.

2.4 γ-ray spectra

The shape of the γ-ray spectrum can provide evidence on the intrinsic distribution of electrons involved in the γ-ray emission processes that might involve acceleration and cooling processes. For all the selected intervals identified for the correlation study, I generated the γ-ray spectra and fitted them with two models, namely a simple power law (PL) model and a log parabola (LP) model. The PL model has the form

$$dN(E)/dE = N_\circ (E/E_\circ)^{-\Gamma} \tag{2.1}$$

where $N_\circ$ is normalization of the energy spectrum and $E_\circ = 300$ MeV, which is constant for all SEDs.

The LP model is defined as below following Nolan *et al.* (2012)

$$dN(E)/dE = N_\circ(E/E_\circ)^{-\alpha-\beta ln(E/E_\circ)} \tag{2.2}$$

here, dN/dE is the number of photons cm^{-2} s^{-1} MeV^{-1}, α is photon index at $E_\circ$, β is the curvature index, E is the γ-ray photon energy, N$_\circ$ and E$_\circ$ are the normalization and scaling factor of the energy spectrum respectively.

I used the maximum likelihood estimator `gtlike` for spectral analysis using likelihood ratio test (Mattox *et al.* 1996) to check the PL model (null hypothesis) against the LP model (alternative hypothesis). $TS_{curve} = 2(\log L_{LP}$ - $\log L_{PL})$ was also calculated (Nolan *et al.* 2012). The presence of a significant curvature was tested by setting the condition $TS_{curve} > 16$.

2.5   Spectral energy distribution modeling

To characterize the nature of the sources during different epochs, I constructed the broad band SED. All the generated SEDs were modelled using the one zone leptonic model of Sahayanathan and Godambe (2012). In this model, the emission region is assumed to be a spherical blob of size R filled with non-thermal electrons following a broken power law distribution

$$N(\gamma)\,d\gamma = \begin{cases} K\,\gamma^{-p}\,d\gamma & \text{for} \quad \gamma_{\min} < \gamma < \gamma_b \\ K\,\gamma_b^{q-p}\gamma^{-q}\,d\gamma & \text{for} \quad \gamma_b < \gamma < \gamma_{\max} \end{cases} \tag{2.3}$$

where, γ is the electron Lorentz factor and, p and q are the low and high energy power-law indices with γ_b the Lorentz factor corresponding to the break energy. The emission region is permeated with a tangled magnetic field B and move down the jet with a bulk Lorentz factor Γ. The broadband SEDs are modelled using synchrotron, SSC and EC emission mechanisms. This model was added as a local model in XSPEC (Arnaud 1996) and the source parameters were obtained through

χ^2 minimization (Sahayanathan *et al.* 2018). There are twelve free parameters in the model, of which six parameters govern the electron energy distribution, namely electron energy index before the break (p), electron energy index after the break (q), the break Lorentz factor (γ_b), minimum Lorentz factor of the electrons (γ_{min}), the maximum Lorentz factor of the electron (γ_{max}) and the electron energy density (U_e). The other six parameters in the model are the magnetic field (B), size of the emission region (R), Lorentz factor (Γ), jet viewing angle (θ), external photon field temperature (T) and the fraction of the external photons that take part in the EC process (f). In order to investigate the different flaring behaviour between optical and γ-ray, firstly I fitted the quiescent epoch to obtain the parameters for all the sources. From the observed SED, I could obtain the high and low energy spectral indices, the synchrotron flux in the optical, the SSC and EC fluxes in the X-ray and γ-ray energies respectively. Consistently for the model fit, I chose five free parameters namely p, q, U_e, Γ and B while the other parameters were frozen to typical values.

To account for the deviation of the model from the optical spectra, I modified the model by including the emission from the accretion disk. The thermal emission from the disk is decided by two parameters, namely the central black hole mass and the mass accretion rate (Shakura and Sunyaev 1973; Jolley and Kuncic 2008). The mass of the black hole is obtained from Chen (2018) and the accretion rate is fitted to reproduce the optical spectra. This procedure significantly improved the resultant χ^2 and the best fit parameters. Through this exercise I also demonstrate the capability to extract the accretion disk component from the broadband SED through a realistic spectral modelling involving different emission mechanisms. To account for the model related uncertainties, I added 12% systematic error evenly over the entire data. For SED model fits, corrections due to galactic absorption were applied to the IR, optical[**], UV (Cardelli *et al.* 1988) and X-ray data points. For UV, optical and IR, all data points over the period in each of the epochs were averaged filter wise to get one data point for each filter. However, for X-ray and

---

[**]http://ned.ipac.caltech.edu

γ-rays, all the available data over the period in each of the epochs was used to construct their average spectra.

Chapter 3

Correlation between optical and γ-ray flux variations in flat spectrum radio quasars *

In this chapter I present the results of the correlation analysis between optical and γ-ray flux variations in FSRQs. The sample selected for this study consists of a total of five FSRQs, namely 3C 454.3, PKS 1510$-$089, 3C 273, 3C 279 and CTA 102. The details of the sample selection, reduction of the data for the generation of multiband light curves, γ-ray spectra and broad band SED are given in Chapter 2. For 3C 454.3 I have used the multiband data that spans the period 2008 August to 2017 February while for the remaining four sources, I have used the data covering the period 2008 August to 2018 February. A brief description of these sources are given below.

TABLE 3.1: Details of the epochs considered for detailed light curve analysis, SED modelling and spectral analysis. The γ-ray fluxes in the 100 MeV to 300 GeV band are in units of 10^{-6} ph cm^{-2} s^{-1} and the optical fluxes in the V-band are in units of 10^{-11} erg cm^{-2} s^{-1}

| | | MJD | | Calender date | | Mean flux | | |
Name	ID	Start	End	Start	End	γ	Optical	Remark
3C 454.3	A	55122	55222	18-10-2009	26-01-2010	4.97	1.76	γ-ray flare and optical flare
	B	55460	55560	21-09-2010	30-12-2010	11.7	2.81	γ-ray flare and optical flare
	C	55650	55750	30-03-2011	08-07-2011	0.54	0.68	Quiescent state
	D	56510	56610	06-08-2013	14-11-2013	0.99	1.67	Optical flare but no γ-ray flare
	E	56780	56880	03-05-2014	11-08-2014	3.75	3.23	Optical flare but weak γ-ray flare
PKS 1510$-$089	A	54937	54957	16-04-2009	06-05-2009	2.97	1.07	γ-ray flare with no optical flare
	B	54951	54971	30-04-2009	20-05-2009	2.26	1.94	γ-ray flare and optical flare
	C	55757	55777	15-07-2011	04-08-2011	1.10	0.66	γ-ray flare with no optical flare
	D	56062	56162	15-05-2012	23-08-2012	0.44	0.62	Quiescent state
	E	57105	57125	24-03-2015	13-04-2015	3.12	0.95	γ-ray flare with no optical flare
	F	57157	57177	15-05-2015	04-06-2015	3.17	2.30	γ-ray flare and optical flare
3C 273	A	55265	55285	10-03-2010	30-03-2010	1.53	16.9	γ-ray flare with no optical flare
	B	56450	56550	07-06-2013	15-09-2013	0.40	16.7	Quiescent state
3C 279	A	55290	55390	04-04-2010	13-07-2010	0.26	0.14	Quiescent state
	B	56742	56762	26-03-2014	15-04-2014	2.21	2.15	γ-ray flare with no optical flare
	C	57178	57198	05-06-2015	25-06-2015	3.94	1.42	γ-ray flare with no optical flare
	D	57828	57848	16-03-2017	05-04-2017	2.33	4.25	optical flare but no γ-ray flare
CTA 102	A	55840	55940	06-10-2011	14-01-2012	0.31	0.39	Quiescent state
	B	57740	57750	18-12-2016	28-12-2016	10.3	44.5	γ-ray flare and optical flare

3.1 3C 454.3

3C 454.3 is a FSRQ at a redshift $z = 0.859$. It was detected first as a bright and variable γ-ray source by EGRET onboard the Compton Gamma Ray Observatory (CGRO; Hartman *et al.* 1993). It has been studied extensively utilizing data over a large range of wavelengths that include, optical, X-ray and γ-ray energies (Bonning *et al.* 2009, 2012; Ackermann *et al.* 2010; Kushwaha *et al.* 2017). 3C 454.3 was found in a highly active state in the γ-ray band by AGILE (Vercellone *et al.* 2010, 2009) in 2007. In 2010 November the highest flare was detected at E > 100 MeV with the LAT instrument, having a flux value of about 6.6×10^{-5}ph cm^{-2} s^{-1}(Abdo *et al.* 2011). According to Shah *et al.* (2017) X-ray and γ-ray

emission from 3C 454.3 cannot be explained by single emission mechanism and to study the high energy observations one needs to consider both EC and SSC emission processes.

3.2 PKS 1510−089

It was identified as a quasar firstly by Bolton and Ekers (1966) with a visual magnitude of 16.5 mag. It is one of the most variable FSRQs in the 3FGL catalog. Located at a redshift of $z = 0.361$ (Tanner *et al.* 1996), it is powered by a black hole of mass 5.4×10^8 M$_\odot$ and accretes at the rate of 0.5 M$_\odot$ yr^{-1} (Abdo *et al.* 2010d). It has been detected at very high energies by HESS (H. E. S. S. Collaboration *et al.* 2013) and MAGIC (Major Atmospheric Gamma-Ray Imaging Cherenkov; Aleksić *et al.* 2014). This source has been studied for multi-wavelength flux variability (Prince *et al.* 2017; Nalewajko 2013) as well as subjected to few SED modelling studies (Prince *et al.* 2019; Nalewajko *et al.* 2012). Considering radio observations with the VLBA coupled with optical long term monitoring data Wu *et al.* (2005) argued for the presence of a binary black hole in PKS 1510−089.

3.3 3C 273

3C 273, the first quasar discovered by Schmidt (1963) at a redshift $z = 0.158$ has a large scale radio jet with a projected size of 57 kpc (Harris and Krawczynski 2006). It was the first quasar that was discovered in the γ-ray band in the energy range of 50−500 MeV (Swanenburg *et al.* 1978). It was later detected by the Energetic Gamma- Ray Experiment Telescope (EGRET; Hartman *et al.* 1999) and then by *Fermi*. It has been studied for flux variations in the optical (Xiong *et al.* 2017)

and also has been found to show dramatic variations in the γ-ray band from *Fermi* observations (Abdo *et al.* 2010b). The γ-ray outburst in 2009 was explained by a time dependent one zone synchrotron self-Compton model (Zheng *et al.* 2013).

3.4   3C 279

At a redshift of $z = 0.536$ (Lynds *et al.* 1965), 3C 279 was among the blazars that were discovered as emitters of γ-rays by EGRET (Hartman *et al.* 1992). In the GeV$-$TeV range it was first detected by the ground based atmospheric Cherenkov experiment MAGIC (MAGIC Collaboration *et al.* 2008). It has been recently suggested that 3C 279 hosts a supermassive black hole binary at its center (Qian *et al.* 2019). The source is found to show flux variations over a range of wavelengths such as radio (Pauliny-Toth and Kellermann 1966), optical (Oke 1967) and γ-rays (Hartman *et al.* 1992). It has also been studied for correlated variations over different wavebands (Chatterjee *et al.* 2008). *Fermi* observations have revealed minute scale flare in this source with a shortest flux doubling time scale lesser than 5 minutes during the outburst in 2015 (Hayashida *et al.* 2017). In addition to flux variability studies, it has also been studied via broad band SED modelling during various activity states. The flares at different epochs of the source were explained by leptonic process (Paliya *et al.* 2015; Shah *et al.* 2019), lepto-hardonic process (Paliya *et al.* 2018) as well as hadronic processes (Petropoulou *et al.* 2017). These observations and subsequent modelling clearly indicate that the same emission mechanisms are not responsible for the high energy emission received from the source at all times.

3.5   CTA 102

This FSRQ at a redshift of $z = 1.037$ (Schmidt 1965) is highly polarized (Moore and Stockman 1981) and variable in the optical band (Maraschi *et al.* 1986). It was detected in the γ-ray band both by EGRET (Fichtel *et al.* 1994) and *Fermi* (Abdo *et al.* 2009). It has been studied for flux variations across different wavebands (Kaur and Baliyan 2018) and minute like time scales of variability were detected in the optical (Osterman Meyer *et al.* 2009) and γ-ray bands (Shukla *et al.* 2018).

3.6   Multi-wavelength light curves

Analysis for the presence or absence of correlation between optical and γ-ray flares requires identification of flares in optical and/or γ-ray light curves. Due to large gaps and/or less number of points in the optical light curves it is not possible to automatically identify epochs (through cross-correlation analysis) on the presence or absence of correlated optical and γ-ray flux variations. Therefore, flares for detailed analysis were selected visually (except for 3C 454.3) as follows. Multi-wavelength light curves that span the 10 year period were first generated for each object. In that, optical and γ-ray light curves were visually inspected for the presence of sharp peaks above their base flux levels. Once identified, expanded multi-wavelength light curves were generated for a total duration of 20 days, centered at the optical and/or γ-ray flares. In an epoch when a γ-ray flare or an optical flare is identified, I imposed the condition of having data in multiple wavelengths such as γ-rays, X-rays, UV, optical and IR so as to constrain both the low energy and high energy hump in the SED analysis. These conditions lead to the identification of few flares. Of these I concentrated only on some epochs for each object. For the source 3C 454.3, I identified an optical flare as follows (i) there is a gradual increase of the optical brightness at least by 0.5 mag from the

quiescent level, (ii) there is a corresponding declining branch from the peak back to the quiescent level and (iii) the rising and decaying phase (both inclusive) lasts for more than 50 days. The details of the epochs selected for the analysis for the sources are given in Table 3.1.

3.6.1   3C 454.3

The multi-wavelength light curves that include γ-ray, X-ray, UV, optical and IR along with the polarization measurements from 2008 August to 2017 February (MJD: $54500-57800$) are shown in Figure 3.1. From Figure 3.1 it is evident that 3C 454.3 has gone through both quiescent and active phases during the period MJD $54500 - 57800$. During this period, I identified four time intervals during which large optical flares were seen. They are denoted by epochs A,B,D and E and cover the period MJD $55122-55222$ (Epoch A), MJD $55460-55560$ (Epoch B), MJD $56510-56610$ (Epoch D) and MJD $56780-56880$ (Epoch E). The above four intervals were chosen such that (i) there is a gradual increase of the optical brightness at least by 0.5 mag from the quiescent level (ii) there is a corresponding declining branch from the peak back to the quiescent level and (iii) the rising and decaying phase (both inclusive) lasts for more than 50 days. The peak of the flares are shown as a vertical dashed red line in Figure 3.1. On either side of the red lines are two black vertical lines, having a total duration of 100 days. I also identified a time interval denoted as Epoch C and covering the period MJD $55650-55750$, where the source was at its quiescent state in IR-optical-UV-Xrays and γ-rays. This quiescent period for a duration of 100 days is indicated by two vertical blue lines in Figure 3.1. The details of the five epochs that were identified for further analysis along with their mean optical and γ-ray flux levels are given in Table 3.1. Detailed analysis of each of these five epochs are given in the following sub-sections.

Epoch A (MJD 55122 − 55222) An inspection of Figure 3.1. indicates that there is a close correlation between IR, optical, UV, X-rays and γ-rays. Optical polarization data though sparse during this period was not available during the peak of the flare making it impossible to comment on the nature of the optical polarization during the peak of the γ-ray flare. The multiband light curves covering for a duration of 100 days centered of the peak of epoch A, along with the polarization measurements when available are given in Figure 3.2. The results of the cross-correlation functions analysis are shown Figure 3.3 both for ICCF and DCF. I found a lag of $2.2^{+0.9}_{-0.9}$ days with the γ-ray leading the optical flux variations. This is similar to the lag of about 4 days found between the γ-ray and optical band by Gaur *et al.* (2012a) on analysis of the data for the time period 2009 November − 2009 December. However, Gupta *et al.* (2017) found that the optical and γ-rays are correlated with zero lag during the period MJD 55150−55200 which is within the range analysed here. During the same period, Gupta *et al.* (2017) found that during the declining phase of the γ-ray flare, the degree of optical polarization increased, showing a clear signature of anti correlation between γ-ray flux variation and optical polarization.

Epoch B (MJD 55460 − 55560) During this period, the peak of the optical flare is about two times larger than the peak of the optical brightness at epoch A. The γ-ray brightness too peaked at nearly the same time of the optical flare. During this epoch, visual inspection indicates close correlation between γ-ray, X-ray, UV optical and IR flux variations. During this period a short duration intense flare in the optical was observed superimposed on the large optical flare at around MJD 55510. This particular short duration optical flare has no corresponding γ-ray flare (Figure 3.2) and is thus a case of an optical flare with no corresponding γ-ray counterpart. At the epoch of this short duration optical flare, there is also enhanced optical polarization, pointing to a strong correlation between optical flux and polarization variations. At this time, enhanced flux levels were also seen in UV and X-ray bands. This remarkable short duration intense optical flare with no

corresponding flare in the γ-ray band was also noticed by Vercellone *et al.* (2011). According to Vercellone *et al.* (2011) this optical flare showed a sharp rise and decay in 48 hours. At the same time, 20% rise was seen in the X-ray with no change at other wavelengths. During the duration of the large optical flare with the peak at MJD 55519, data on the degree of optical polarization is missing to make any statement on the correlation or anti-correlation between optical flux and polarization variations. DCF and ICCF analysis between optical and γ-ray flux variations, shown in Figure 3.3 indicate that the time delay between optical and γ-ray flux variations is $0.8^{+1.1}_{-1.0}$ days. Thus, during this major optical flare in epoch B, the optical and γ-ray flux variations are correlated with zero lag.

Epoch D (MJD 56510 − 56610) The optical flux during this epoch has nearly the same amplitude as the optical flare at epoch B. Considering the correlation between optical and γ-ray flux variations during both epochs A and B, it is natural to expect the γ-ray flare at epoch D to have similar brightness to that of epoch B. However, the source was barely detected in the γ-ray band during this period. This is an indication of an optical flare with no/weak corresponding γ-ray flare (Figure 3.2). Correlation analysis between the optical and γ-ray light curves during this epoch gives a time delay of $1.0^{+0.7}_{-0.5}$ days. This shows that the optical and the very weak γ-ray variations are correlated with 1 day lag. The results of the cross-correlation function analysis are shown in Figure 3.3. Polarizaion data was not available during the period of the flare and therefore the correlation if any between optical flux and polarization variations could not be ascertained.

Epoch E (MJD 56780 − 56880) During this epoch the optical flare has a peak brightness similar to that of the optical flare at epoch B, but the source has minor γ-ray flare during this epoch. This same period was also independently analyzed by Kushwaha *et al.* (2017) for correlation between γ-ray and optical flux variations. They find no lag between optical and γ-ray flux variations during the period overlapping the duration of epoch E. I noticed an interesting feature by

careful examination of the optical total flux and polarization variations shown in Figure 3.2. The degree of optical polarization is anticorrelated with the optical flare both during the rising phase and the decaying phase of the flare. Though such anti-correlations between optical flux and polarization variations were known before in the blazar BL Lac (Gaur *et al.* 2014) and 3C 454.3 (Gupta *et al.* 2017), I noticed anticorrelation between optical flux and polarization variations both during the rising part of the flare as well as the decaying part of the flare. The correlation analysis between the optical and γ-ray light curves during this epoch gives a time delay of $0.3^{+0.7}_{-0.5}$ days.Correlation analysis for this epoch shown in Figure 3.3.

3.6.2   PKS 1510−089

The multi-wavelength light curves that include γ-ray, X-ray, UV, optical and IR are given in Figure 3.4. The figure also includes polarization measurements. Inspection of the light curves indicates that the source has displayed varied activity levels that includes both flaring and quiescent periods. From visual inspection of the light curves I selected 6 epochs (A, B, C, D, E and F) in the source for studying the correlations between optical and γ-ray variations. These epochs were identified by the presence of optical and/or γ-ray flares in the light curves and a quiescent state in both the optical and γ-ray bands. A summary of these epochs is given in Table 3.1 and the multi-wavelength light curves covering a shorter duration during these epochs are shown in Figure 3.5 and Figure 3.6. More details on these six epochs are given below:

Epoch A: During this epoch, the γ-ray has increased in flux by a factor of about 10, while the optical and the IR J and K-band fluxes have not shown any variability and are indeed steady. There is also a hint that the X-ray flux from the source is non-variable, however, due to the lack of data during part of the γ-ray flare, no

conclusive statement could be made on the nature of X-ray flux variations. The optical polarization too has not shown noticeable variability during the steady optical/IR brightness state of the source. I conclude that in this epoch I observed a γ-ray flare with no optical counterpart.

Epoch B: During this epoch, the optical flux has increased by a factor of 6, while the flux variations in the IR band are at a reduced level. There is also a hint of a very low amplitude γ-ray flare during the peak of the optical flare, but it is very small. The lack of X-ray data and optical polarization data during the epoch of the optical flare has prevented us to make any statement on the nature of X-ray variations as well as the degree of optical polarization during this epoch. Thus in this epoch the source has shown correlated optical and γ-ray flux variations, though the amplitude of variations in the γ-ray band is much lower than that of the optical and IR bands.

Epoch C: The flux variations noticed in this epoch is similar to that observed during epoch A. A minor flare is observed in the γ-ray band, but the source is stable in the X-ray, optical and IR bands. Optical polarization data is not available during the γ-ray flare to ascertain the nature of optical V-band polarization. Thus, during this epoch, the source has shown a γ-ray flare without a counterpart in the low energy X-ray, optical and IR bands.

Epoch D: During this period, the source is in the quiescent state in all the energy bands analyzed here.

Epoch E: During this epoch, the source has shown a strong γ-ray flare, however, such a flare is not seen in the X-ray, optical and IR bands. Here too, optical polarization data is not available during the period of the γ-ray flare. Thus, in this epoch, the source has shown a γ-ray flare without similar flaring in the other wavelengths such as X-rays, optical and IR.

Epoch F: A weak γ-ray flare is seen in the source during this period. Simultaneous to the γ-ray flare, there is an indication of a minor optical flare which is also accompanied by an increase in the degree of optical polarization. There is paucity of X-ray and IR data during the peak of the γ-ray flare. Thus, the optical and γ-ray flux variations are closely correlated during this epoch.

3.6.3   3C 273

I show in Figure 3.7 the multi-wavelength light curves for the source 3C 273. The source is mostly quiescent during the period 2008 to 2018 August except for few instances where it has flared in the γ-ray band. I identified two epochs in this source for studying the correlation between optical and γ-rays. The details of these two epochs are given in Table 3.1. They are also marked in Figure 3.7, and an expanded version of these two epochs are given in Figure 3.8.

Epoch A: There is a prominent γ-ray flare during this epoch, wherein the γ-ray flux has increased by a factor of two at the peak of the γ-ray flare. During the peak of the γ-ray flare, the X-ray, optical and IR brightness do not show significant changes. Also, the source lacks optical polarization data during the peak of the γ-ray flare. The source has thus shown a γ-ray flare without an optical counterpart in this epoch.

Epoch B: During this epoch the source is found to be in the quiescent state in all the wavebands namely γ-rays, X-ray, optical and IR. The source is also weakly polarized in the optical V-band during this period.

3.6.4   3C 279

I show in Figure 3.9 the multi-wavelength light curves. From visual inspection, I identified four epochs in this source for studying the correlation between optical and γ-ray flux variations. I give in Table 3.1 the summary of those four epochs. An expanded view of the multi-wavelength flux variations in the source is shown in Figure 3.10. Below, I summarize the salient aspects of these four epochs.

Epoch A: In this epoch the source is in the quiescent state. In the one day binned γ-ray light curve the source is below the detection limit for many days during this 100 days period. Also, in the X-ray, optical and IR bands, the source is non-variable during this period. However, during the middle of this epoch, the optical polarization increased by a factor of about 5 from $\sim$6% to $\sim$25.8%. During this period of increased optical polarization, the source did not show flux variations in any of the bands.

Epoch B: During this epoch, the source has shown a minor flare in the γ-ray band with no corresponding flare in the optical, IR and X-ray bands. Polarization data is not available during the peak of the γ-ray flare thereby making it impossible to know the polarized nature of the source. By comparing the multi-wavelength light curves during this epoch, I conclude that the source showed a γ-ray flare without an optical counterpart.

Epoch C: During this epoch, a strong γ-ray flare was observed wherein the γ-ray flux increased by a factor of about 3. During the peak of the γ-ray flare, X-ray too showed a flare, however, in the optical and IR bands, the source was found to be stable with no signs of flux variability. An interesting behaviour displayed by this source is an apparent negative correlation of γ-ray and X-ray flux variations to the optical polarization. During the epoch when the γ-ray and X-ray were at their peaks, the optical polarization was low, and it gradually increased when the

X-ray and γ-ray fluxes declined.

Epoch D: During this epoch, the source showed a prominent optical and IR flare. The flare was found be be asymmetric with a fast rise and slow decay. During the epoch of the optical and IR flare the source did not show any variation in the γ-ray band. Due to the lack of polarization data during the peak of the optical and IR flare, I could not make any statement on the optical polarization state during the time of the optical and IR flare. Thus this epoch is a clear example of the source showing an optical flare without a γ-ray counterpart.

3.6.5 CTA 102

The source was found to be in a steady and low brightness state during most of the time between 2008 August to 2018 August, except for a spectacular γ-ray flare in the beginning of 2016. The multi-wavelength light curves are shown in Figure 3.11. I identified 2 epochs in this source for studying the correlation between optical and γ-ray variations. A summary of these two epochs is given in Table 3.1 and expanded plots of these two epochs are shown in Figure 3.12. More details on these two epochs are given below.

Epoch A: During this epoch the source was in the quiescent state in all the wavebands considered in this work.

Epoch B: The source showed a major γ-ray flare during this epoch. This flaring in the γ-ray band was also accompanied by flaring behaviour in the X-ray and optical wavelengths. The nature of IR flux during this period is uncertain due to the non-availability of IR data during this flaring period. Thus, during this epoch, the source showed correlated flux variations in the optical and γ-ray bands.
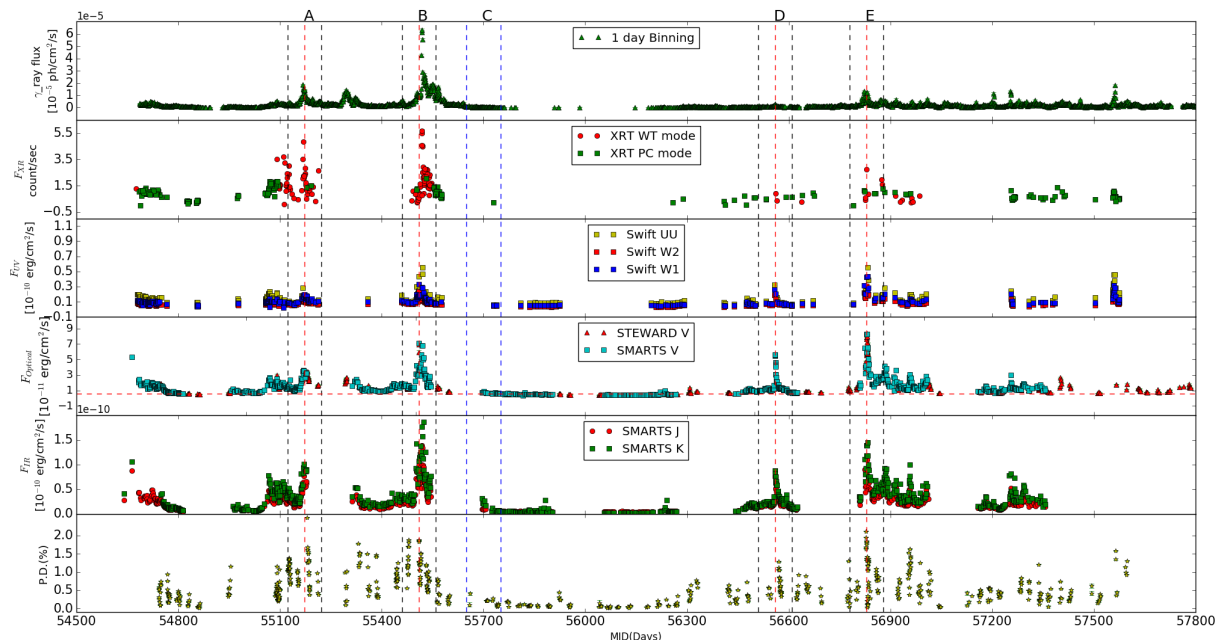
FIGURE 3.1: Multi-wavelength light curves of the source 3C 454.3. From the top, the first panel shows the 1 day binned γ-ray lightcurve for the time range MJD 54500-57800; the second panel shows the *Swift*-XRT lightcurve in both PC and WT modes, the third panel shows the *Swift* UVOT lightcurves in W1, W2 and UU bands; in the fourth panel optical light curve in V-band is given; the fifth panel shows the IR light curves in J and K bands and in the bottom panel variation of the degree of polarization is presented. The red vertical lines correspond to the peaks of the optical flares and the two black vertical lines denote a width of 50 days each on either side of the peak of the flare. The two vertical blue lines have a width of 100 days and correspond to the quiescent period. In γ-ray light curve only points with TS > 9 are shown.

3.7 γ-ray spectra

To study the intrinsic distribution of electrons in the jets that are involved in the γ-ray emission process, I generated γ-ray spectra for all the selected epochs of the five sources. I fitted the γ-ray spectra with the two models namely (i) the simple power law (PL) model and (ii) the log-parabola (LP) model. The details of this two models and the procedure followed to generate the γ-ray spectra are specified in Chapter 2. The results of the γ-ray spectral analysis are given in Table 3.2. One example of the PL model that best fits the data (for the source 3C 273 at Epoch
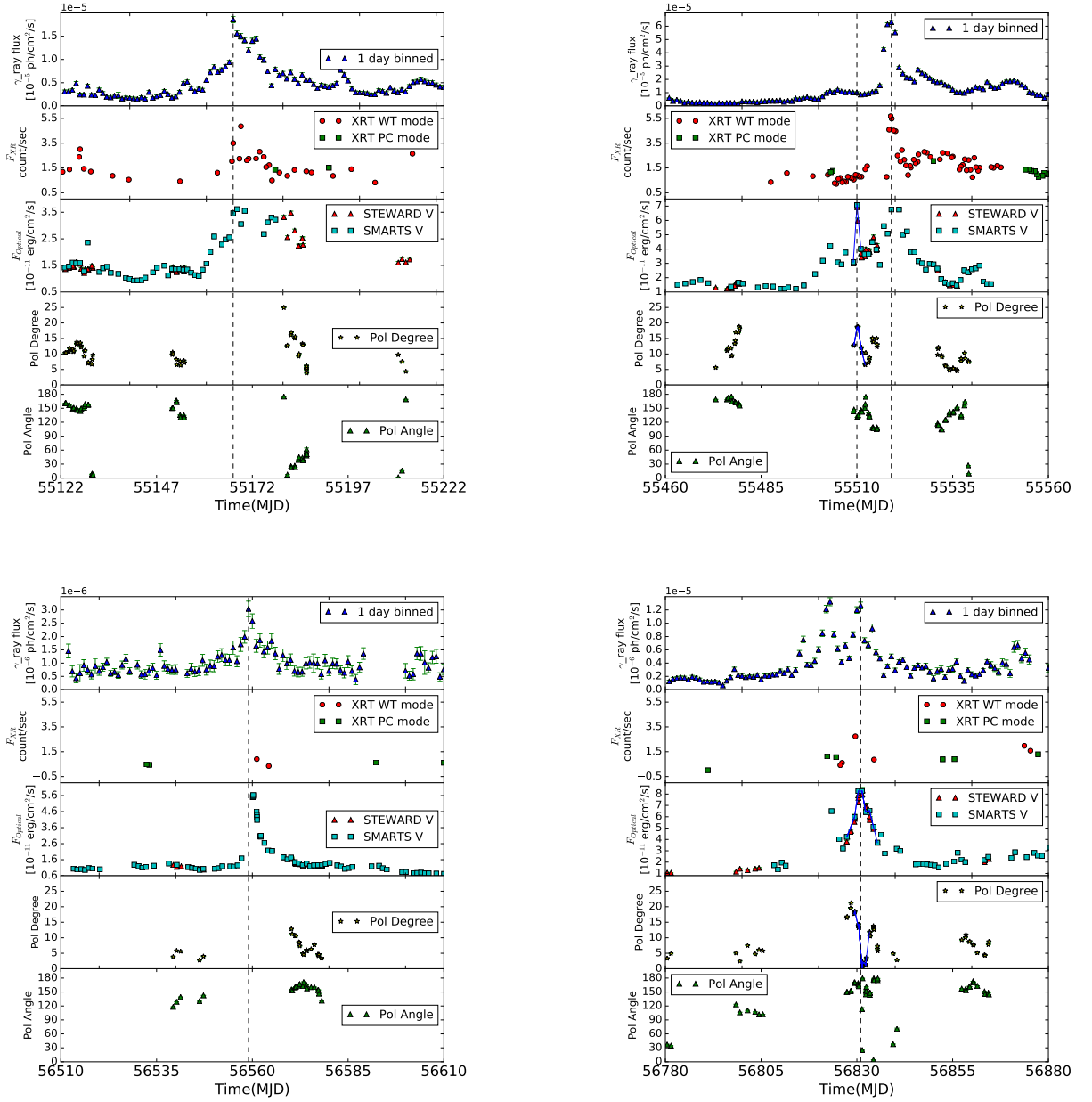
FIGURE 3.2: Multi-wavelength light curves covering a period of 100 days during epochs A (top left), B (top right), D (bottom left) and E (bottom right) for the source 3C 454.3. Here, from the top the first panel shows the γ-ray variations, the second and third panels show the variations in X-ray and optical bands and the bottom two panels show the variations in degree of optical polarization and polarization position angle. The vertical dashed line shows the peak of optical/γ-ray flare.
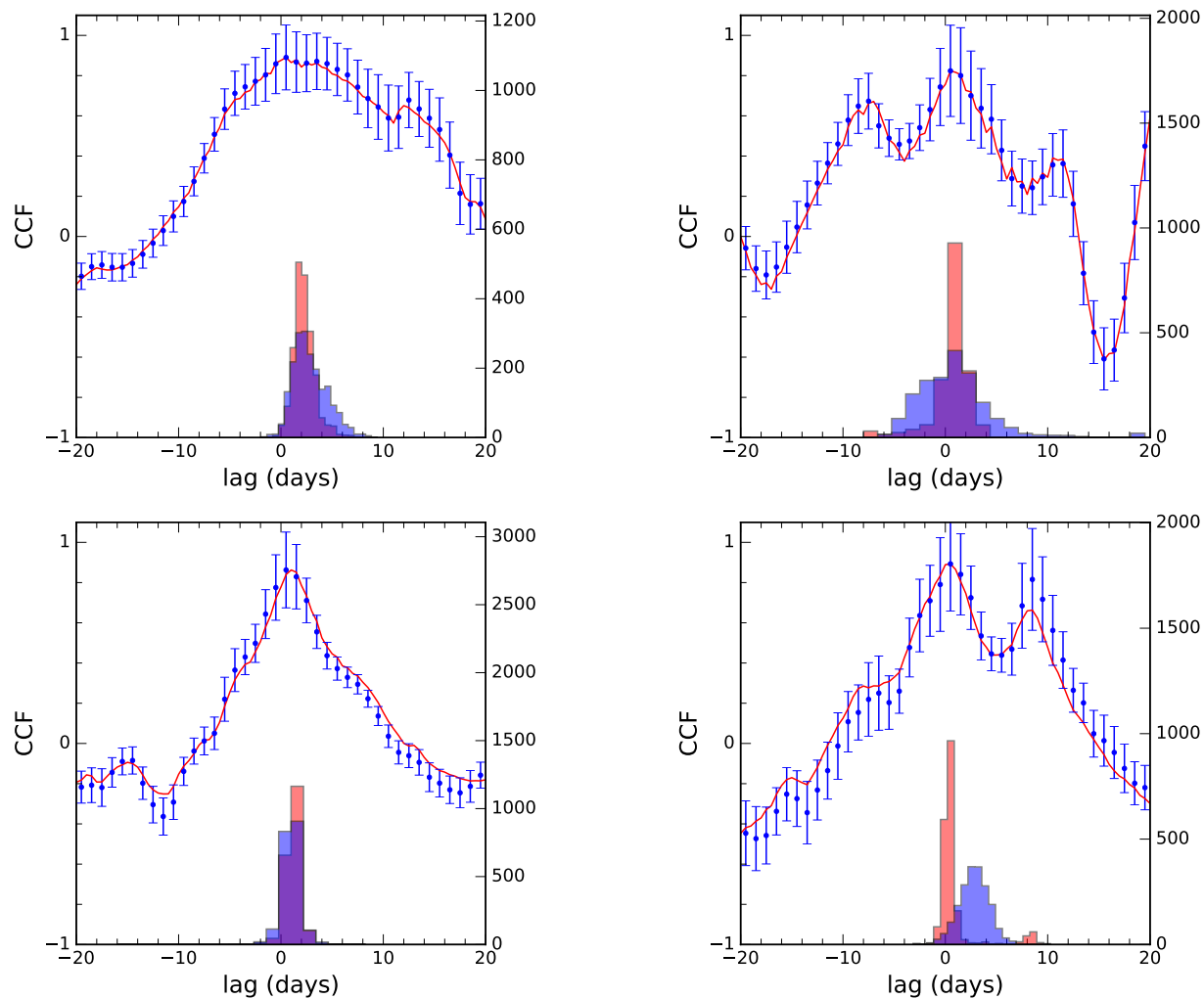
FIGURE 3.3: Cross-correlation analysis between γ-ray and optical flux variations during epoch A (top left), epoch B (top right), epoch C (bottom left) and epoch D (bottom right). The solid line is for ICCF and the filled circles refer to DCF. The histograms in blue and orange show the distribution of cross-correlation centroids for ICCF and DCF respectively.

B) and another example of a LP model that best fits the data (for the source 3C 454.3 at Epoch A) is shown in Figure 3.13.
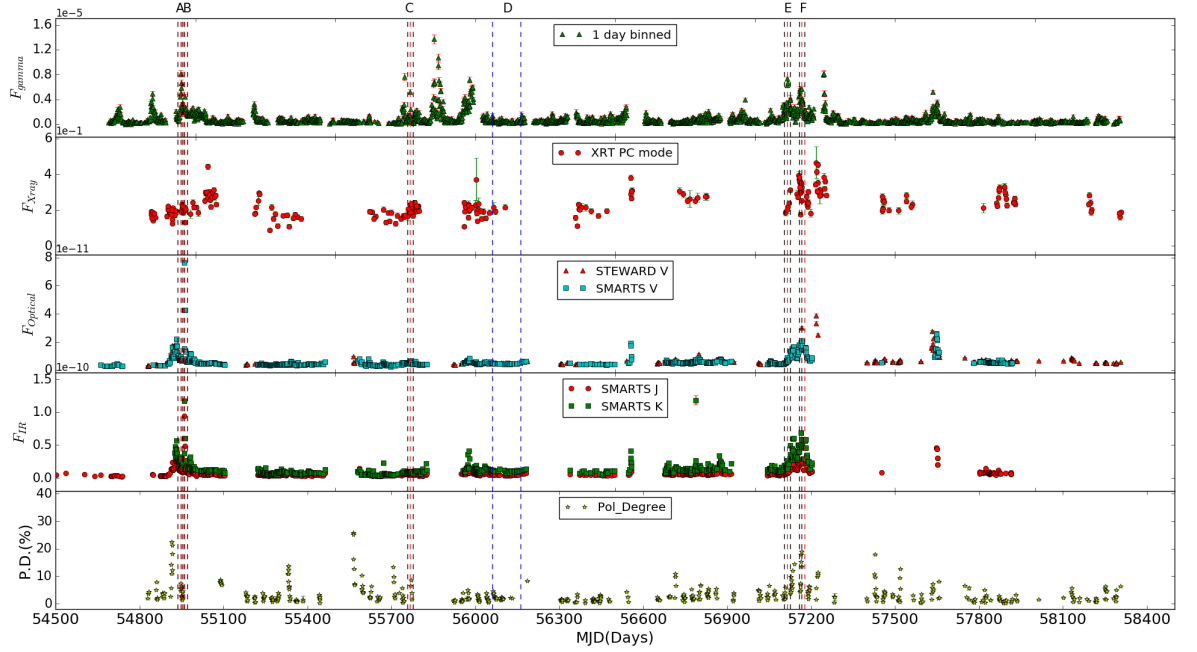
FIGURE 3.4: Light curves of the source PKS 1510−089. The top one is the one day binned γ-ray light curve, the second panel from the top is the X-ray light curve, the next two panels are the optical and the IR light curves and the bottom panel is the optical V-band polarization. The peak of either the optical or γ-ray light curve is shown by red dotted lines, while the two black solid lines on either side of the red line correspond to a width of 10 days each. The two blue lines show the quiescent period of 100 days. For γ-ray light curve, upper limits are not shown and only points with TS > 9 are plotted.

3.8 Spectral energy distribution modelling

The sources studied here showed various characteristics in their optical and γ-ray flux variations. There are instances when (a) optical and γ-ray flux variations are correlated, (b) there are optical flares without γ-ray counterparts and (c) there are γ-ray flares without optical counterparts. To further characterize the nature of the sources during the various epochs, I constructed their broad band SED during these epochs and studied them using simple one zone leptonic emission model. Chapters 1 and 2 provide a brief introduction to the one zone leptonic model and the methodology used for this work. The adopted values of the seven
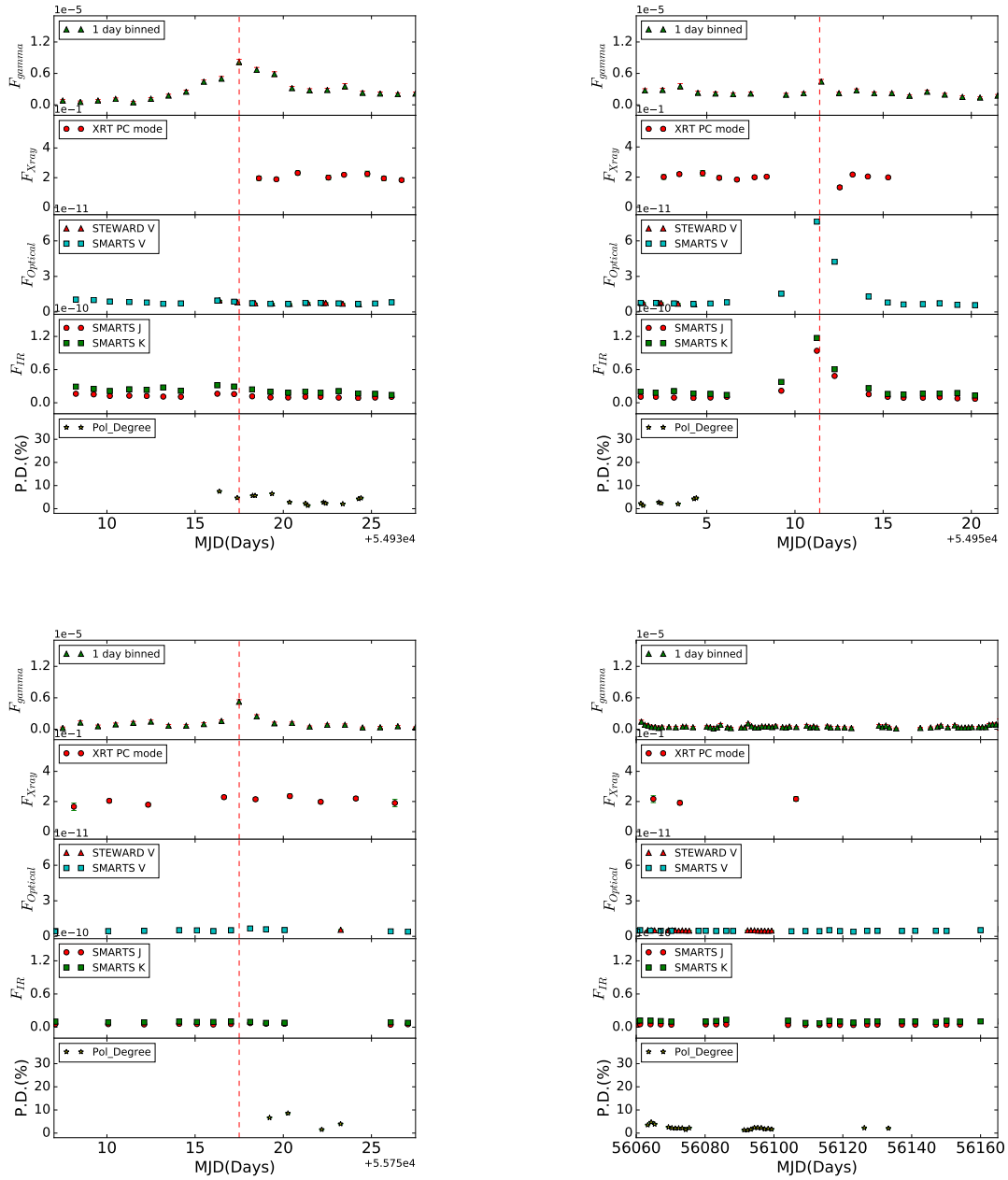
FIGURE 3.5: Multi-wavelength light curves for epochs A (top left), B (top right), C (bottom left) and D (bottom right) for the source PKS 1510−089. In all the panels γ-ray fluxes are in units of 10^{-5} ph cm^{-2} s^{-1}. The optical fluxes are in units of 10^{-11} erg cm^{-2} s^{-1} and the IR fluxes are in the units of 10^{-10} erg cm^{-2} s^{-1}. The vertical dotted line shows the peak of the optical/γ-ray flare.
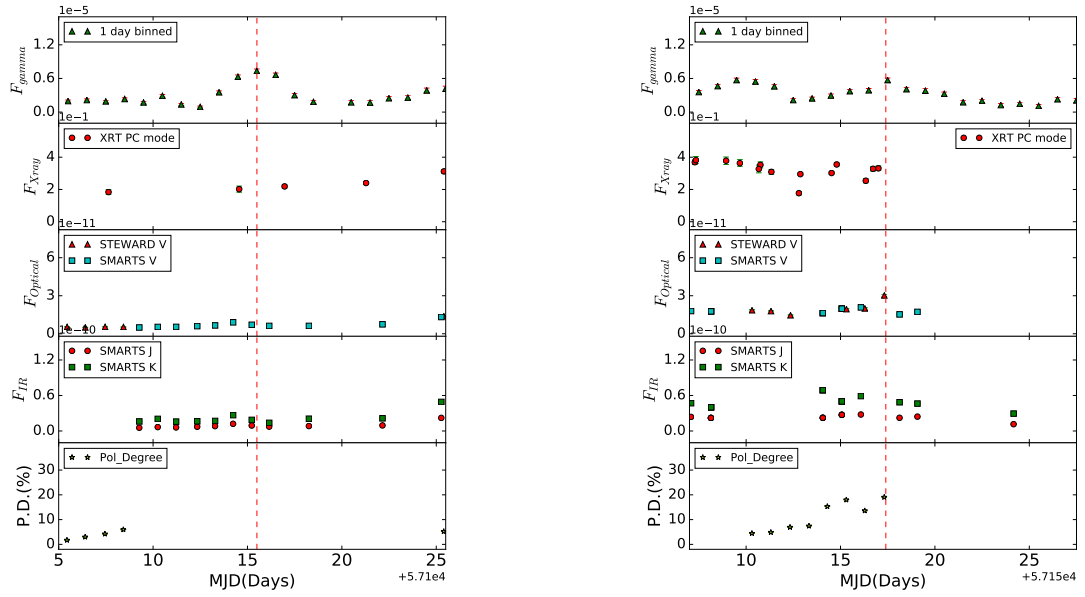
FIGURE 3.6: Muti-wavelength light curves for the source PKS 1510−089 during epochs E (left) and F (right). Labels have the same meaning as that of Figure 3.5.
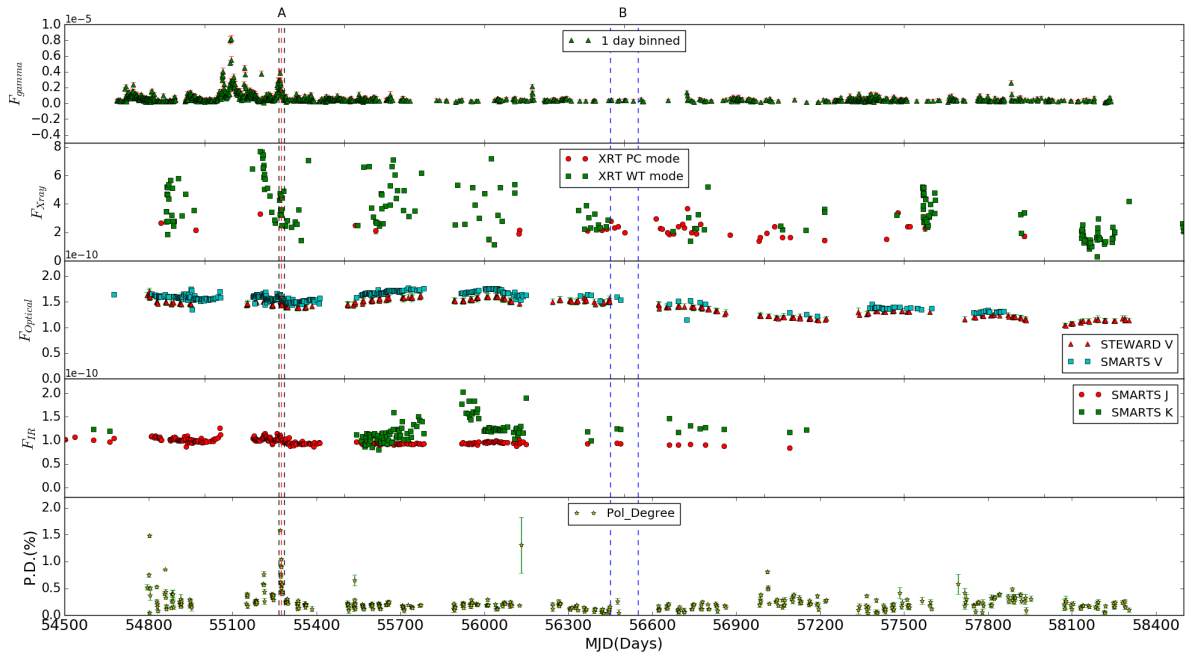
FIGURE 3.7: Multi-wavelength light curves of the source 3C 273. The panels and the vertical lines have the same meaning as that of Figure 3.4
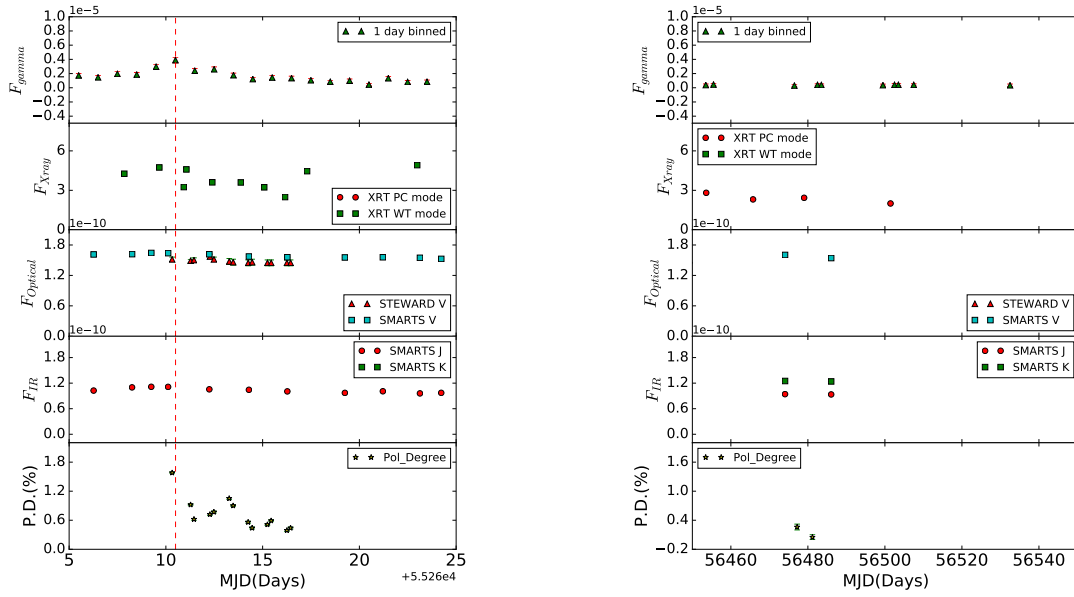
FIGURE 3.8: Light curves of 3C 273 for epoch A (left panel) and epoch B (right panel). The γ-ray fluxes are in units of 10^{-6} ph cm^{-2} s^{-1} and the optical and IR fluxes are in units of 10^{-10} erg cm^{-2} s^{-1}. The vertical dashed line shows the peak of the γ-ray flare.
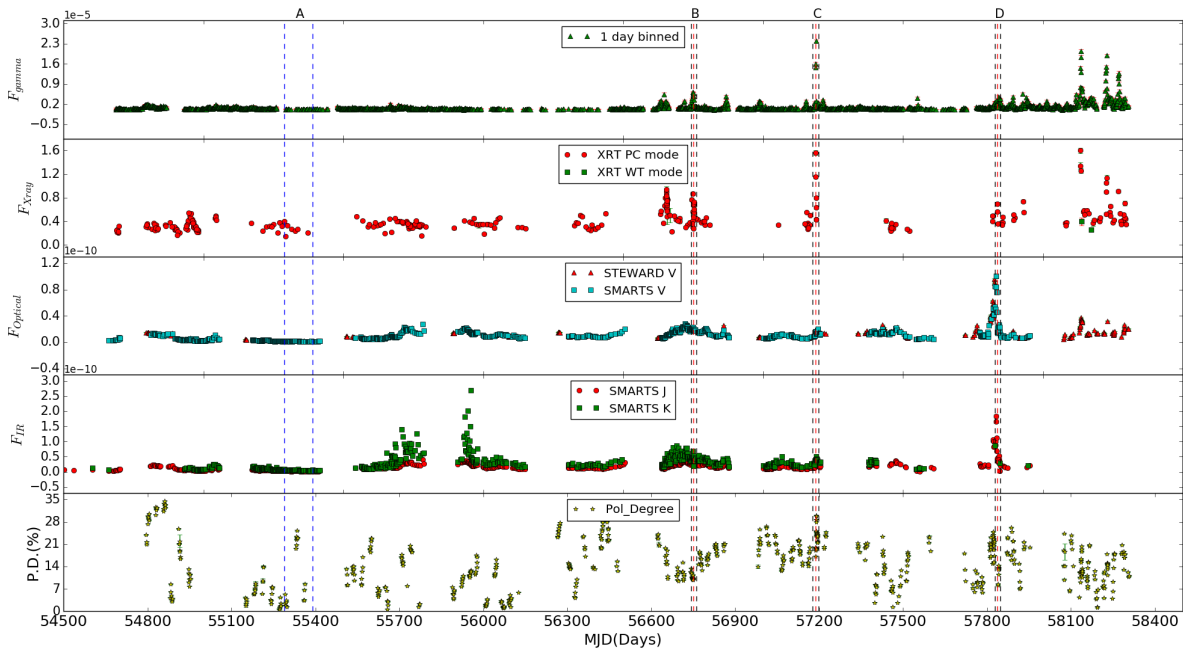
FIGURE 3.9: The light curves of the source 3C 279 in different wavelengths. The panels and the dashed lines have the same meanings as that of Figure 3.4.
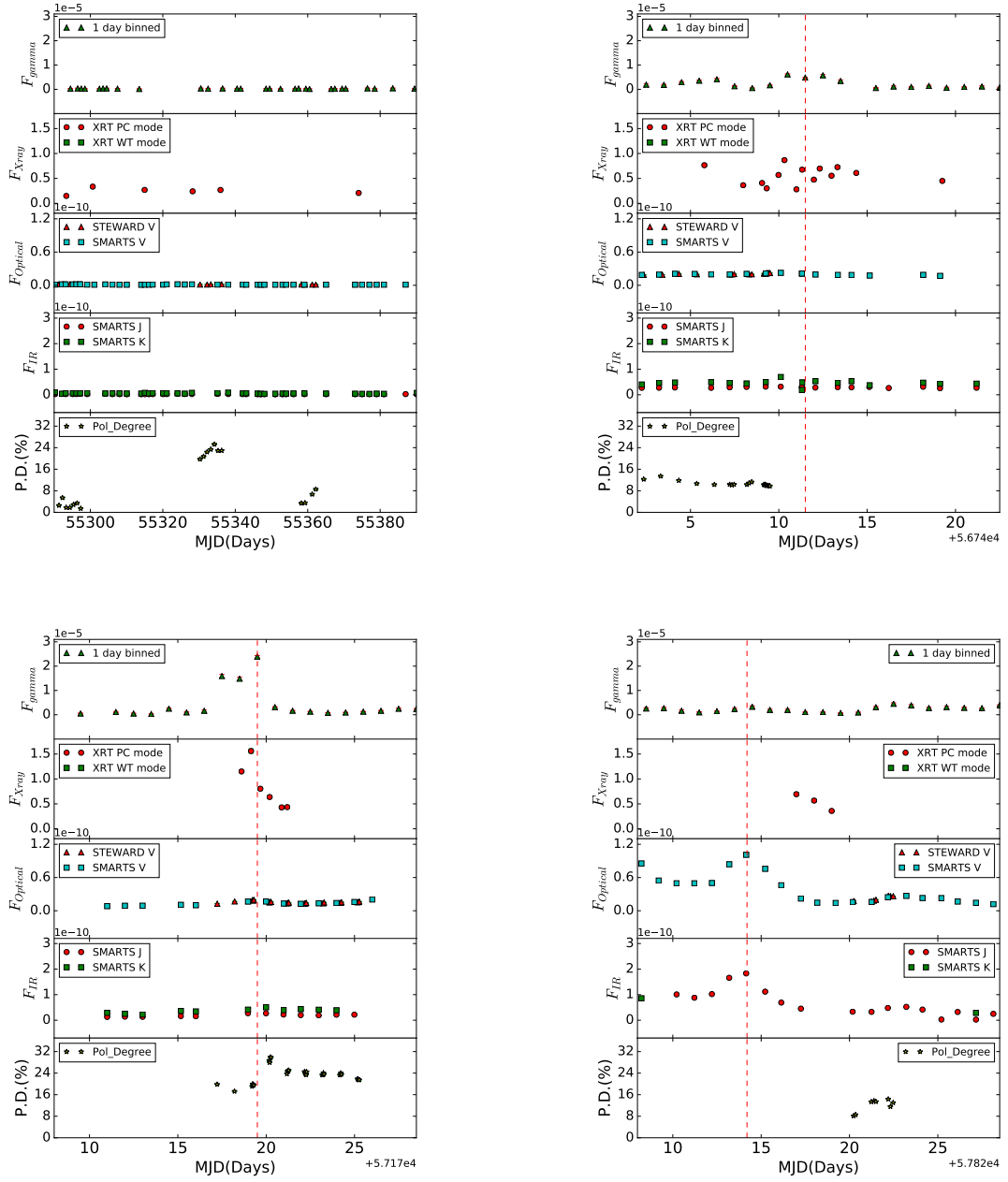
FIGURE 3.10: Multi-wavelength light curves of the source 3C 279 for epoch A (top left), epoch B (top right), epoch C (bottom left) and epoch D (bottom right). The optical and IR light curves have units of 10^{-10} erg cm^{-2} s^{-1}, while the γ-ray light curves have units of 10^{-5} ph cm^{-2} s^{-1}. The dashed lines indicate the peak of the optical/γ-ray flare.
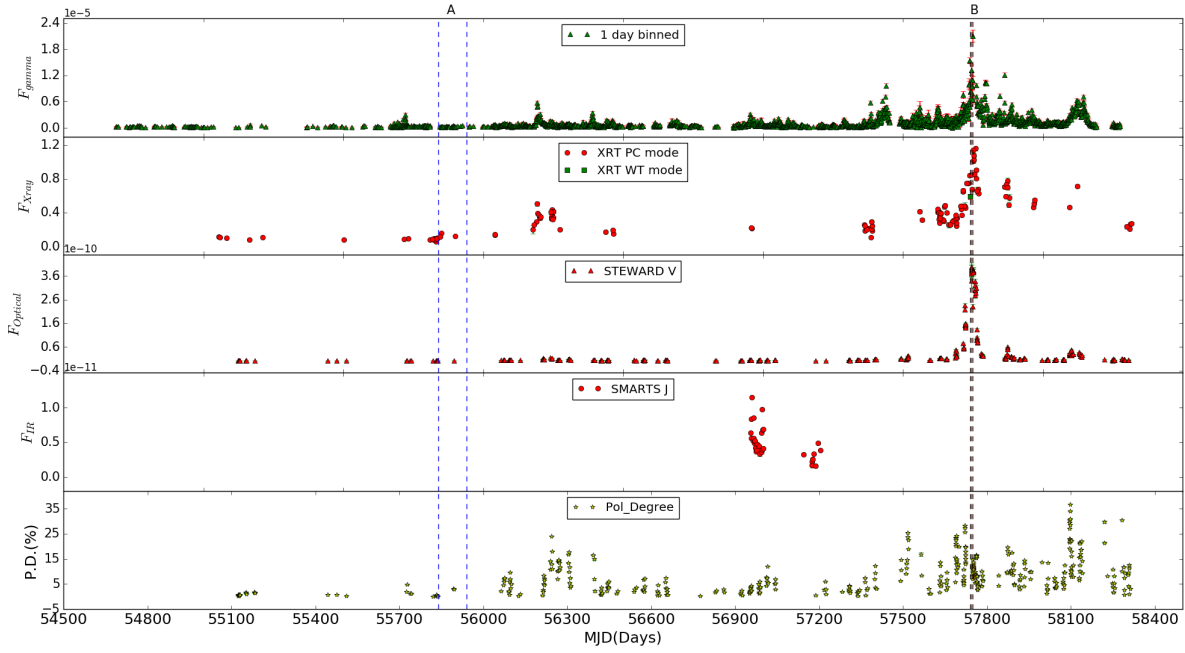
FIGURE 3.11: Long term light curves of the source CTA 102 in different wavelengths. Details in this figure are similar to that of Figure 3.4.
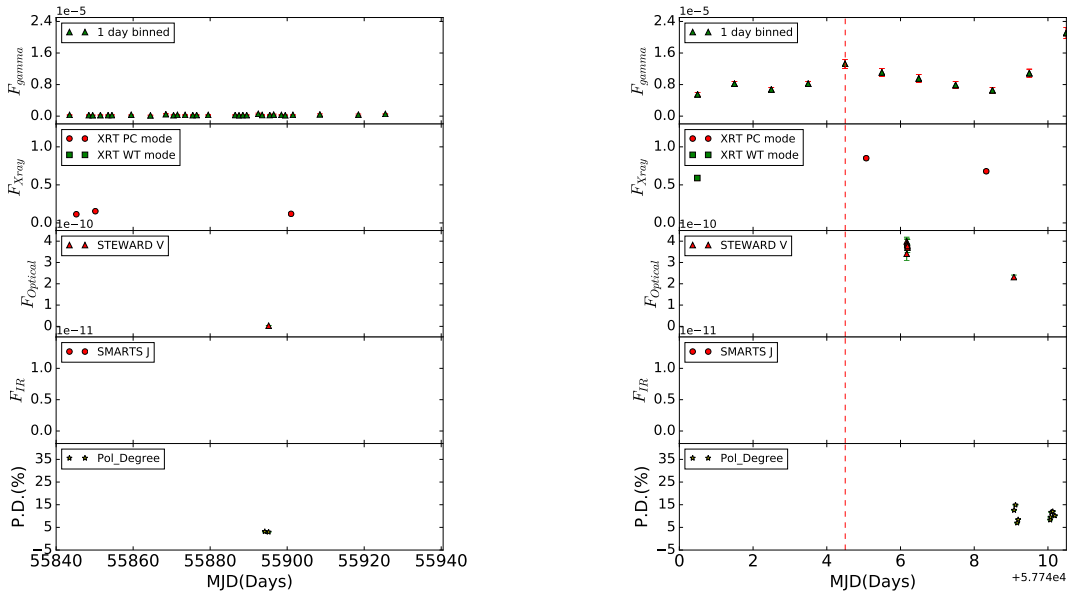
FIGURE 3.12: The left and right panels show the multi-wavelength light curves of the source CTA 102 for epoch A and B respectively. The dashed line shows the peak of the γ-ray flare. The optical and γ-ray fluxes are in units of 10^{-10} erg cm^{-2} s^{-1} and 10^{-5} ph cm^{-2} s^{-1} respectively.

TABLE 3.2: Details of the PL and LP model fits for the different epochs of the source 3C 454.3, PKS 1510−089, 3C 273, 3C 279 and CTA 102. Here the γ-ray flux values are in units of 10^{-6}ph cm^{-2} s^{-1}

	PL				LP					
Epochs	Γ	Flux	TS	$-$Log L	α	β	Flux	TS	$-$Log L	TS$_{curve}$
3C 454.3										
A	-2.34±0.01	5.68±0.06	87024.8	138177.8	1.91±0.03	0.15± 0.01	4.93±0.07	79568.2	137962.7	430.1
B	-2.33±0.01	13.3±0.08	278585.0	80508.1	2.21±0.00	0.09± 0.00	12.79±0.12	283811.0	80238.2	539.8
C	-2.42±0.03	0.57±0.02	3422.6	151787.4	1.97±0.10	0.24± 0.04	0.47±0.03	3392.8	151756.9	61.0
D	-2.25±0.02	1.03±0.03	9890.6	142338.0	2.04±0.04	0.14± 0.02	0.88±0.03	9768.6	142299.7	76.6
E	-2.14±0.00	4.42±0.00	66161.9	146140.9	1.53±0.00	0.15± 0.00	3.71±0.03	62145.3	145896.2	489.4
PKS 1510-089										
A	-2.41±0.04	0.08±0.006	1502.89	32666.94	2.35±0.03	0.10± 0.02	2.89±0.08	6626.5	30287.04	4759.8
B	-2.38±0.01	1.10±0.02	4484.27	40710.69	2.31±0.04	0.05± 0.02	2.30±0.03	6046.02	39865.06	1691.24
C	-2.29±0.05	1.05±0.03	2143.16	26980.49	2.24±0.06	0.06± 0.04	1.16±0.01	2149.74	26918.59	123.8
D	-2.46±0.01	0.36±0.007	1396.18	71986.58	2.40±0.05	0.009± 0.007	0.38±0.009	1383.28	71943.76	85.64
E	-2.35±0.02	0.10±0.006	3632.06	41998.12	2.21±0.04	0.05± 0.02	3.00±0.02	12254.5	37916.38	8163.48
F	-2.26±0.02	0.44±0.008	7069.12	33739.65	2.18±0.02	0.06± 0.01	3.05±0.05	11891.14	31131.89	5215.52
3C 273										
A	-2.48±0.04	0.03±0.003	384.26	18366.24	2.45±0.06	0.02± 0.04	0.49±0.01	1965.47	17796.95	1138.58
B	-2.91± 0.10	0.005±1.13	22.10	53603.31	2.91±0.11	0.13± 0.16	0.46±0.02	-328.63	53791.17	-375.72
3C 279										
A	-2.42±0.03	0.02±0.003	193.899	61574.51	2.46±0.07	0.06± 0.01	0.16±0.004	341.966	61472.92	203.18
B	-2.28± 0.04	0.29±0.003	5059.59	28075.17	2.13±0.05	0.09± 0.02	0.61±0.03	6630.85	27337.68	1474.98
C	-2.22±0.00	0.60±0.01	14113.31	41165.00	2.05±0.03	0.10± 0.01	4.09±0.001	25625.3	37399.62	7530.76
D	-2.28±0.03	0.16±0.003	2426.62	24463.13	2.14±0.04	0.08± 0.02	1.44±0.01	5391.43	23282.19	2361.88
CTA 102										
A	-2.49±0.00	0.002±0.91	26.02	57614.41	2.58±0.06	0.02± 0.05	0.16±0.004	565.75	57358.15	512.52
B	-2.12± 0.004	0.36±0.008	10266.7	35236.65	1.84±0.03	0.09± 0.01	0.63±0.02	14952.58	35028.19	416.92

frozen parameters for the five sources are given in Table 3.3. In Table 3.4, and Figure 3.14 to Figure 3.20, I summarize the results of the fitting.
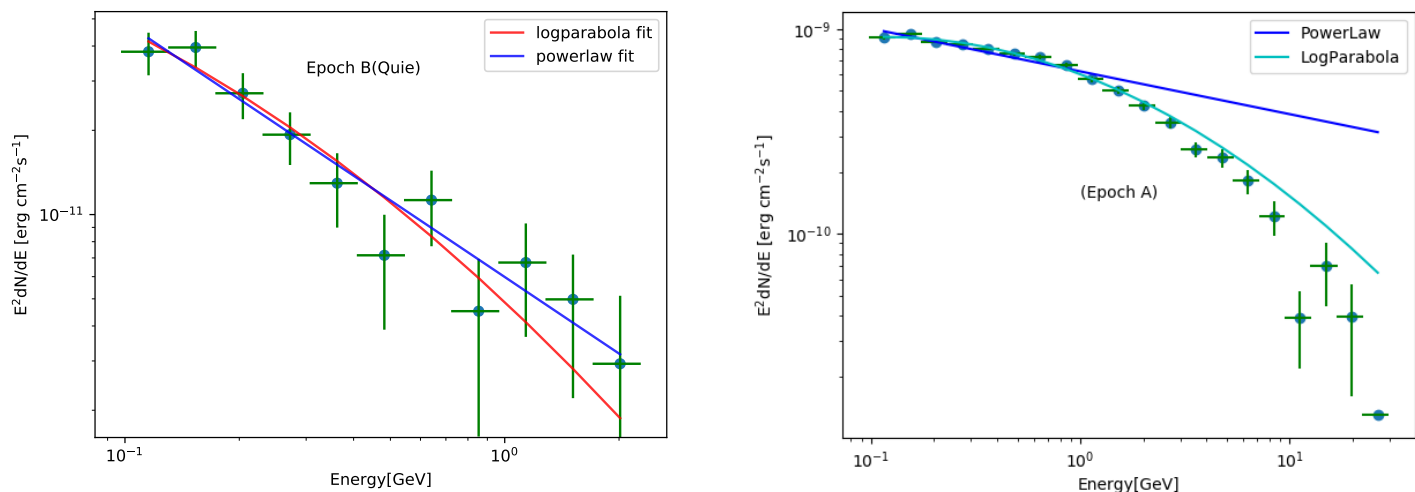
FIGURE 3.13: Observed and model fits to the γ-ray spectra of the source 3C 273 for epoch B (left panel) and of 3C 454.3 for epoch A (right panel).

TABLE 3.3: Values of the parameters that were frozen during the model fits to the observed SEDs. The size of the emission region R is in units of 10^{15} cm, the temperature T is in Kelvin and viewing angle θ is in degree.

Object	R	γ_{min}	γ_{max}	γ_b	T(K)	θ	f	State
3C 454.3	3.0	40	1×10^4	1200	1000	1	0.9	A, B, C, D
	90	40	4×10^4	1500	800	1	0.8	E
PKS 1510−089	7.9	40	2×10^4	1500	800	2	0.9	A, B, C, D, E, F
3C 273	15.8	50	1×10^4	1200	800	2	0.9	A, B
3C 279	15.8	40	2×10^4	1200	800	2	0.9	A, B, C, D
CTA 102	100	50	2×10^4	2100	800	2	0.02	A, B

3.9 Results and Discussion

3.9.1 γ-ray spectra

The high energy γ-ray spectra of FSRQs and low synchrotron peaked BL Lacs deviate from the power law behaviour and are phenomenologically better represented either as a broken power law (BPL) or a LP model. Such departures from simple
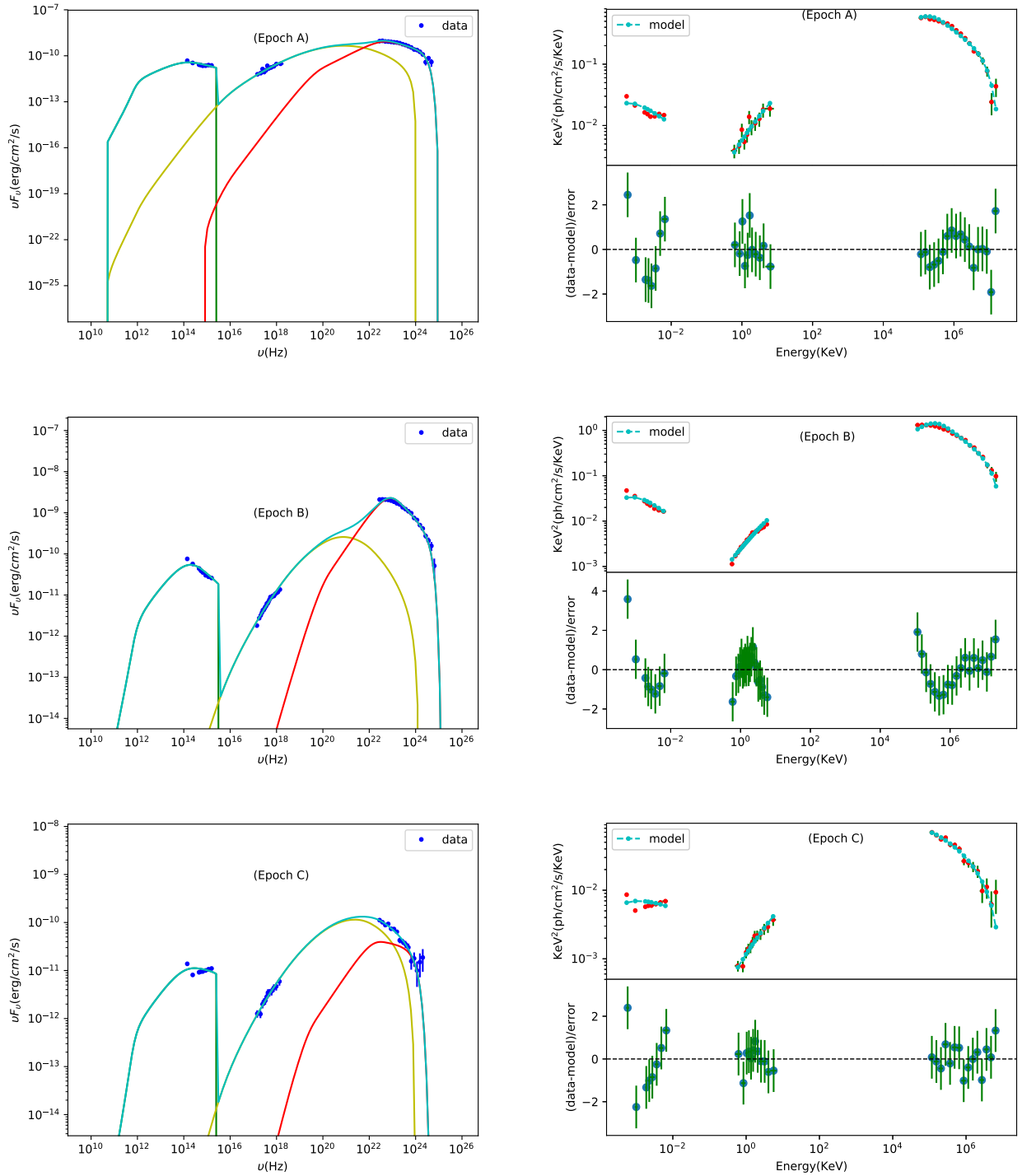
FIGURE 3.14: Broad band spectral energy distribution along with the one zone leptonic emission model fits for epochs A, B and C. In the left panels the green line refers to the synchrotron model, the yellow line refers to the SSC process and the red line refers to the EC process. The cyan line is the sum of all the components. In the right hand panels for each epoch the first panel shows the fitting of the model to the data carried out in XSPEC and the second panel shows the residuals.

TABLE 3.4: Results of the broad band SED analysis on the sources at different epochs

Name	Epoch	Bulk Lorentz factor	Low energy particle index	High energy particle index	Eletron energy density (cm^{-3})	Magnetic field (Gauss)	Accretion rate	IC peak (MeV)	χ^2/dof
3C 454.3	A (with out AD)	11.79±0.82	1.47±0.16	3.64±0.11	5.15±1.08	1.77±0.11	—	246	1.0
	B (with out AD)	16.63±0.96	1.34±0.13	3.93±0.09	2.05±0.36	1.78±0.09	—	402	1.0
	C (with out AD)	7.30±0.30	1.56±0.09	3.12±0.11	3.62±0.32	2.82±0.16	—	118	0.84
	D (with out AD)	11.88±1.07	1.98±0.15	3.49±0.15	1.15±0.24	4.01±0.23	—	226	1.30
	E (with out AD)	5.00±0.71	1.37±0.11	3.14±0.08	0.04±0.01	0.73±0.03	—	84	1.07
PKS 1510−089	A (with out AD)	10.29 ± 1.12	1.10 ± 0.52	3.85 ± 0.11	0.12 ± 0.04	0.97 ± 0.08	—	227	1.9
	A (with AD)	10.62 ± 1.20	1.10 ± 0.58	4.22 ± 0.16	0.12 ± 0.04	0.84 ± 0.07	1.48 ± 0.32		0.8
	B (with out AD)	8.56 ± 0.65	1.10 ± 0.37	3.66 ± 0.09	0.22 ± 0.05	1.05 ± 0.06	—	198	0.8
	B (with AD)	9.01 ± 0.69	1.10 ± 0.38	3.86 ± 0.12	0.20 ± 0.05	0.98 ± 0.06	1.24 ± 0.48		0.5
	C (without AD)	5.72 ± 0.61	1.10 ± 0.35	3.04 ± 0.13	0.66 ± 0.19	0.66 ± 0.03	—	163	1.2
	C (with AD)	7.31 ± 0.63	1.39 ± 0.23	3.55 ± 0.13	0.37 ± 0.09	0.64 ± 0.05	0.85 ± 0.22		0.7
	D (without AD)	5.00 ± 1.31	1.10 ± 0.36	3.20 ± 0.13	0.32 ± 0.09	1.34 ± 0.08	—	116	2.4
	D (with AD)	6.41 ± 1.27	1.10 ± 1.26	3.95 ± 0.18	0.21 ± 0.15	0.98 ± 0.16	1.26 ± 0.22		1.2
	E (without AD)	8.62 ± 0.86	1.10 ± 0.51	3.45 ± 0.08	0.27 ± 0.09	0.72 ± 0.06	—	209	1.6
	E (with AD)	9.22 ± 0.96	1.13 ± 0.27	3.63 ± 0.10	0.24 ± 0.08	0.68 ± 0.06	0.79 ± 0.28		1.3
	F (without AD)	12.31 ± 1.19	1.10 ± 0.37	3.68 ± 0.09	0.08 ± 0.02	1.18 ± 0.07	—	333	2.2
	F (with AD)	12.53 ± 1.11	1.10 ± 0.33	3.81 ± 0.12	0.07 ± 0.02	1.12 ± 0.06	1.49 ± 0.67		1.9
3C 273	A (with AD)	9.42 ± 1.37	2.44 ± 0.27	3.94 ± 0.15	0.01 ± 0.004	2.21 ± 0.42	16.00 ± 4.13	121	1.9
	B (with AD)	5.00 ± 0.52	1.92 ± 0.12	5.48 ± 0.44	0.07 ± 0.009	2.33 ± 0.20	16.00 ± 2.72	32	1.5
3C 279	A (without AD)	7.13 ± 1.03	1.89 ± 0.46	4.27 ± 0.10	0.07 ± 0.02	1.05 ± 0.14	—	64	1.5
	A (with AD)	7.13 ± 1.09	1.89 ± 0.48	4.25 ± 0.20	0.07 ± 0.02	1.05 ± 0.15	0.01 ± 0.15		1.7
	B (without AD)	11.22 ± 1.10	1.15 ± 0.26	3.71 ± 0.08	0.04 ± 0.01	1.16 ± 0.09	—	177	1.1
	B (with AD)	11.22 ± 1.12	1.15 ± 0.26	3.71 ± 0.10	0.04 ± 0.01	1.16 ± 0.09	0.01 ± 1.18		1.2
	C (without AD)	8.80 ± 0.04	1.24 ± 0.20	3.51 ± 0.07	0.22 ± 0.03	0.66 ± 0.04	—	147	1.8
	C (with AD)	8.80 ± 0.60	1.24 ± 0.21	3.51 ± 0.09	0.22 ± 0.04	0.66 ± 0.04	0.01 ± 1.86		1.9
	D (without AD)	11.75 ± 1.53	1.72 ± 0.25	3.70 ± 0.01	0.05 ± 0.01	1.52 ± 0.13	—	154	3.0
	D (with AD)	11.75 ± 1.50	1.72 ± 0.26	3.70 ± 0.11	0.05 ± 0.01	1.52 ± 0.18	0.01 ± 4.92		3.1
CTA 102	A (without AD)	7.98 ± 1.50	1.10 ± 0.64	3.84 ± 0.46	0.006 ± 0.004	0.39 ± 0.10	—	196	2.4
	A (with AD)	8.42 ± 1.19	1.10 ± 0.70	4.35 ± 0.38	0.006 ± 0.003	0.32 ± 0.07	10.00 ± 6.09		1.4
	B (without AD)	32.17 ± 13.61	1.29 ± 0.08	3.17 ± 0.15	0.007 ± 0.001	0.42 ± 0.03	—	1295	1.0
	B (with AD)	36.44 ± 11.84	1.28 ± 0.09	3.11 ± 0.17	0.008 ± 0.003	0.42 ± 0.10	0.08 ± 325.54		1.0

PL fits noted as a common feature in FSRQs firstly in the early observations from *Fermi*-LAT (Abdo *et al.* 2010a) are now observed in the high energy spectra of several FSRQs (Harris *et al.* 2014; Paliya *et al.* 2015; Rajput *et al.* 2019; Sahakyan 2020). The cause of the spectral curvature seen in the γ-ray spectra from *Fermi*-LAT is still not known. Several scenarios, both intrinsic and extrinsic origins are proposed in the literature to explain the break in the γ-ray spectrum of FSRQs.
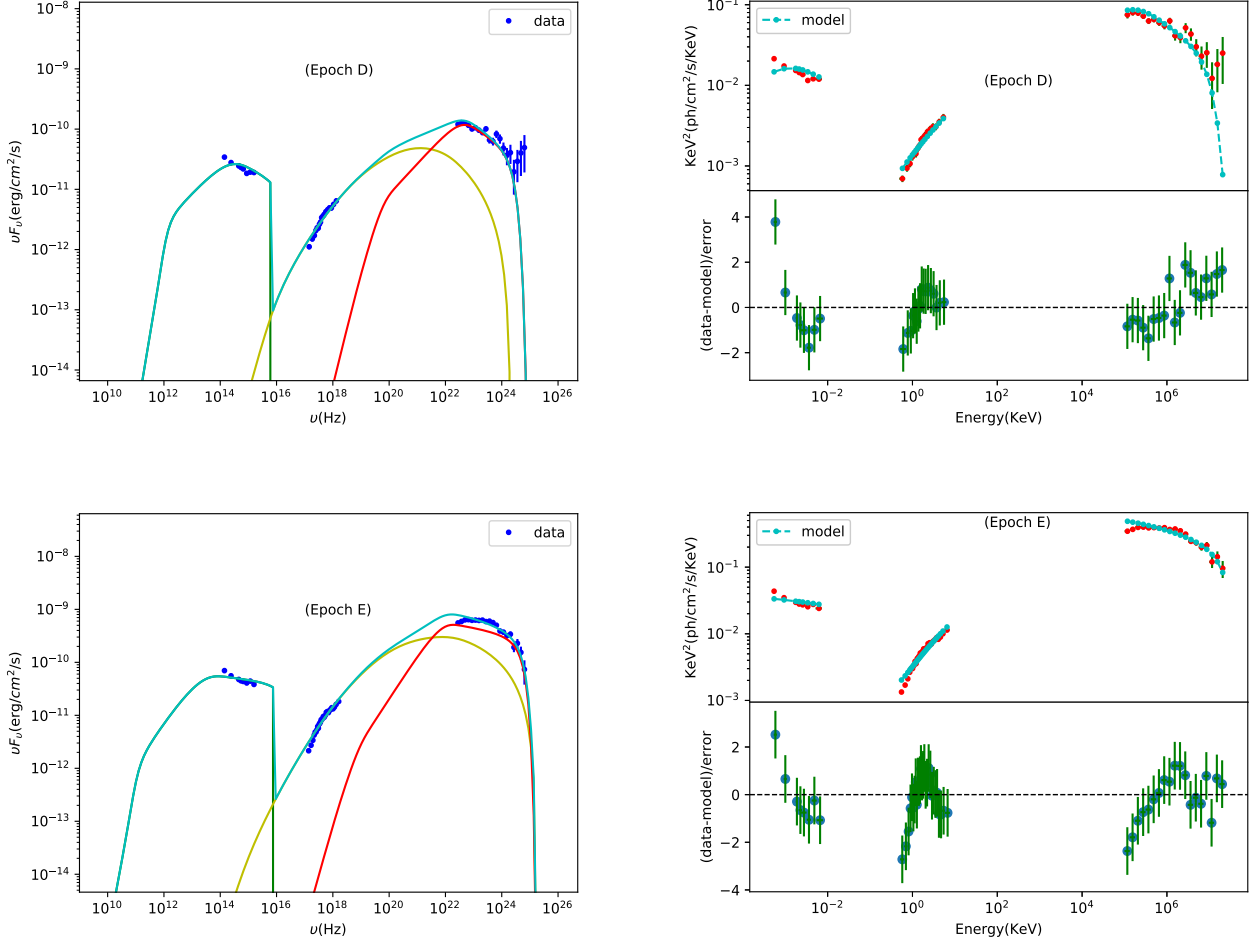
FIGURE 3.15: Model fits to the broad band SED during epochs D and E. The panels have the same meanings as that of Figure 3.14.

One of the causes could be due to the attenuation of γ-rays by photon-photon pair production within the BLR due to HeII recombination and HI recombination. In this scenario termed as the double absorber model (Poutanen and Stern 2010), one expects to see a break around $4-7$ GeV and another break around $19.2-30$ GeV. Such an observation would imply absorption of γ-rays by BLR photons and the γ-ray production site must lie within the BLR. However, observations do not support the double absorber model (Harris *et al.* 2012). Alternatively, the break in the GeV spectra of FSRQs can happen by Klein-Nishina effect on the inverse Compton scattering of BLR photons by relativistic jet electrons with a curved distribution (Cerruti *et al.* 2013). But, from an analysis of the γ-ray spectra of
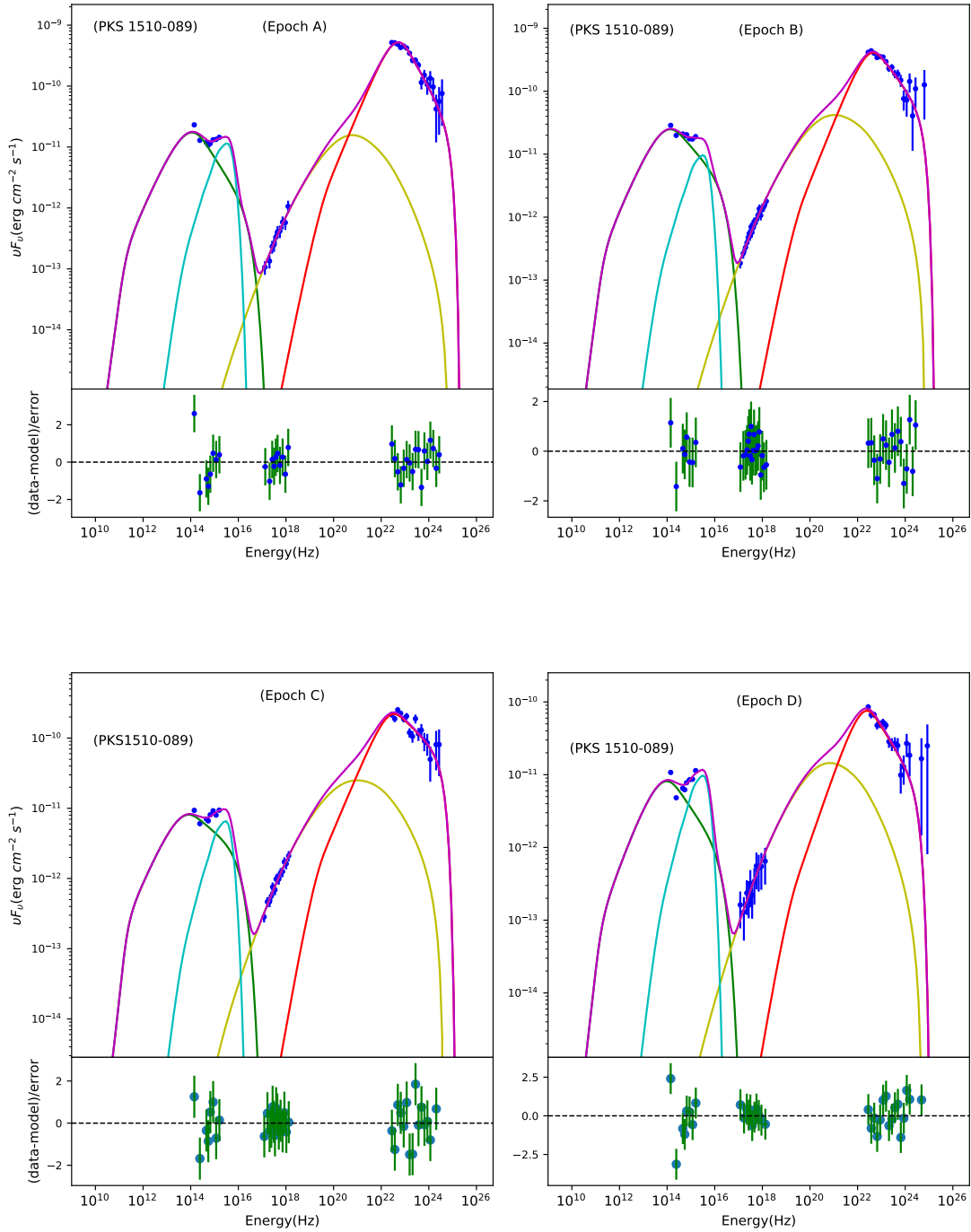
FIGURE 3.16: Observed broad band spectral energy distribution for the source PKS 1510−089 along with model fits for the epochs A,B C and D. The various components are the synchrotron emission (green line), the SSC process (yellow line), the EC process (red line) and the accretion disk component (cyan line). The magenta line is the sum of all the components. The bottom panel in each SED shows the residuals between SED fits and the observed points.
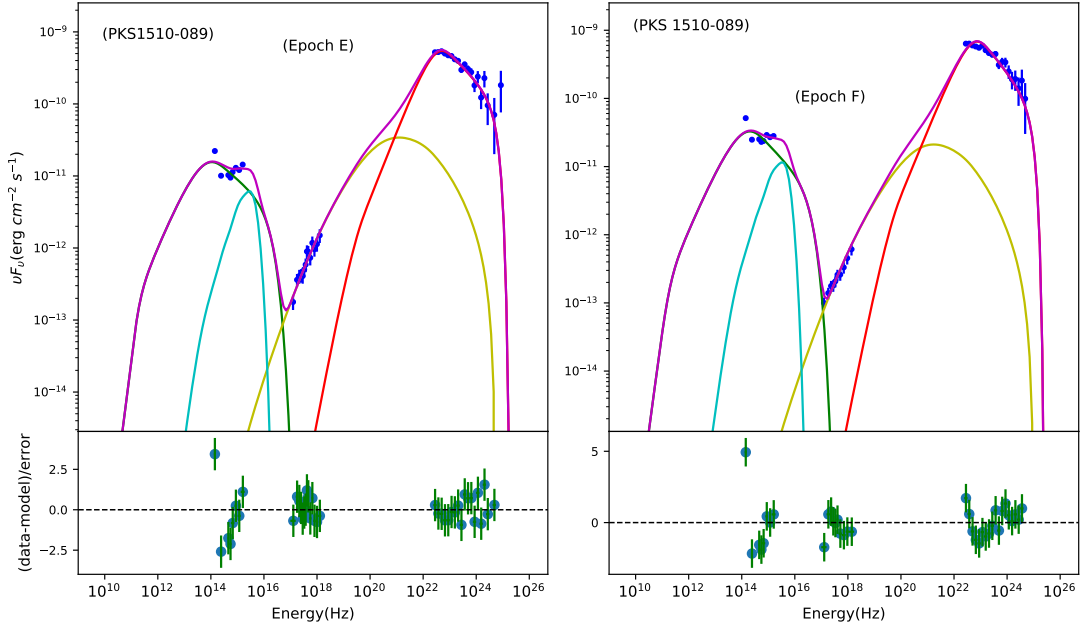
FIGURE 3.17: Model fits to the broad band SED during epochs E and F for the source PKS 1510−089. The panels have the same meanings as that of Figure 3.16.
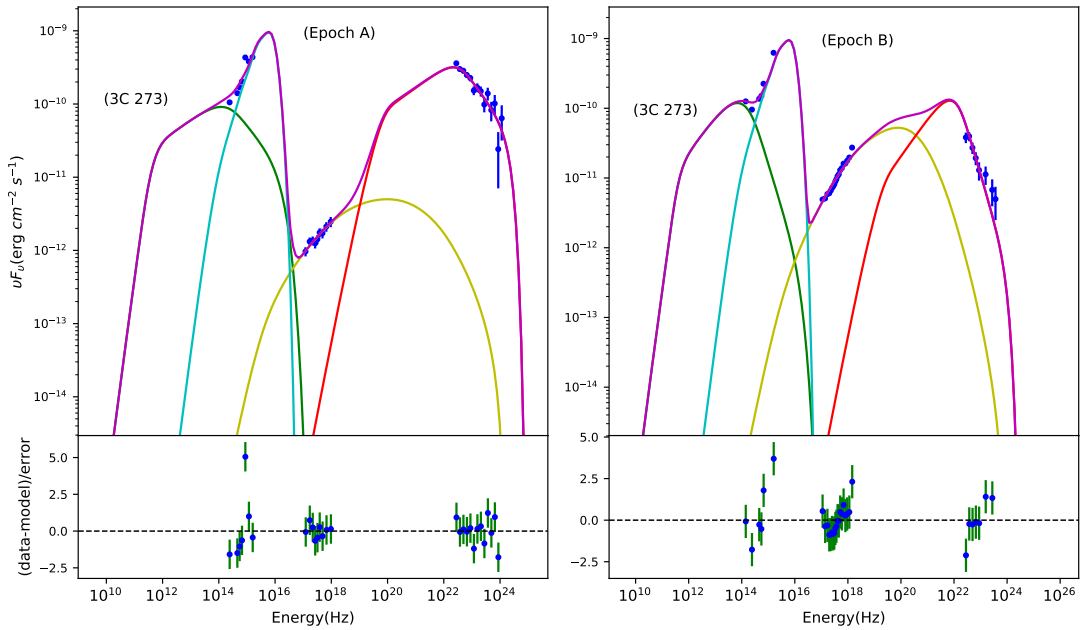
FIGURE 3.18: Model fits to the broad band SED during epochs A and B for source 3C 273. The panels have the same meanings as that of Figure 3.16.
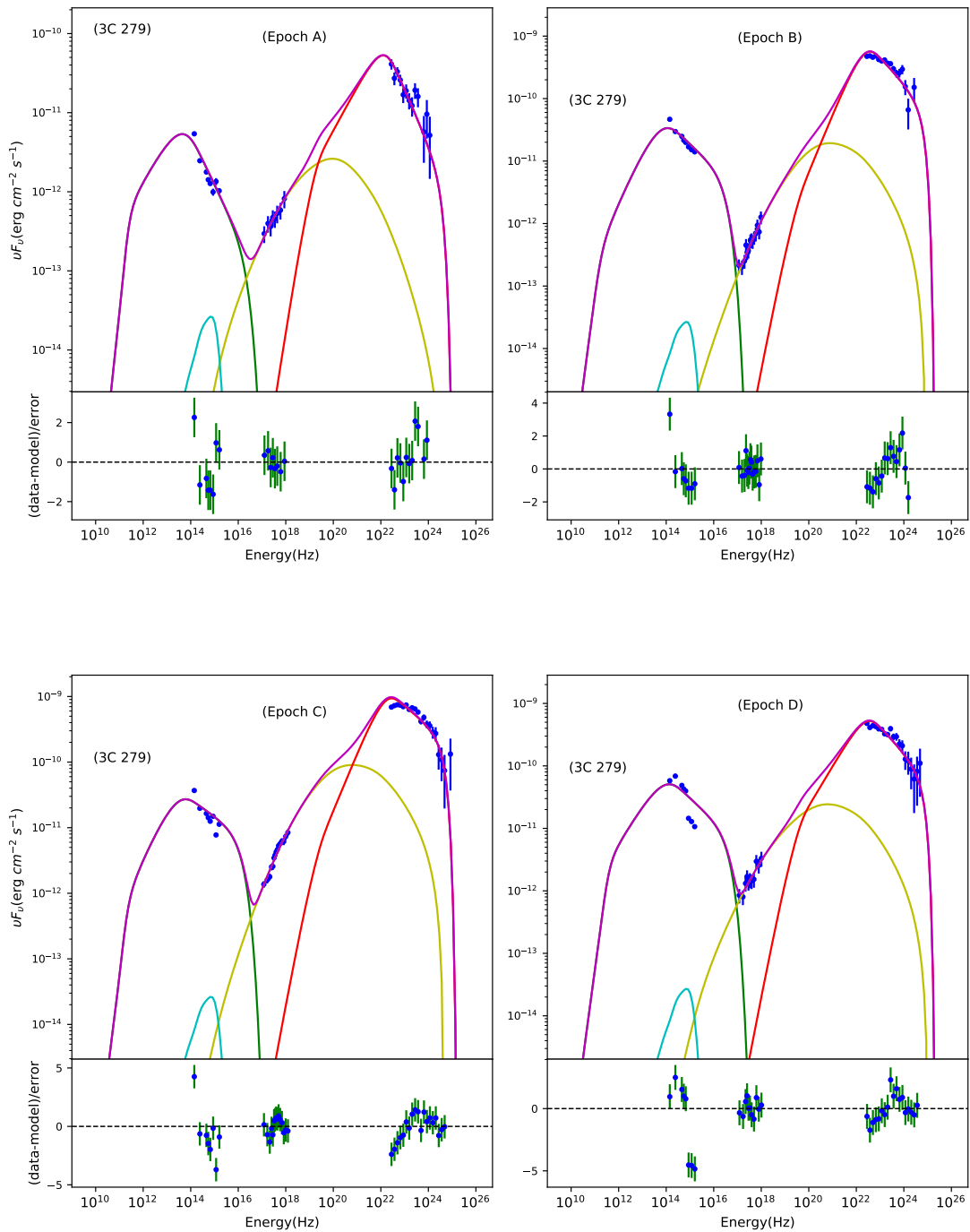
FIGURE 3.19: Model fits to the broad band SED during epochs A, B, C and D for the source 3C 279. The panels have the same meanings as that of Figure 3.16.
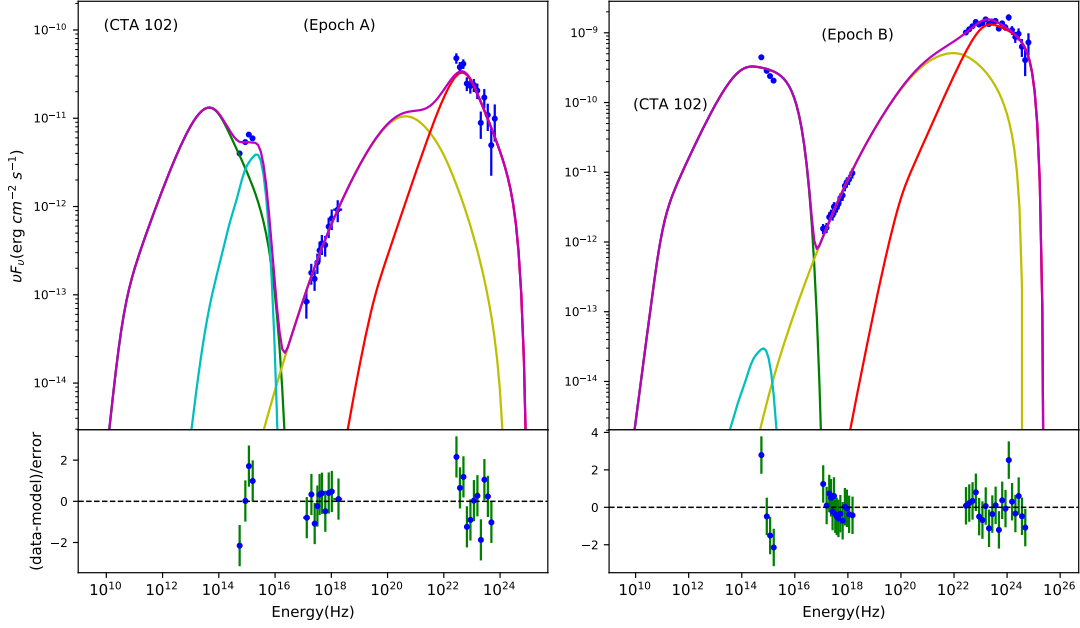
FIGURE 3.20: Model fits to the broad band SED during epoch A and B for the source CTA 102. The panels have the same meanings as that of Figure 3.16.

a large number of blazars, Costamante *et al.* (2018) found that in FSRQs, the observed γ-ray spectra is not by IC scattering of BLR photons and the γ-ray emission site lies outside the BLR.

Apart from the above, the break in the γ-ray spectra of FSRQs can also happen due to intrinsic effects because of the electrons in the relativistic jets of these sources either having a cut-off in their energy distribution or a log-parabola energy distribution. In this work, the SEDs of all the sources in the different epochs are well modelled by IC scattering of the photons from the obscuring torus, and the γ-ray emission region lies outside the BLR where IC takes place in the Thomson regime. The results of the γ-ray spectral analysis carried out on all the epochs in the objects and reported in Table 3.2. I note that in the 3FGL catalog (https://www.ssdc.asi.it/fermi3fgl/), the γ-ray spectra of all the sources studied here are better described by the LP model than the PL model except for the source 3C 273 at epoch B. The parameters α and β in the LP model fits to the

data carry very important information on the characteristics of the γ-ray spectra. In this model, α gives the slope of the spectra and β is a measure of the curvature in the spectra. A smaller value of α and β implies a harder spectrum with a mild curvature. Any changes in the value of α and β during different epochs is a measure of the changes in the γ-ray spectral shape. The dependence of α and β values against the fluxes of the sources are given in Figure 3.21. For all the sources I found the spectra to harden with increasing flux. I found decreasing as well as increasing trend of β with flux. The variation in the γ-ray spectral shape can be associated with the shift in IC peak frequency. This is evident from the results of our SED analysis. Our model fits to the observed SED also gives the IC peak frequency (see Table 3.4). Analysis of the IC peak indicates that as the IC peak shifts towards lower energies, the spectrum is harder and the curvature (β) is sharper which too demonstrates that the γ-ray spectral variation is closely related to the changes in the IC peak. Alternatively, γ-ray spectral variation can also be attributed to the changes in the location of the γ-ray emission region during different activity states of the sources (Coogan *et al.* 2016). Besides, since the γ-ray emission in FSRQs is due to EC scattering of the external target photons, the γ-ray peak energy will depend on the dominant external photon frequency. If the target photon field is the IR emission from the dusty torus, then the temperature of the dust emission will depend on the location of the emission region from the central black hole (Dermer *et al.* 2014; Ghisellini and Tavecchio 2009).

3.9.2 Connection between optical and GeV flux variation

The capability of *Fermi* to scan the sky once in three hours and supporting ground based monitoring observations in the optical band has enabled one to study close correlations between flux variations in the GeV band and other low energy bands. From multiband observations of the blazar 3C 454.3 over a period of about 5 months, Bonning *et al.* (2009) found close correlation between the optical and

GeV band flux variations. This argues for co-spatiality of the optical and GeV emission regions. This correlation is also easily understood in the one zone leptonic emission model, wherein relativistic electrons in the jet produce optical emission by synchrotron process, and the same relativistic electrons produce γ-ray emission by inverse Compton process. However, mismatch between optical and GeV flux variations are also known in few other blazars such as PKS 0208−512, (Chatterjee *et al.* 2013), PKS 0454−234, S4 1849+67, BZQ J0850−1213, OP 313 (Cohen *et al.* 2014), PKS 2142−75 (Dutka *et al.* 2013), PKS 1510−089 (MacDonald *et al.* 2015) and PKS 2155−304 (Wierzcholska *et al.* 2019a). From the analysis of multi-band light curves of the sources, I found instances where the optical and γ-ray flux variations are closely correlated, cases where there are optical flares without γ-ray counterpart and instances when there are γ-ray flares without optical counterparts. Thus, it is evident that the correlations between the optical and GeV flux variations in *Fermi* blazars are complex. Recently, from correlation analysis between the optical and γ-ray light curves of 178 blazars, Liodakis *et al.* (2019) found that statistically about 50% of their optical flares have no GeV counterparts and this fraction is less in the case of γ-ray flares, i.e., about 20% of γ-ray flares have no optical counterparts. While in the leptonic scenario a close correlation between optical and GeV variations is expected, the results found in this work as well as the other recent results by Rajput *et al.* (2019) and Liodakis *et al.* (2019) indicate that correlated variability analysis between the optical and GeV bands may also not be definitive in constraining the leptonic v/s hadronic scenario for the high energy emission process in blazars. Most of the correlation studies between different energy bands of the blazars indicate positive correlation. But there are exceptions and cases of anticorrelation are also found for some sources (Chatterjee *et al.* 2013; Cohen *et al.* 2014; Dutka *et al.* 2013; MacDonald *et al.* 2015; Rajput *et al.* 2019). I found various behaviours between optical and γ-ray energy bands for our selected sample of sources. During the 9 years of monitoring data analyzed for the source 3C 454.3 I found four flaring epochs in the optical, namely A,B, D and E. During epochs A and B, the optical flare is accompanied by a γ-ray flare, while at the

other two epochs D and E, though the optical flares have amplitudes similar to that of epochs A and B, the γ-rays during epochs D and E were either weak or undetected. This is clearly seen in Figure 3.22 where the logarithm of γ-ray flux is plotted against the logarithm of optical flux. I looked for the correlation between the optical V-band and the γ-ray band for all the epochs for other four sources which are chosen for the analysis and I only consider epochs where the correlation is significant at the 90% level. The results are shown in Figure 3.22 and the results of the fit are given in Table 3.5. I convert the gamma-ray fluxes from ph cm^{-2} s^{-1} to erg cm^{-2} s^{-1} at 100 MeV (Singal *et al.* 2014) to match the optical flux units. The fit takes into account the errors in both the optical and γ-ray flux values.

To have an insight into this anomalous variability behavior I fitted the broad band SED of the source in all the epochs using simple one zone leptonic emission model. For the source 3C 454.3 during epochs A and B, where the optical and γ-ray flux variations are correlated, there is enhancement in the bulk Lorentz factor relative to the quiescent epoch C. During epoch D, I found an enhancement of the magnetic field related to the quiescent state C, which could explain the high optical flare accompanied by a very weak γ-ray flare. Such a change in magnetic field could also produce enhanced optical polarization and X-ray flux. But, the non-availability of optical polarization and X-ray flux measurements during epoch D, preclude us to make a firm conclusion on the enhancement of the magnetic field as the cause for the occurrence of optical flare with weak γ-ray flare during epoch D, however, is the most favorable scenario. In epoch E,where there is an optical flare with a weak γ-ray counterpart our SED modeling indicates decrease in electron energy density, magnetic field and bulk Lorentz factor and also the emission region could be located at a region farther than the emission region of other epochs. I therefore conclude that the observations of optical flare with weak/no corresponding γ-ray flare during epochs D and E, could be due to one or a combination of parameters such as the bulk Lorentz factor, magnetic field and electron energy density or due to changes in the locations of the γ-ray emitting regions. A possible cause for optical flux variations without γ-ray counterparts could be attributed to hadronic

processes (Mücke and Protheroe 2001), however based on our SED analysis, I conclude that the leptonic model is also capable of explaining the emission from 3C 454.3 during all the epochs.

For the source PKS 1510−089 during epochs B and F the optical and γ-ray flares are correlated. During this epoch Γ is larger than that of the quiescent period. This has given rise to increased flare in optical and γ-rays. The difference in the amplitude of variations between optical and γ-ray flares during epochs B and F must be due to a combination of Γ and B. For epochs A, C and E the magnetic field is lower than the quiescent period by a factor of 1.2 - 1.5. This has led to decreased optical variations. At the same time Γ has increased from 1.1 - 1.7 times the quiescent period leading to increased γ-ray flare, but no corresponding optical flare (see Figure 3.5 and Figure 3.6).

In the source 3C 273, using our criteria, I were able to identify one quiescent period and a flaring period. At epoch A, the bulk Lorentz factor increased compared to the quiescent state B, whether the magnetic field is nearly the same (Table 3.4). It is natural to expect increased optical and γ-ray flares during epoch A, but I found a γ-ray flare without an optical counterpart. This absence in optical flux variations might be due to sub-dominant optical synchrotron emission compared to the prominent accretion disk emission. The prominent accretion disk component is very well evident in the broad band SED both in the quiescent and active states (Figure 3.18).

In the source 3C 279, I identified four epochs, A,B, C and D of which during epoch A, the source was quiescent while it was active during the other epochs. During epoch D, magnetic field is about 1.5 times larger than the quiescent period leading to larger optical synchrotron emission. At the same epoch, Γ has increased from about 7 to 12. This explains the increased γ and optical flaring in epoch D. During epochs B and C, Γ has increased relative to the quiescent state giving rise to larger γ-ray fluctuations. During epoch B, magnetic field is marginally larger

than the quiescent period, while the particle density is lower than the quiescent period. However, in epoch C, the magnetic field and particle density is lower and higher respectively than the quiescent period. The interplay between low magnetic field and high particle density and vice versa could lead to lower optical variations. This could be the reason for γ-ray flares without optical counterparts in epochs B and C in 3C 279.

In CTA 102, I found one flaring epoch when the optical and γ-ray seems to be correlated. Many short term flares with optical and γ-ray counterparts are seen during this epoch. For SED analysis I considered only 10 days due to the availability of γ-ray, X-ray and optical data points for SED modelling. During Epoch B, Γ was nearly four times greater than the quiescent epoch. The magnetic field during epoch B and the quiescent period agree with each other within errors (see Table 3.4). This increase in Γ relative to the quiescent epoch is the cause of the increased γ-ray flare and optical flare during epoch B. Prominent accretion disk component is visible in the SED during the quiescent phase, however, this is not evident in the flaring epoch B (Figure 3.20). This is also reflected in the high accretion rate found during the quiescent epoch A and a negligibly small accretion rate during epoch B.

3.10 Summary

I have carried out detailed investigations of the correlation between optical and GeV flux variations in five FSRQs namely 3C 454.3, PKS 1510$-$089, 3C 273, 3C 279 and CTA 102. The study includes (a) identification of epochs in those sources with anomalous optical$-$GeV flux variations, (b) analysis of the broad band SEDs of the sources in those epochs and (c) the analysis of γ-ray spectra. The results of those analysis are summarized below:
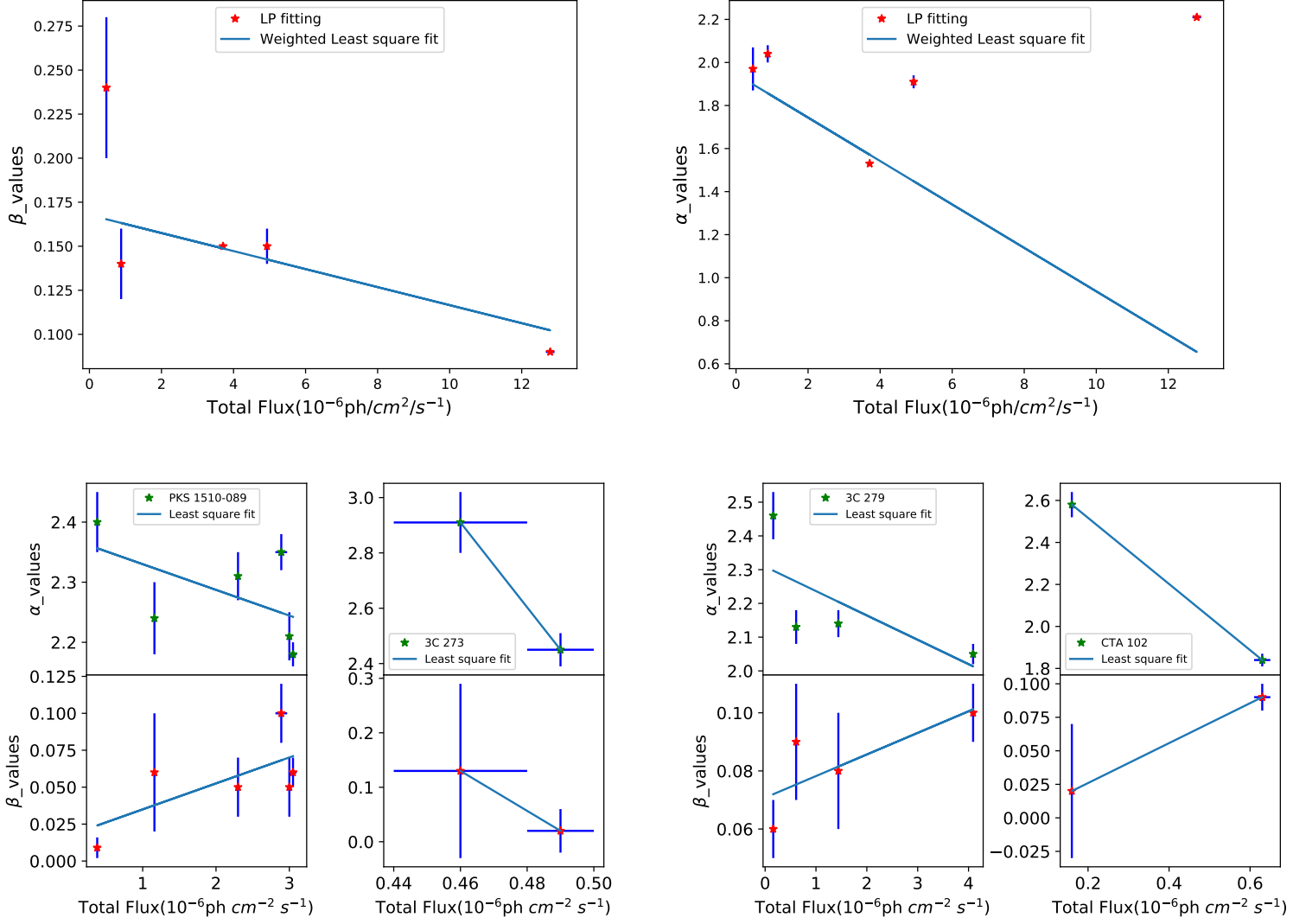
FIGURE 3.21: Variations of the parameters α and β with flux for the sources 3C 454.3 (top panels), the bottom left panels are for PKS 1510$-$089 and 3C 273 while the bottom right panels are for 3C 279 and CTA 102.

1. All the five FSRQs studied here, namely 3C 454.3, PKS 1510$-$089, 3C 279, 3C 273 and CTA 102 showed varied correlations between optical and GeV flux variations. I found cases when the optical and γ-rays are closely correlated, epochs when there are optical flares without γ-ray and epochs when there are γ-ray flares without optical counterparts. From analysis of these epochs through broad band SED fits, I found that the regions giving rise to optical and γ-ray emission in all the sources are largely co-spatial.

TABLE 3.5: Results of the linear least squares fit to the optical and γ-ray flux measurements, during different epochs for the sources 3C 454.3, PKS 1510$-$089, 3C 273, and 3C 279. Here R and P are the Spearman rank correlation coefficient and the probability for no correlation respectively.

Object	Epoch	Slope	Intercept	R	P
3C 454.3	A	1.54 ± 0.12	8.04 ± 1.29	0.81	0.00
	B	1.23 ± 0.15	4.94 ± 1.51	0.61	0.00
	D	0.52 ± 0.04	-3.50 ± 0.40	0.60	0.00
	E	0.98 ± 0.07	1.71 ± 0.71	0.80	0.00
PKS 1510$-$089	C	3.23 ± 1.07	27.11 ± 12.09	0.55	0.08
	E	1.45 ± 0.60	7.13 ± 6.73	0.57	0.07
3C 273	A	16.93 ± 3.52	156.64 ± 34.52	0.94	0.00
3C 279	B	4.78 ± 1.66	41.96 ± 17.90	0.50	0.06
	C	1.96 ± 1.45	12.02 ± 16.01	0.55	0.05

2. SED analysis indicates that the optical emission is often well explained by synchrotron emission process and the γ-ray emission is well explained by EC process with the seed photons from the torus. Inclusion of accretion disk component to the model, improves the spectral fit, yielding low χ^2 relative to the non-inclusion of accretion disk component. However, prominent accretion disk component is seen in all the epochs of the SEDs in PKS 1510$-$089, 3C 273 and the quiescent state SED of CTA 102. For the sources 3C 454.3, 3C 279, the low energy part of the SED is dominated by the jet synchrotron without a prominent accretion disk.

3. From model fits I found that (a) correlated optical and γ-ray flux variations are caused by increase in the bulk Lorentz factor (b) γ-ray flares with no optical counterparts are due to an increase in the bulk Lorentz factor and/or increase in the electron number density and (c) an optical flare with no γ-ray counterpart is due to an increase in the magnetic field.
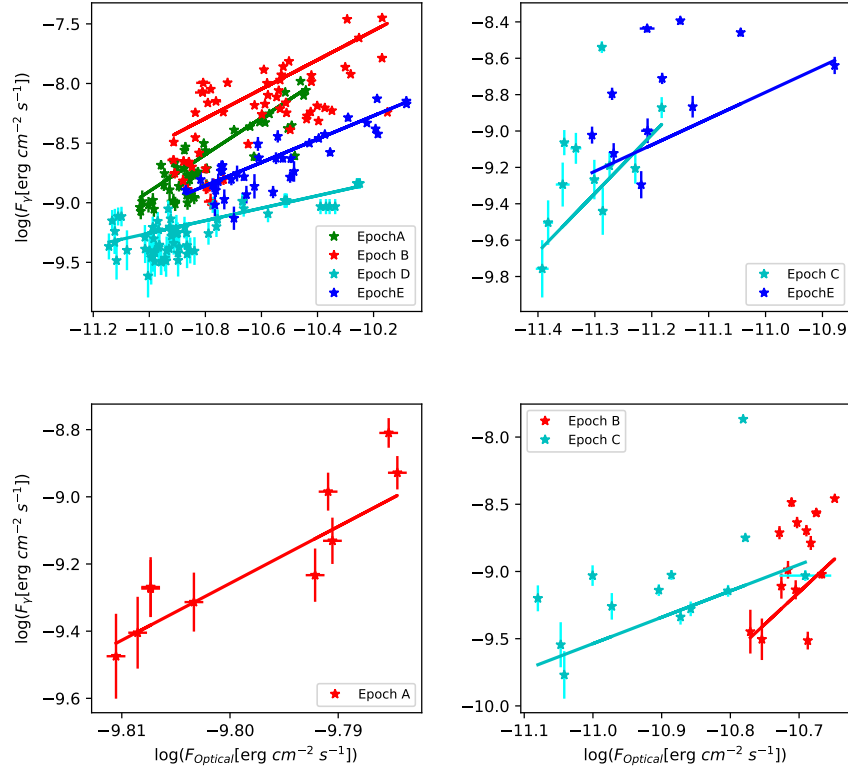
FIGURE 3.22: Optical flux v/s γ-ray flux for the sources 3C 454.3 (top left), PKS 1510−089 (top right), 3C 273 (bottom left) and 3C 279 (bottom right) respectively.

4. The γ-ray spectra of the sources during various epochs are well represented by the LP model.

Chapter 4

Correlation between optical and γ -ray flux variations in BL Lacs *

Results of the analysis on the correlations between optical and γ-ray flux variations in the BL Lac category of AGN is presented in this chapter. A total of 3 BL Lac objects were selected. They are AO 0235+164, OJ 287 and PKS 2155−304. The details on the selection of the above three objects and the data used are given in chapter 2. Brief details on the three objects are given below.

4.0.1   AO 0235+164

AO 0235+164 was first classified as a BL Lac object based on its variability and featureless optical spectrum (Spinrad and Smith 1975). Cohen *et al.* (1987) measured the redshift of the object at $z = 0.94$. It has shown violent variations across the electromagnetic spectrum that includes optical, X-rays and γ-rays (Raiteri

---

TABLE 4.1: Summary of the epochs considered for detailed light curve analysis, SED modelling and spectral analysis. The γ-ray fluxes are between 100 MeV to 300 GeV and in units of 10^{-6} ph cm^{-2} s^{-1} and the optical fluxes are in units of 10^{-11} erg cm^{-2} s^{-1}.

	MJD		Calender date		Mean Flux		Peak Flux		
Name/ID	Start	End	Start	End	γ	Optical	γ	Optical	Remark
AO 0235+164									
A	54720	54740	11-09-2008	01-10-2008	1.03±0.26	0.96±0.56	0.86±0.14	2.26±0.01	γ-ray and optical flare
B	54743	54763	04-10-2008	24-10-2008	0.90±0.23	0.88±0.42	1.41±0.20	1.57±0.01	γ-ray and optical flare
C	55100	55200	26-09-2009	04-01-2010	0.11±0.11	0.07±0.02	—	—	Quiescent State
D	57040	57060	18-01-2015	07-02-2015	0.13±0.08	0.35±0.19	0.22±0.10	0.67±0.01	γ-ray and optical flare
OJ 287									
A	54870	54970	08-02-2009	19-05-2009	0.04±0.06	1.62±0.46	—	—	Quiescent state
B	55127	55147	23-10-2009	12-11-2009	0.11±0.14	3.49±1.10	0.50±0.18	5.88±0.02	γ-ray and optical flare
C	56735	56755	19-03-2014	08-04-2014	0.26±0.18	2.10±0.39	0.59±0.18	2.69±0.01	γ-ray and optical flare
D	57350	57370	24-11-2015	14-12-2015	0.28±0.13	4.34±1.78	0.47±0.14	8.20±0.02	γ-ray and optical flare
PKS 2155−304									
A	55740	55840	28-06-2011	06-10-2011	0.08±0.06	5.82±0.61	—	—	Quiescent state
B	56790	56810	13-05-2014	02-06-2014	0.41±0.30	9.88±0.81	1.04±0.20	10.70±0.02	γ-ray and optical flare

et al. 2001, 2009; Abdo *et al.* 2010c). The high optical flux variability shown by the source during December 2006 is explained by the high optical polarization degree (30% - 50%) and small changes in the viewing angle of the jet (Hagen-Thorn *et al.* 2008). Raiteri *et al.* (2001) found quasi-periodic behaviour in radio outburst with a periodicity of ~ 5.7 years. It is classified as a LSP blazar (Ackermann *et al.* 2015a) and its γ-ray spectrum is will fit by a LP function (Acero *et al.* 2015). From detailed multi-wavelength observations of the source spanning about six months and including observations from the radio to the γ-ray bands, Ackermann *et al.* (2012) found the γ-ray activity to be well correlated with the optical/IR flares. They also found the broad band SED to be well explained by leptonic model with the seed photons for the IC scattering from the torus.

4.0.2   OJ 287

OJ 287 first identified as a blazar in 1967 by Dickel *et al.* (1967) is a LSP blazar (Ackermann *et al.* 2015a) at redshift $z = 0.3056$. In the long term optical light curve, a periodicity of $\sim$12 years was observed which in the binary super massive black hole model is attributed to the secondary SMBH striking the accretion disk around the primary SMBH (Sillanpaa *et al.* 1988). In addition to flux variations in the optical band (Rakshit *et al.* 2017; Paliya *et al.* 2017b), it has also shown polarization variations (Rakshit *et al.* 2017). Flux variations are also seen in the GeV γ-ray energy band (Agudo *et al.* 2011). The broadband spectral analysis of the source at various activity levels points to the high energy hump explained by IC scattering of both emission line photons (Kushwaha *et al.* 2018) as well as the torus (Kushwaha *et al.* 2013).

4.0.3   PKS 2155$-$304

PKS 2155$-$304 was first discovered in the Parkes survey (Shimmins and Bolton 1974) and identified as a BL Lac object by Hewitt and Burbidge (1980). It is a HSP blazar at a redshift of $z =$0.116 (Bowyer *et al.* 1984), and its γ-ray spectrum is consistent with a LP function (Acero *et al.* 2015). Correlated optical and γ-ray flare was seen in 2014, while in 2016, there was a large optical flare with no corresponding flare both in the GeV band as well as at very high energies (Wierzcholska *et al.* 2019b). Simultaneous observations of the source in 2008, showed evidence of correlated flux variations between optical and VHE bands, however, the increased flux in the optical band has no correspondence with the X-ray and the GeV flux consistent with being constant (Aharonian *et al.* 2009). Quasi-periodic variations in the optical emission with a time scale of 317$\pm$12 days
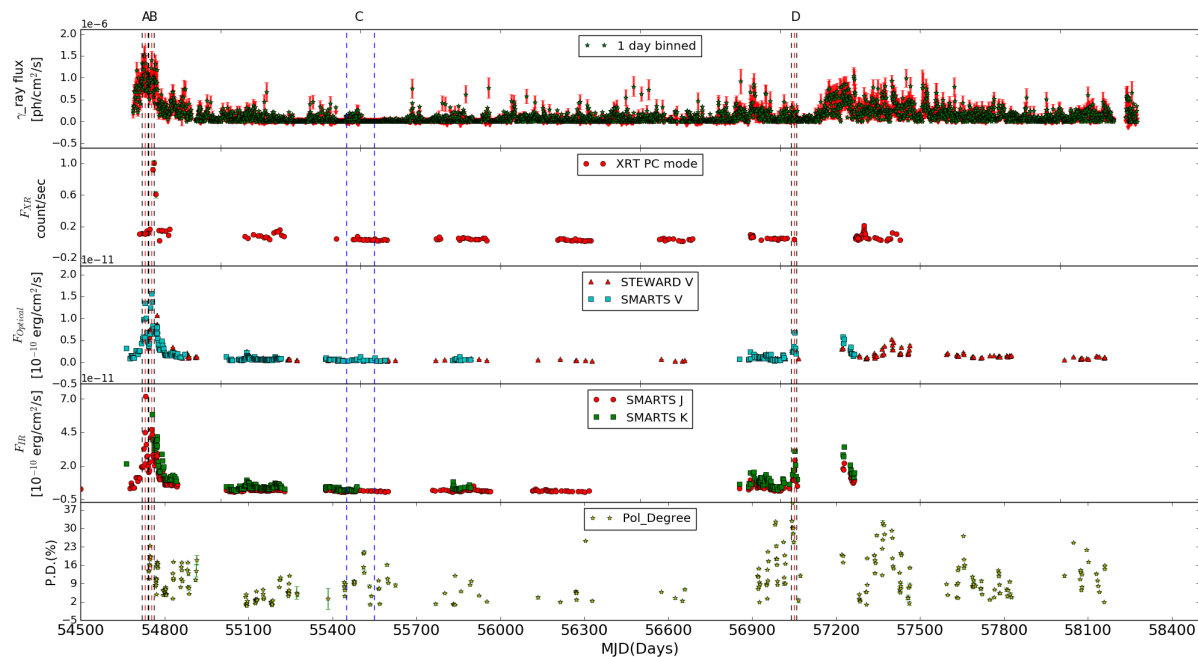
FIGURE 4.1: Multi-wavelength light curves of the source AO 0235+164. From the top, panels refer to the one day binned γ-ray light curve, the X-ray light curve, the optical light curve, the IR light curves and the degree of optical polarization. The vertical red lines refer to the optical flare peaks and γ-ray flare, and the two vertical black lines indicate a period of 10 days each on either side of the peak of the flare. The two vertical blue lines are for the period of 100 days and shown correspond to the quiescent period. The upper limit points, which are defined for TS < 9 are shown with vertical arrow in the γ-ray light curve.

(Zhang *et al.* 2014) and in the GeV emission with a time scale of 1.74±0.013 years are known in PKS 2155−304 (Zhang *et al.* 2017).
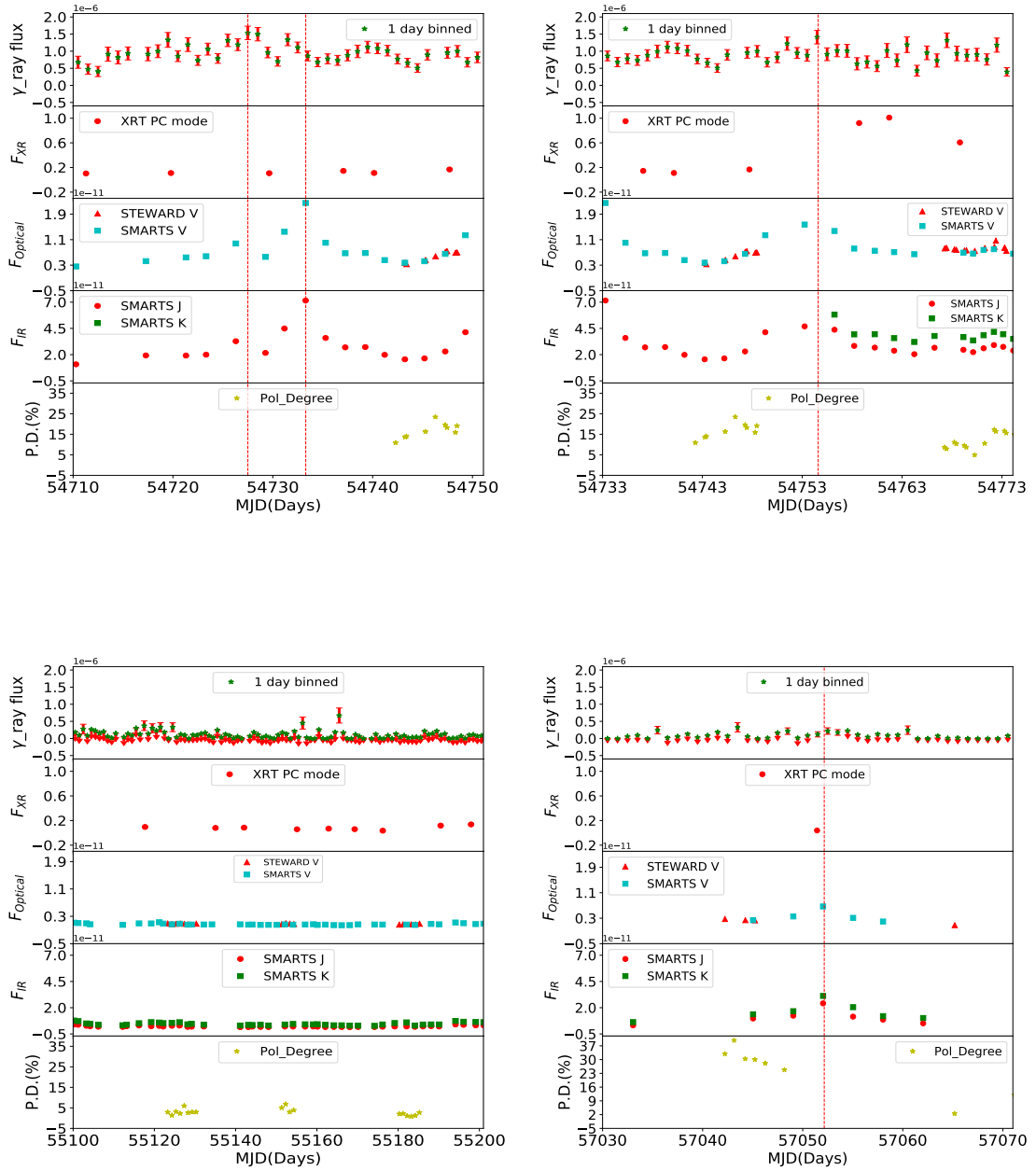
FIGURE 4.2: Multi-wavelength light curves for the selected epochs of the source AO 0235+164. Epoch A is in the top left panel and epoch B is shown in the top right panel. The bottom left and right panels show the light curves for epochs C and D respectively. The dashed lines show the peak of the optical and GeV flare.

4.1 Analysis

4.1.1 Multi-wavelength light curves

Multi wavelength light curves of all the BL Lacs were generated as per the procedures outlined in chapter 2. From these, flares need to be identified to study the correlation between optical and gamma-ray flux variations. However, an automated procedure to identify this was hindered due to gaps and less number of data points in the optical light curves. Therefore, flares were first identified visually. Once those flares were identified expanded light curves were generated for a duration of 20 days centered on the optical or γ-ray flare. This is to make sure the availability of data at multiple wavelengths that are needed for broad band SED modelling. This condition of data availability at multiple wavelengths lead to the identification of few epochs for each object. A summary is given in Table 4.1 and the details of the epochs selected for each object are given below.

4.1.1.1 AO 0235+164

Multi-wavelength light curves from *Fermi*, *Swift*-XRT, SMARTS and Steward observatory are shown in Figure 4.1. Two major flares in the optical/IR bands are evident in the light curves. X-ray and γ-rays too have measurements simultaneous to the flares in the optical/IR. Close inspection of the light curves indicates that these large optical flares are composed of many short term flux variations. I identified four epochs in this source namely A,B,C and D for studying the correlations between optical and GeV flux variations. Table 4.1 provides a summary of these epochs and the multi-wavelength light curves covering a 40 day period for each epoch (except for the quiescent epoch which is 100 days) are given in Figure 4.2. However, for SED analysis during flaring epochs, data covering a period of

20 days centered around the flare was used. The details of those four epochs are given below.

Epoch A: During this epoch, the γ-ray and optical flares have increased by the same factor relative to the quiescent epoch, however, the amplitude of IR variation is larger than the variation in the optical. During this epoch, there are two optical flares, a major one around MJD 54733 and a minor one around MJD 54726. The nature of X-ray flux variations during the peak of the optical flare could not be ascertained due to the lack of X-ray flux measurements. No optical polarization measurements were available during the 20 days period of this epoch. I conclude that in this epoch the optical and GeV flares are correlated.

Epoch B: During this epoch the available peak optical flux is about a factor of 2 larger than the mean level during the 20 days period of this epoch. Similar enhancement in the γ-ray flux is there during the same epoch of the optical flare (see Table 4.1). In IR too, there are indications of increased brightness during this epoch, however, the nature of the X-ray state of the source could not be ascertained during this epoch due to the lack of flux measurements. Optical polarization measurements were not available during the peak of the optical flare, but the measurements during the 20 day period centered around the optical flare show that the source is strongly polarized at the 20% level, relative to the quiescent state where the PD is around 2%. Thus in this epoch, there is an optical flare with a GeV counterpart.

Epoch C: During this period, the source was at its quiescent phase in all the wavelengths analyzed in this work. The source was also less polarized during this epoch with a PD of around 2%.

Epoch D: The source has shown an optical flare during this epoch. Simultaneous to the optical flare, the IR fluxes too have increased with the peak of the IR

measurements coinciding with the peak of the optical flare. Around the peak of the optical flare the source is detected in the γ-ray band with high significance (TS > 9). Considering points also with TS < 9 during this epoch, the presence of a γ-ray flare is evident. There is lack of X-ray flux measurements during the peak of the optical flare and therefore, the exact X-ray flux state of the source during the optical flare is not known. Though there are no simultaneous polarization measurements during the peak of the optical flare, the few measurements available during the 20 days period of this epoch show that the PD during this epoch is about 30%, a factor of about 15 larger relative to the polarization at the quiescent state. Thus in this epoch too, there is an optical flare with a GeV counterpart.

4.1.1.2   OJ 287

I show in Figure 4.3 the multi-wavelength light curves of the source, that include data from *Fermi*, *Swift*-XRT, SMARTS and the Steward Observatory. The source is active all the times in the optical. I identified four epochs in this source, namely A,B,C and D. The brief details of these four epochs are given in Table 4.1. An expanded view of those four epochs, that covers a time span of 40 days for the flaring epochs and 100 days for the quiescent epoch is shown in Figure 4.4.

Epoch A: During this epoch, the source was at a quiescent state at all the wavelengths, though some small scale variations are seen in the optical light curve. It was below the detection limit (TS < 9) in the γ-ray band for most of the time during this epoch. During this quiescent period of 100 days, dramatic changes were noticed in the degree of optical polarization. During the beginning of the epoch, PD decreased from about 30% to around 15% in about 20 days, remained steady at around 20% in the middle of the epoch and again increased to about 30% during the end of this epoch. No changes in optical flux were noticed during the times of polarization variations.

Epoch B: There is a weak γ-ray flare in this epoch that has a corresponding enhancement in flux in the optical band. The X-ray brightness state of the source during the epoch of the weak optical and γ-ray flare is unknown due to the absence of X-ray measurements. Polarization measurements during the beginning of this epoch indicate that the source has high optical polarization of about 20% to 30%. During this epoch optical and γ-ray flares are correlated.

Epoch C: During this epoch from visual inspection there is a weak optical flare, which again has a correlated γ-ray flare that is moderate. The optical polarization also showed a marginal increase during the peak of the optical and γ-ray flare. Thus in this epoch there is a correlated optical and γ-ray flare.

Epoch D: During this epoch, the source showed a large optical flare. In the IR band too, a flare is noticed albeit with low amplitude. However, the source was detected in the γ-ray band with high significance (TS > 9) only during the peak of the flare while during most of the time in this epoch, the source was detected with less significance (TS < 9). Considering all the detections indicate the presence of a γ-ray flare along with an optical flare. The X-ray brightness during this epoch was consistent with a constant flux level. Polarization observations available during the end of the epoch indicate the source to have lower polarization compared to the values of PD at epoch B. Thus, during this epoch too I have an optical flare with a γ-ray counterpart.

4.1.1.3   PKS 2155−304

During the 10 year period analyzed here for flux variations, the source was found to be variable all the times in the optical band. This is evident in Figure 4.5 where I show the multi-wavelength light curves of the source. In this source I identified two epochs namely A and B. The summary of these two epochs are given in Table

4.1 and an expanded view of these two epochs are shown in Figure 4.6. For the quiescent period this expanded plot is shown for a 100 day period, while for epoch B, it is shown for a duration of 40 days. The details of these two epochs are given below.

Epoch A: I considered this epoch as the quiescent state of the source. During this period, the one day binned $\gamma-$ray light curve was nearly stable. In the optical and IR bands too, the flux of the source remained stable. Available X-ray flux measurements during this period too points to the source being weak in X-rays. No changes were noticed in the optical polarization with the PD remaining nearly constant at a value of about 3%. This epoch thus represents the true quiescent period of the source.

Epoch B: The source displayed a strong γ-ray flare during this epoch. Coincident with the γ-ray flare I noticed a low amplitude optical and IR flare. X-ray too showed increased flux during the optical and γ-ray flare however the peak of the X-ray does not coincide with the peak of the γ-ray flare. Although the overall optical brightness state of the source is larger compared to the other periods, there is lack of optical data at the peak of the γ-ray flare. However visual inspection of Figure 4.5 indicates a γ-ray flare correlated with a weak optical flare. Optical polarization was also higher during this epoch relative to the quiescent epoch A. Thus during this epoch I observed correlated flux variations in IR, optical, and γ-rays.

4.1.2 γ-ray spectrum

In order to explore the behaviour of γ-ray spectra for different epochs and to discern the intrinsic distribution of electrons in the jet of BL Lacs, I performed the fitting of the γ-ray spectra with two models namely PL and LP. For γ-ray
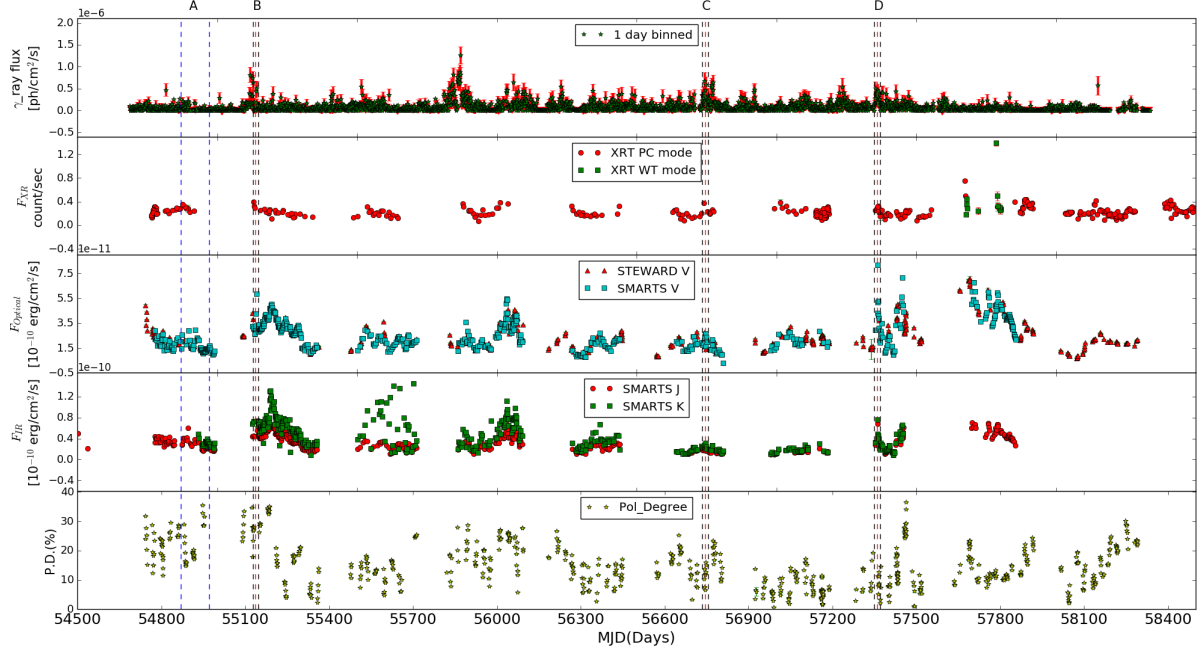
FIGURE 4.3: Multi-wavelength light curves of the source OJ 287. The other details are similar to that given in the caption to Figure 4.1.

spectral analysis, the data were averaged over a duration of 100-days in the case of quiescent periods and 20 days during other periods. Two sample spectral fits are shown in Figure 4.7, one in which the spectrum is well described by the LP model and the other in which the spectrum is well described by the PL model. The large error bars in the γ-ray spectra are due to poor photon statistics. The results of the model fitting are given in Table 4.2. For most of the epochs, the γ-ray spectra is well fit by a LP model.

4.1.3   Spectral energy distribution modelling

To characterize the physical properties of the sources during the epochs of optical and γ-ray flux variations, I generated the broad band SED of the sources at the different epochs and modelled them using the one zone leptonic emission model.
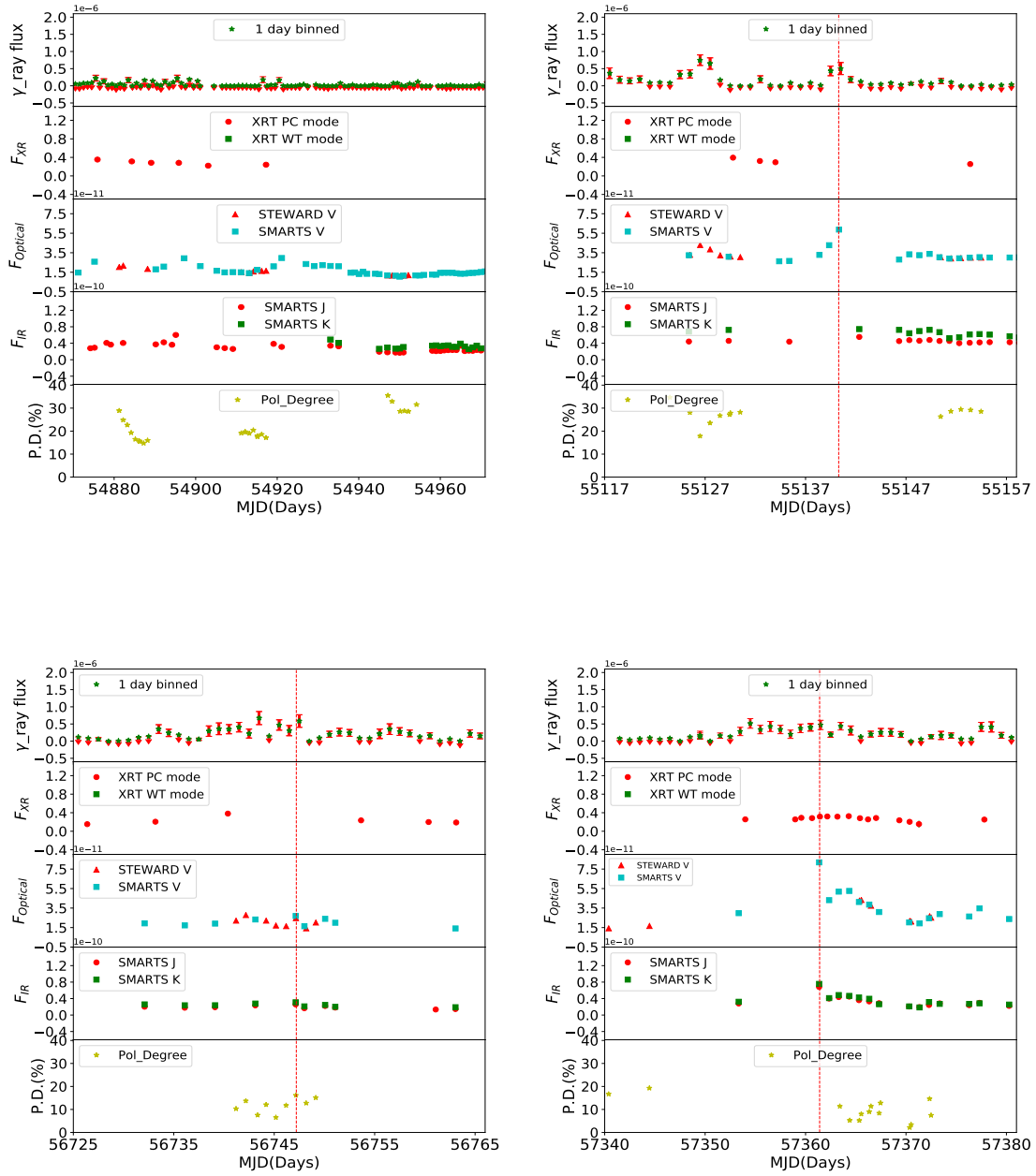
FIGURE 4.4: Multi-wavelength light curves for the selected epochs of the source OJ 287. The top left and right panels are for epochs A and B, while the bottom left and right panels are for epochs C and D respectively.
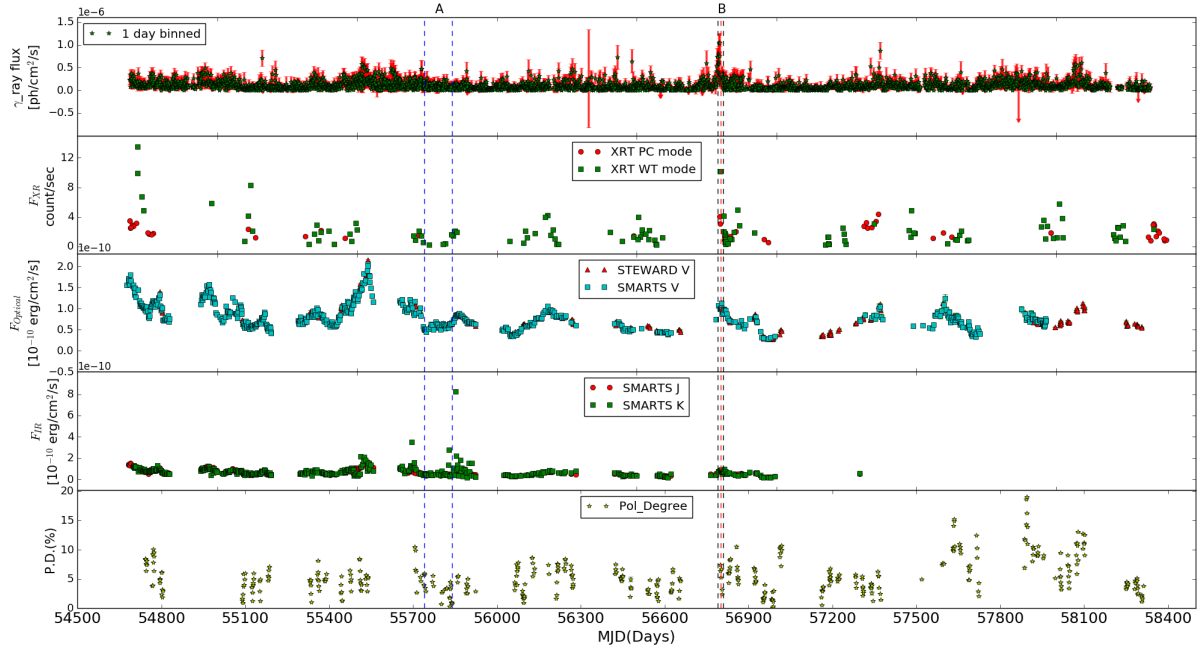
FIGURE 4.5: Multi-wavelength light curves of the source PKS 2155−304. Other details to the figure are similar to that given in the caption to Figure 4.1.
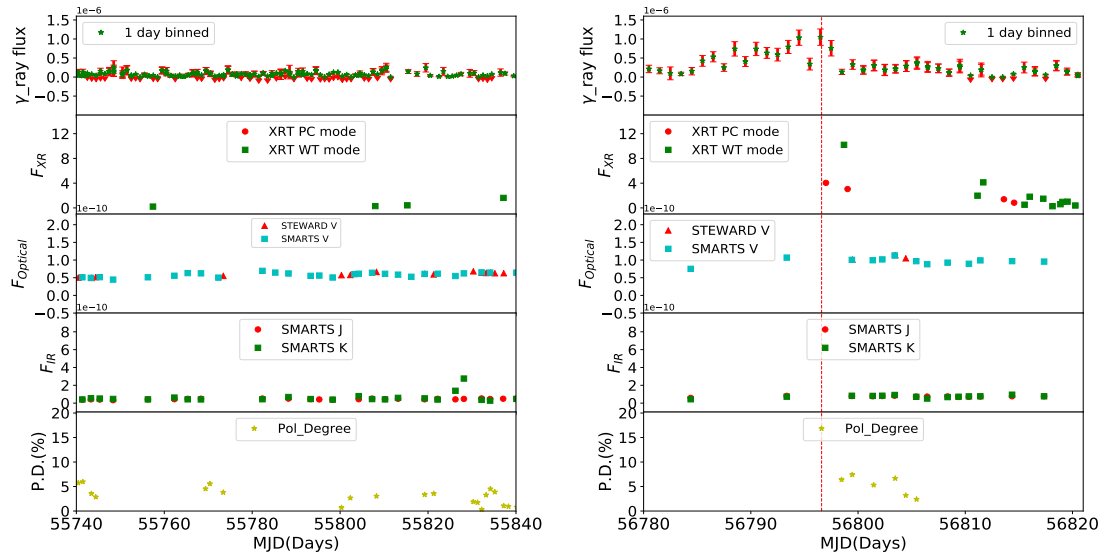
FIGURE 4.6: Multi-wavelength light curves for the selected epochs of the source PKS 2155−304. The left and right panels are for the epochs A and B respectively.

TABLE 4.2: Details of the PL and LP model fits for the selected epochs of the sources AO 0235+164, OJ 287 and PKS 2155−304. Here the γ-ray flux value is in units of 10^{-7}ph cm^{-2} s^{-1}. The value of Γ, α and β mentioned here are obtained by fits to the data which matches with the values returned by fermipy.

| | PL | | | | LP | | | | | |
Epochs	Γ	Flux	TS	$-$Log L	α	β	Flux	TS	$-$Log L	TS$_{curve}$
AO 0235+164										
A	-1.90±0.02	3.90±0.13	3874.64	31241.99	1.94±0.03	0.05± 0.02	9.64±0.12	4413.69	30888.09	707.8
B	-1.95±0.01	3.60±0.05	2617.2	27655.91	1.98±0.03	0.08± 0.03	8.64±0.12	2982.15	27330.24	651.36
C	-2.40±0.16	0.19±0.11	71.97	69867.23	2.40±0.18	0.06± 0.06	0.92±0.12	133.52	69843.77	46.94
D	-1.91±0.16	1.03±0.12	87.59	21402.72	1.91±0.18	0.07± 0.00	1.42±0.05	95.85	21422.97	-40.50
OJ 287										
A	-2.44±0.13	0.43±0.05	104.512	57896.37	2.48±0.16	0.07± 0.17	0.40±0.02	98.39	57897.17	-0.16
B	-2.51± 0.16	0.87±0.19	109.77	15636.63	2.95±0.41	0.30± 0.27	1.47±0.09	143.06	15634.43	4.40
C	-1.88±0.11	1.77±0.37	205.64	8613.66	1.87±0.15	0.07± 0.02	2.46±0.20	242.103	8601.86	23.60
D	-2.72±0.14	1.97±0.24	184.95	9139.01	2.88±0.40	0.09± 0.23	3.01±2.32	254.03	9129.45	19.12
PKS 2155−304										
A	-1.78±0.04	0.41±0.04	831.04	51370.55	1.84±0.05	0.09± 0.04	0.85±0.06	934.67	51344.24	52.62
B	-1.62± 0.04	4.09±0.40	1541.92	14844.11	1.83±0.06	0.02± 0.03	4.97±0.54	1621.77	14822.00	44.22
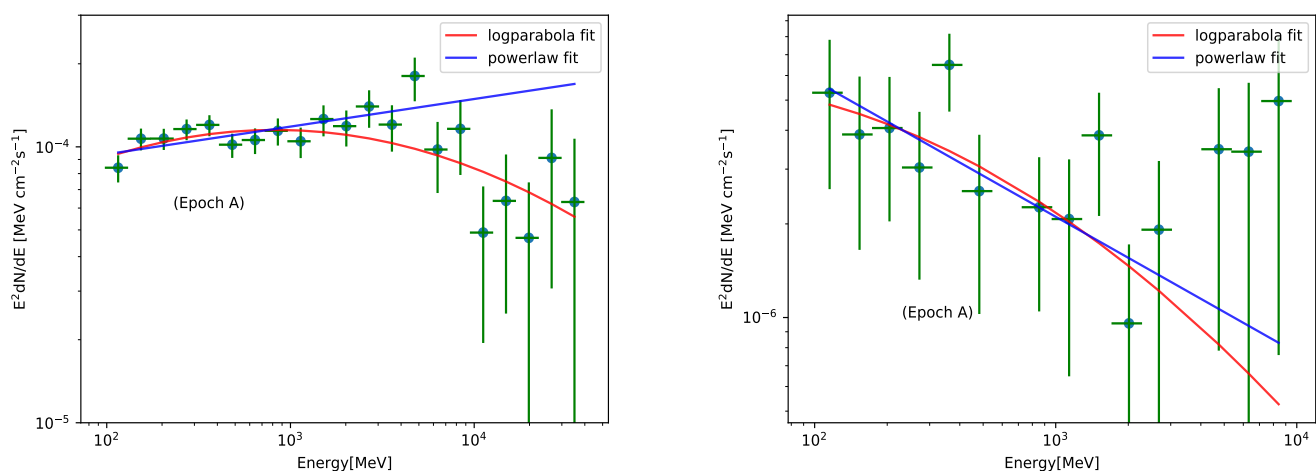
FIGURE 4.7: Observed and model fits to the γ-ray spectra. Left: Epoch A of AO 0235+164 well fit by the LP model and Right: Epoch A of OJ 287 well described by the PL model.

For comparison, I also generated the broad band SED for a quiescent state in each of the sources. To generate the SEDs, all photometric measurements during each epoch as summarized in Table 4.1 were averaged filter wise in the optical and IR bands to get one photometric point for each epoch. For X-rays and γ-rays, average X-ray and γ-ray spectra were generated using all data during the period of each epoch. Blazars are known to show flux variations over a range of time scales (Wagner and Witzel 1995). Also during the time ranges considered here for SED analysis, the brightness states of the sources were not stable in most of the wavelengths. Therefore, the source parameters obtained by fitting the time averaged SED could be treated as average/typical values applicable for the duration that is considered. In the one zone leptonic emission model the low energy hump of the broad band SED of BL Lacs is due to synchrotron emission from relativistic electrons in the jet, while the high energy hump is mostly attributed to SSC processes. For example in the source PKS 2155$-$304, Wierzcholska *et al.* (2019b) explains the high energy part of the SED using SSC process. The flare of the source in June 2013 was well fit by leptonic model, while the flare of April 2013 was fit with lepto-hadronic model (Abdalla *et al.* 2020). Also, the interest in the modelling of blazar SED has increased due to the finding of an association of the IceCube neutrino with blazars such as TXS 0506+056 (IceCube Collaboration *et al.* 2018a) and BZB J0955+3551 (Paliya *et al.* 2020). In spite of the different model fits attempted on BL Lac sources such as PKS 2155$-$304 at different periods, I performed a statistical fitting of the broad band SEDs using synchrotron, synchrotron self Compton and external Compton mechanisms. The details of the model as implemented within XSPEC can be found in Sahayanathan *et al.* (2018). This XSPEC implementation of the model also gives the errors in the best fitting parameters through the χ^2 minimization technique. To account for the model as well as observational (for example, non-removal of host galaxy contribution in the optical brightness of the sources) uncertainties, we added 12% systematics to the data. The model has twelve free parameters, namely particle spectral index

before the break (p), the particle spectral index after the break (q), electron energy density (U_e), minimum Lorentz factor of the electrons (γ_{min}), the maximum Lorentz factor of the electrons (γ_{max}), the break Lorentz factor of the electrons (γ_b), magnetic field (B), size of the emission region (R), bulk Lorentz factor of the jet (Γ), viewing angle of the jet (θ), the temperature of the external photon field (T), and the fraction of the external photons that take part in the EC process (f). The number of parameters defining the model SED is larger than the spectral information extracted from observed SED and this force us to freeze some parameters to typical values and perform the fitting procedure. Hence, the fitting was performed only on five parameters namely p, q, B, Γ and U_e; while the remaining seven parameters are frozen to their typical values (Table 4.3). Consistently, the validity of the fitted parameters will heavily depend on the choice of these frozen parameters. The observed SED along with the model fits are given in Figure 4.8 to Figure 4.10. The best fit model parameters are given in Table 4.4. A quick look into the best fit power-law indices of the particle spectrum disfavors the radiative cooling origin of the broken power-law electron distribution. Under this interpretation, one may expect the difference in the power-law index to be $\sim$1 (p and p+1). The corresponding difference in the synchrotron spectral index will be $\sim$0.5 (Rybicki and Lightman 1986). However, the spectral index difference of blazars exceeds this value (Figure 27. of Abdo *et al.* 2010c). The large difference in particle indices is also seen in case of CGRaBS catalog (Figure 9 of Paliya *et al.* 2017a). An alternate explanation for the broken power-law distribution with large index difference could be the presence of multiple acceleration scenarios (Sahayanathan 2008). In addition, the excessively large index difference can also be an artifact introduced by a steeply decaying spectrum. For the sources AO 0235+164 and OJ 287, during all the epochs, the high energy component is well fit by EC with the seed photons for the EC scattering coming from the dusty torus. For the source PKS 2155−304, the high energy component is well fit by SSC model.
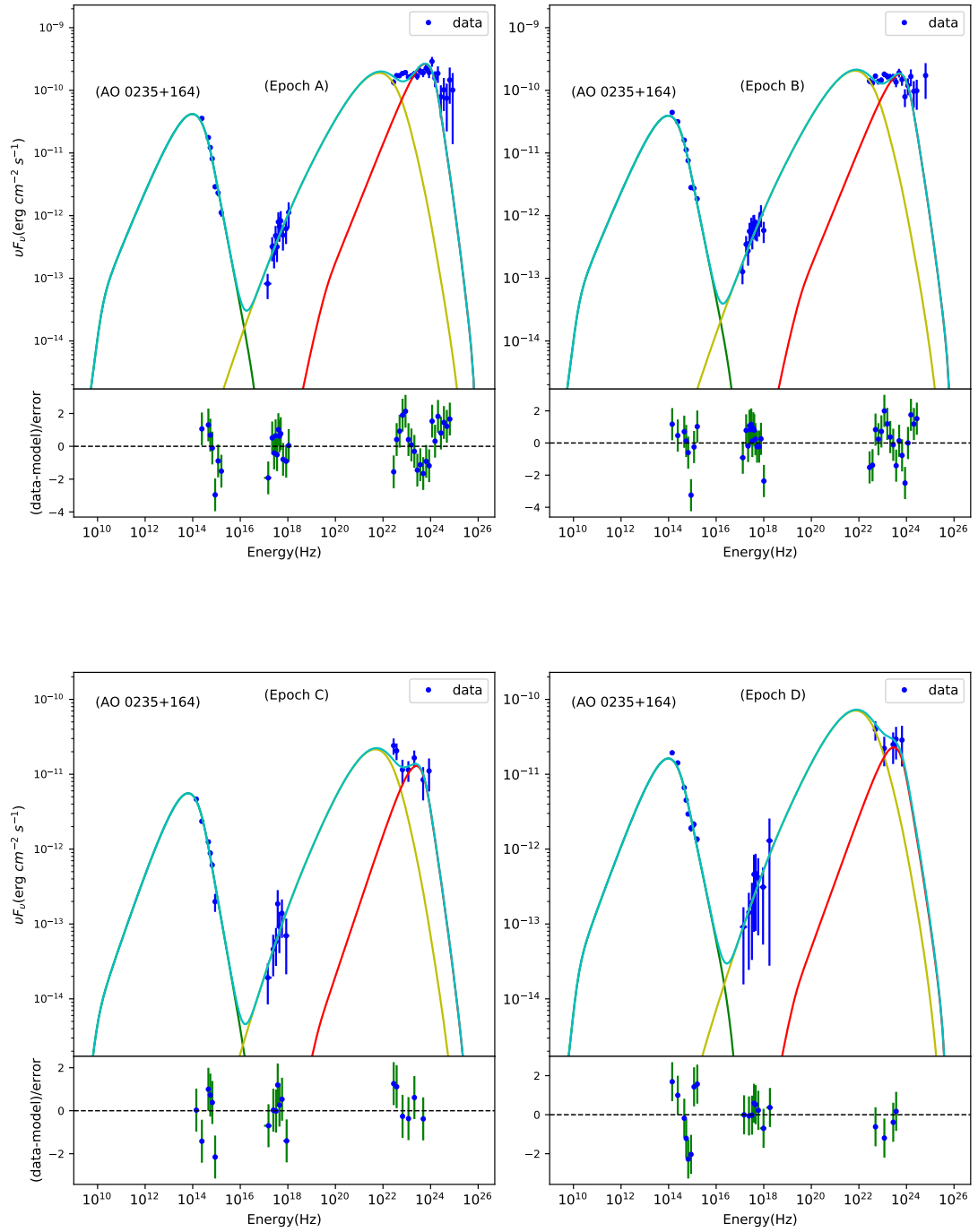
FIGURE 4.8: One zone leptonic model fits to the broad band SED for epochs A, B, C and D for the source AO 0235+164. In the figures, the green line is the synchrotron emission, the yellow and red lines are the SSC and EC components respectively. The cyan line is the sum of all the components. The second panel in the figures show the residuals.
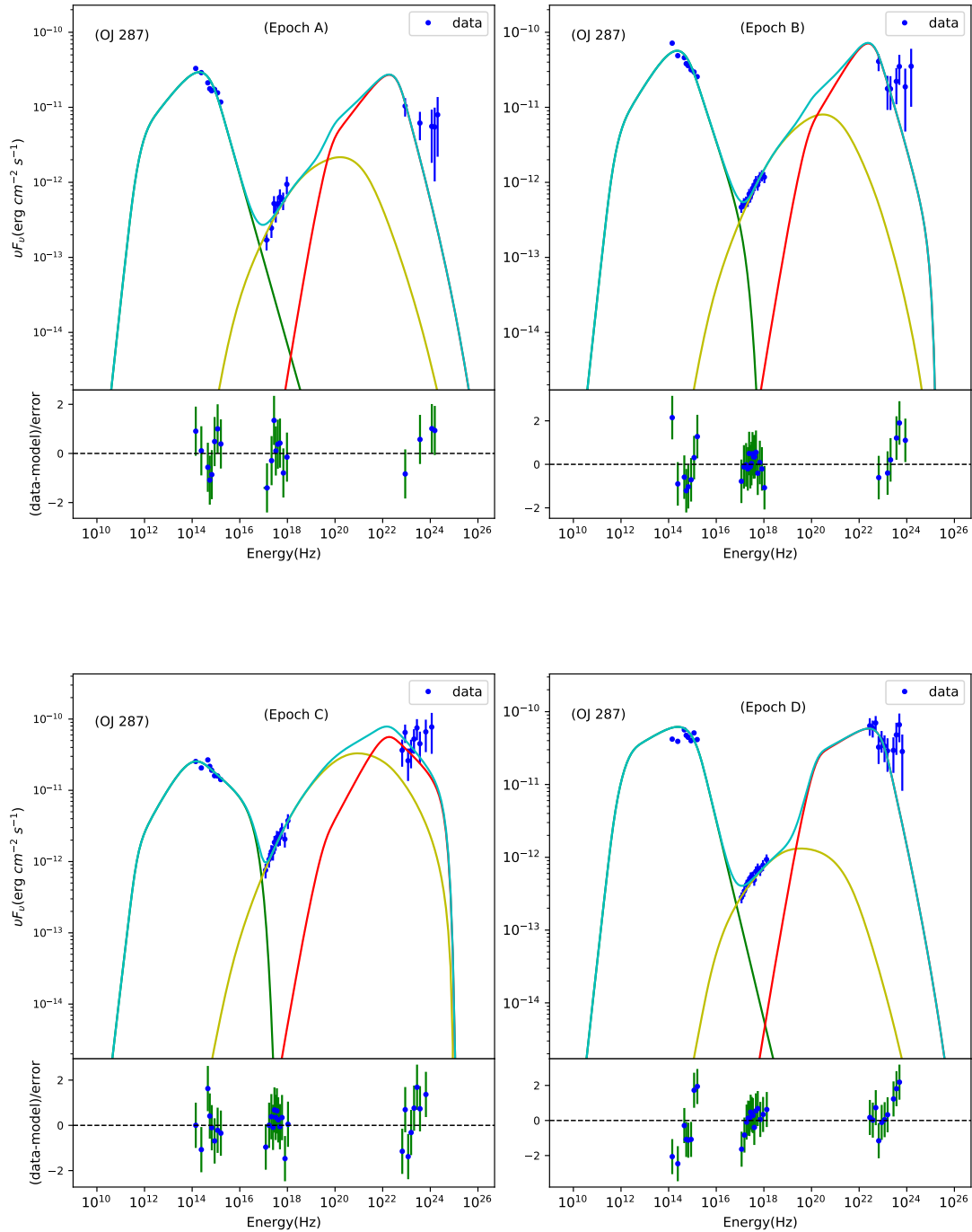
FIGURE 4.9: One zone leptonic model fits to the broad band SED for epochs A, B, C and D for the source OJ 287. The details to the figures are the same as those given in Figure 4.8.

TABLE 4.3: Values of the parameters that were frozen during the model fits to the observed SED. The viewing angle of 2° was assumed in all the SED model fits. The size of the emission region is in units of 10^{16} cm.

Object	R	γ_{min}	γ_{max}	γ_b	Temperature (K)	f	State
AO 0235+164	25.1	50	1×10^5	8000	800	0.001	A, B, C, D
OJ 287	0.63	50	2×10^4	1200	800	0.9	A,B,C,D
PKS 2155−304	15.8	50	1×10^6	2.5×10^4	−	−	A, B

TABLE 4.4: Results of the broad band SED analysis for the sources at different epochs

Name	Epoch	Bulk Lorentz factor	Low energy particle index	High energy particle index	Electron energy density (cm^{-3})	Magnetic field (Gauss)	χ^2/dof
AO 0235+164	A	10.31 ± 0.33	1.10 ± 0.12	7.00 ± 0.62	0.005 ± 0.0004	0.06 ± 0.002	1.7
	B	9.23 ± 0.31	1.13 ± 0.05	6.77 ± 0.23	0.006 ± 0.0005	0.06 ± 0.002	1.6
	C	5.86 ± 0.47	1.10 ± 0.25	6.61 ± 0.42	0.004 ± 0.0008	0.06 ± 0.004	1.2
	D	6.43 ± 0.80	1.24 ± 0.14	6.08 ± 0.21	0.005 ± 0.001	0.08 ± 0.009	1.5
OJ 287	A	6.12 ± 1.40	1.10 ± 0.95	4.26 ± 0.26	0.16 ± 0.09	3.15 ± 0.30	0.8
	B	10.57 ± 1.97	1.93 ± 0.36	4.97 ± 0.39	0.06 ± 0.02	4.12 ± 0.58	0.9
	C	6.82 ± 1.21	1.75 ± 0.29	3.58 ± 0.20	0.30 ± 0.12	2.12 ± 0.17	0.8
	D	19.03 ± 8.60	2.62 ± 0.41	5.74 ± 0.83	0.02 ± 0.007	6.48 ± 1.16	1.4
PKS 2155-304	A	6.05 ± 2.43	2.26 ± 0.05	6.38 ± 0.65	0.001 ± 0.0003	0.12 ± 0.10	1.3
	B	11.78 ± 6.90	2.02 ± 0.15	3.26 ± 0.08	0.001 ± 0.0006	0.03 ± 0.02	0.7

4.2 Results and Discussion

4.2.1 Connection between optical and GeV flux variations

The nature of seed photons that participate in the IC process to explain the high energy emission in BL Lac objects is highly debated. Cross-correlation analysis between variations in the optical band and Gev γ-ray band on a large sample of blazars tend to support the scenario of EC to be the dominant process in FSRQs and SSC being the dominant process in BL Lacs (Cohen *et al.* 2014). On analysis
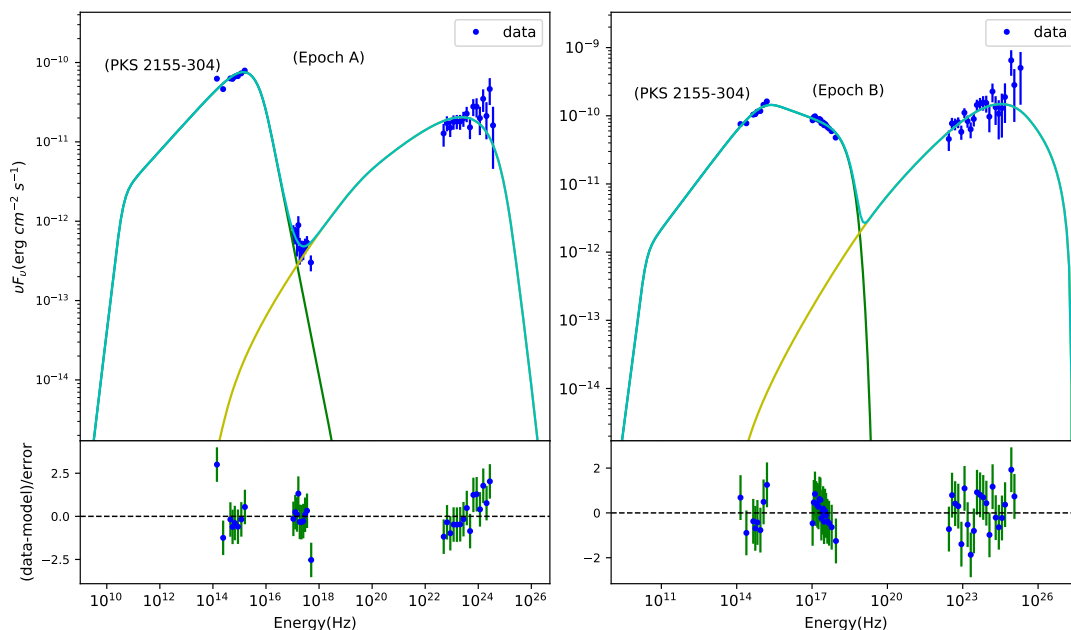
FIGURE 4.10: One zone leptonic model fits to the broad band SED for epochs A and B for the source PKS 2155−304. The different components in the figure have the same meaning as that of Figure 4.8.

of the relation between optical and γ-ray flux variations on a large sample of blazars, Hovatta *et al.* (2014) found SSC to be the dominant high energy emission mechanism in ISP and HSP sources, while EC is more dominant in LSP sources. Though these studies broadly support the one-zone leptonic emission from blazar jets, the recent observations of uncorrelated optical and GeV flares challenge one zone models of blazar emission. The existence of such uncorrelated flux variations between the optical and GeV bands are known today owing to the capabilities of *Fermi* and supporting ground based observations at longer wavelengths in the optical bands. I have examined here on the prevalence of uncorrelated optical and GeV flux variations in the BL Lac objects. Based on the criteria outlined in chapter 2, I arrived at a sample of three objects namely A0 0235+164, OJ 287 and PKS 2155−304. In all the three objects in the epochs where flares are studied in this work, the optical and γ-ray flux variations are correlated. However, some observations point to scenarios of uncorrelated optical and GeV flux variations to be a common feature in blazars. Recently, from a discrete correlation function

analysis of a sample of 178 blazars, Liodakis *et al.* (2019) found that about 50% of optical flares have no γ-ray counterparts and about 20% of γ-ray flares have no optical counterparts. This has increased our knowledge on the prevalence of correlated optical and gamma-ray flux variations in blazars manifold compared to the earlier reports available on few individual sources (Chatterjee *et al.* 2013; Dutka *et al.* 2013; Cohen *et al.* 2014; MacDonald *et al.* 2015; Rajput *et al.* 2019, Rajput et al. 2020).

In AO 0235+164, during epochs A, B and D, I found variations in the optical and GeV γ-rays are closely correlated. This is a LSP source (Ackermann *et al.* 2015a) and the high energy emission in the broad band SEDs during all the epochs of this source is well fit by EC process with the seed photons for inverse Compton scattering being the IR emission from the torus (see Figure 4.8). The high energy emission is via EC process is also studied by Hovatta *et al.* (2014). The multi-wavelength analysis of the source AO 0235+164 conducted by Baring *et al.* (2017) also suggests the presence of EC process, which is responsible for the high energy emission. The radiation output from inverse Compton emission, that constitutes the high energy component is a function of the energy density of the electrons U_e, Lorentz factor Γ and the density of the external photon field that participates in IC scattering. At the same time, the radiation output from synchrotron process that constitutes the low energy component in the SED depends on U_e, Γ and magnetic field B. During epochs A and B, compared to the quiescent period, I found the bulk Lorentz factor to increase by a factor of around 1.8 and 1.6 in epochs A and B respectively. At the same time the electron energy density during epochs A and B has increased relative to the quiescent state. This increase in bulk Lorentz factor and electron energy density has lead to increased optical and γ-ray flare. Thus the correlated optical and γ-ray flux variations during epochs A and B can be attributed to the increase of Γ and U_e. At epoch D, I have an optical flare with a γ-ray counterpart. Our leptonic model fit showed marginal increase in B-field during this epoch, relative to the quiescent period. This has given rise to

increased optical emission. A plausible reason for the increase in magnetic field B can be due to the alignment of B-field via shocks in the jets. Though Γ during the epoch is greater than the quiescent period. U_e has also increased relative to the quiescent period. Hence, the correlated optical and γ-ray flare seen during epoch D can be inferred as a result of increase in Γ, B and U_e.

OJ 287 is a LSP BL Lac and here too the high energy part of the SED at different epochs is described by EC process with the seed photons from the dusty torus. In this source, I found during all the flaring epochs considered here the optical flare is correlated with the γ-ray flare (see Figs. 4.3 and 4.4). For epoch B, comparison of the model parameters obtained from SED fits (see Table 4.4) shows that U_e has decreased by a factor of about 2.5, while Γ has increased by a factor of about 2, and the B field has increased marginally. The correlated optical and γ-ray flare during epoch B is due to a factor of 2 increase in Γ coupled with a marginal increase in the B-field. During epoch C, again we noticed correlated optical and γ-ray flare. At this epoch relative to the quiescent period, Γ is similar while U_e has increased by about a factor of 2, which could lead to increased optical and γ-ray flare. For epoch D too, I observed an optical flare with a γ-ray counterpart. The magnetic field and Γ obtained from SED model fit during this epoch is a factor of 2 and 3 larger than the quiescent period. Thus, the correlated optical and γ-ray flare seen during this epoch is due to a change in the magnetic field in the emitting region and increase in Γ.

For the source PKS 2155$-$304, I identified two epochs, epoch A, a quiescent period and epoch B, an active period with an increased optical state coinciding with a γ-ray flare (see Figure 4.5). This is a HSP BL Lac and the high energy emission in the broad band SED both during the quiescent and flaring state is fit by SSC process in our one-zone leptonic modelling approach. This source has also been extensively studied by various authors for multi-wavelength variability and broad band SED modelling, however, different processes have been invoked at different

periods of the source to explain the observations. For example multi-wavelength observations carried out on the source during 25 August 2008 − 06 September 2008, Aharonian *et al.* (2009) found correlation between the optical brightness changes with the changes in the VHE γ-rays, but the optical variations did not correlate with the GeV γ-rays. The authors argue that the population of electrons that were responsible for optical emission may be different from those responsible for GeV and VHE γ-rays. From an analysis of the optical and GeV γ-rays during the period 2007 to 2009, H. E. S. S. Collaboration *et al.* (2014) found varied correlations between the optical and GeV γ-rays. They found instances of (a) correlation between optical and GeV γ-rays, (b) anti-correlation between optical and GeV γ-rays and (c) no-correlation between optical and GeV γ-rays. In this work too, during epoch B, I have an enhanced γ-ray with a peak value of about two times the quiescent level. Similarly in the optical too there is an enhancement of about a factor of 2 relative to the base optical brightness, but available observations lack optical measurements during the peak of the γ-ray flare. X-ray flux enhancement too is not coincident with the GeV flare. From SED modelling, the Γ during epoch B is ~ 1.9 times larger than that at the quiescent epoch. The correlated optical and gamma-ray flare at this epoch is thus due to an increase in Γ. In this work, though the observed high energy SEDs are modelled well with either the EC (for AO 0235+164 and OJ 287) or SSC (PKS 2155−304), in all the sources I noticed that the γ-ray spectra have hard component which were not fit with our one-zone leptonic model. This is also seen in the residuals of the broad band SED fits. Such rising γ-ray spectrum is also seen at certain epochs in the blazar 3C 279 (Paliya *et al.* 2016). The hard γ-ray spectrum in 3C 279 is also not fit by the one zone leptonic model and is explained by either the two-zone leptonic model or the lepto-hardronic model. Co-ordinated multi-wavelength observations of many blazars are indeed needed to see if such complicated variability patterns and broad band SEDs are witnessed in many other blazars. Though in the leptonic scenario a correlation between optical and GeV flux variations is expected, contrary to the hadronic scenario, in which a close correlation is not expected, the observations

of varied variability behaviours in the same source suggest that variability studies might not be definitive in constraining leptonic v/s hadronic models of emission in blazar jets. Also, I note that even in the case of the association of the IceCube neutrino detection with the blazar TXS 0506+056, which argues for the hadronic component in the SED of blazars, SED modelling of the source points to leptonic process for the observed GeV and high energy γ-rays (Gao *et al.* 2019).

4.3 Summary

In an effort to identify correlated as well as uncorrelated flux variations between optical and GeV γ-ray band in BL Lac objects, I carried out a systematic analysis of flux variations in three BL Lac objects namely AO 0235+164, OJ 287 and PKS 2155−304. The results of this work are summarized below.

1. All the three BL Lacs showed correlated variations between optical and γ-rays during the flares analyzed in this work.

2. The high energy hump of the broad band SED of AO 0235+164 and OJ 287 at all epochs are described by inverse Compton scattering of IR photons from the torus. For PKS 2155−304, the SEDs at all epochs are fit by synchrotron and synchrotron self Compton process. However, in all the sources, there is a hard γ-ray component that is not fit by the one-zone leptonic model.

3. The instances of correlated flux variations in the optical and GeV bands in the one-zone leptonic scenario can be explained by changes in the bulk Lorentz factor, magnetic field and electron density.

Chapter 5

Long-term γ-ray variability in blazars *

Blazars have been studied for their γ-ray variability since the launch of *Fermi* in the year 2008. However, most of the time, individual sources were analysed for variability, which, in addition to γ-rays utilizes data from other wavelengths (Bonning *et al.* 2009; Chatterjee *et al.* 2012; Paliya *et al.* 2015; Rajput *et al.* 2019). There are a limited number of studies in the literature that focus on the γ-ray flux variability characteristics of a large sample of blazars. The first study focusing on the γ-ray flux variability of blazars is by Abdo *et al.* (2010e) who analysed 11 months of data from the *Fermi* LAT for a total of 106 objects. Similarly, the γ-ray flux variability of high redshift ($z > 3$) blazars has recently been investigated by Li *et al.* (2018). Quasi-periodic oscillation on year-like time scales has also been reported from the analysis of the long term γ-ray light curves of blazars (Ackermann *et al.* 2015b; Zhang *et al.* 2017; Gupta *et al.* 2019; Bhatta 2019). However, a careful re-analysis of the same data set for a few objects for

---

*The contents of this chapter are from
Bhoomika Rajput, C. S. Stalin, Suvendu Rakshit, 2020, AA, 634A, 80

which quasi-periodicities were reported did not yield any solid evidence as to the existence of year-long periodicities in the γ-ray light curves (Covino *et al.* 2019; Castignani *et al.* 2017). This as well as our limited knowledge on the long term γ-ray flux variability characteristics of blazars necessitates a systematic analysis on the γ-ray flux variability properties of blazars carried out in a homogeneous manner. Such a study is now possible due to the availability of γ-ray data for a large number of blazars for a long duration of time.

In this chapter, I present the results on the long term γ-ray flux variability characteristics (that includes flux variability amplitude and time scale of variability) of different classes of blazars. The sample consists of 1120 blazars of which 481 are FSRQs and 639 are BL Lacs. In addition to characterising variability, I also looked for a correlation of variability with other physical properties of the sources such as the mass of the black hole (M_{BH}) and Doppler factor (δ).

5.1 Monthly binned light curves

The γ-ray light curves of my sample of sources were generated for a period of about nine years from 2008 August 11 to 2017 December 31. The light curves were generated with a time binning of one month which results in 114 bins for each light curve. For each interval I calculated the flux and test statistic (TS) values for every source. The TS values were calculated using the maximum likelihood function `gtlike`. I considered a source to be detected at any epoch if its TS > 9 (3σ detection). At epochs where TS < 9, the source was considered undetected. In Figure 5.1 and Figure 5.2, I show the light curves of a few FSRQs and BL Lacs from the sample. It is likely that many light curves do not have flux measurements every month and missing flux points are due to the source's flux below the detection threshold.
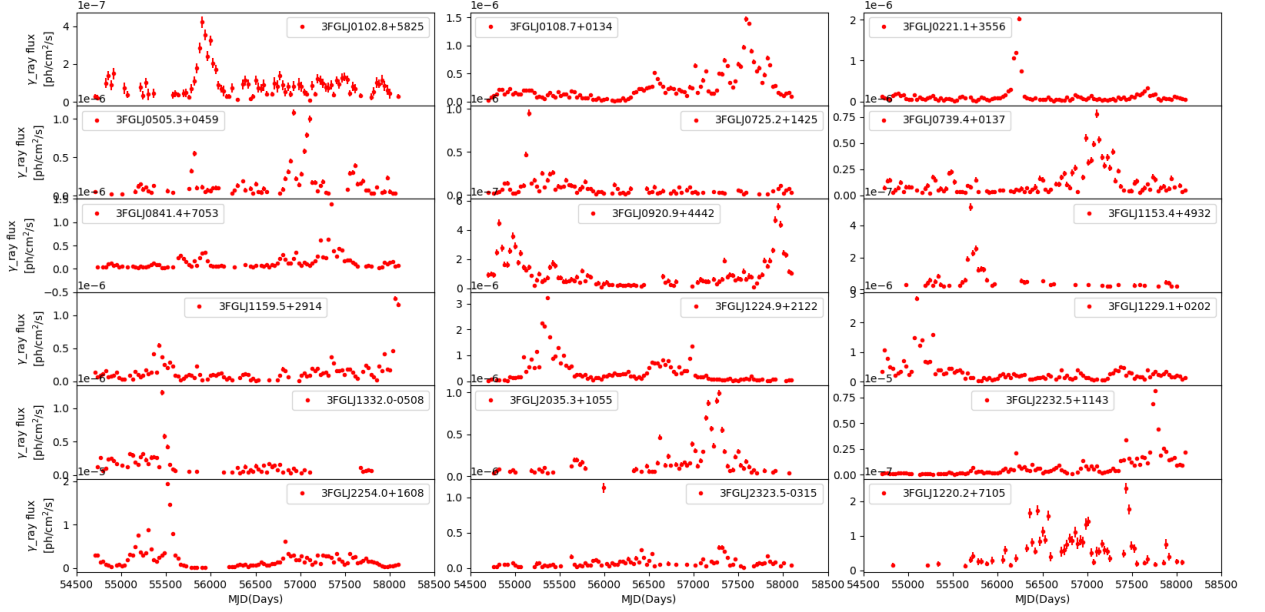
FIGURE 5.1: Example light curves for variable FSRQs. The light curves generated on monthly time bins have their integrated fluxes measured between 100 MeV−300 GeV. The points are the flux values in the monthly bins with TS > 9 (approximately 3 σ) and the error bars are their 1 σ values. The names of the sources are given in each panel.

5.2 Flux variability amplitude

To quantify flux variability, I used the fractional root mean square variability amplitude (F_{var};Vaughan *et al.* 2003). This is defined as

$$F_{var} = \sqrt{\frac{S^2 - \overline{\sigma_{err}^2}}{\bar{x}^2}} \tag{5.1}$$

where S^2 is the sample variance and $\overline{\sigma_{err}^2}$ is mean square error. They are given as

$$S^2 = \frac{1}{N-1} \sum_{i=1}^{N} (x_i - \bar{x})^2 \tag{5.2}$$
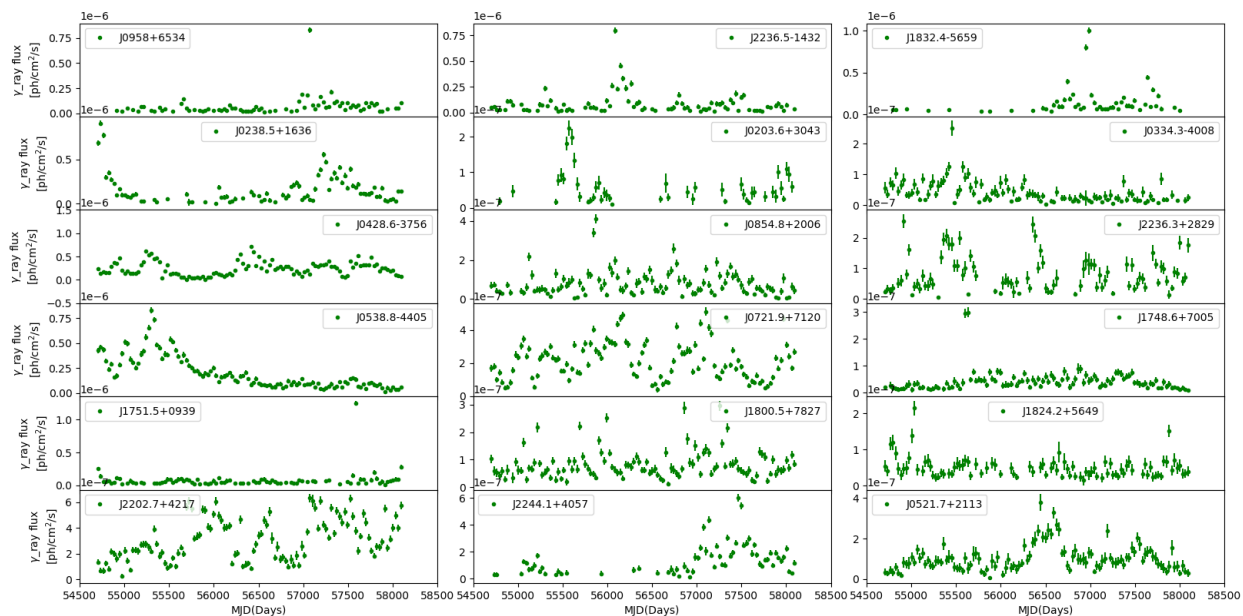
FIGURE 5.2: Example monthly binned light curves (TS > 9) along with their 1 σ errors for BL Lacs. The names of the sources are given in each panel. Each point in the light curves refers to flux measured in the 100 MeV−300 GeV band

and

$$\sigma_{err}^{\bar{2}} = \frac{1}{N} \sum_{i=1}^{N} \sigma_{err,i}^2 \,, \tag{5.3}$$

Here, σ_i is the statistical uncertainty, to which I added the systematic uncertainty $\sigma_{syst} = 0.03 < \mathrm{x}_i >$ in quadrature (Abdo *et al.* 2009) to get the total error σ_{err} defined as

$$\sigma_{err}^2 = \sigma_i^2 + \sigma_{sys}^2 \tag{5.4}$$

The uncertainty in F_{var} is defined as (Rani *et al.* 2017)

$$err(F_{var}) = \sqrt{\left(\sqrt{\frac{1}{2N}} \frac{\sigma_{err}^{\bar{2}}}{\bar{x}^2 F_{var}}\right)^2 + \left(\sqrt{\frac{\sigma_{err}^{\bar{2}}}{N}} \frac{1}{\bar{x}}\right)^2} \tag{5.5}$$
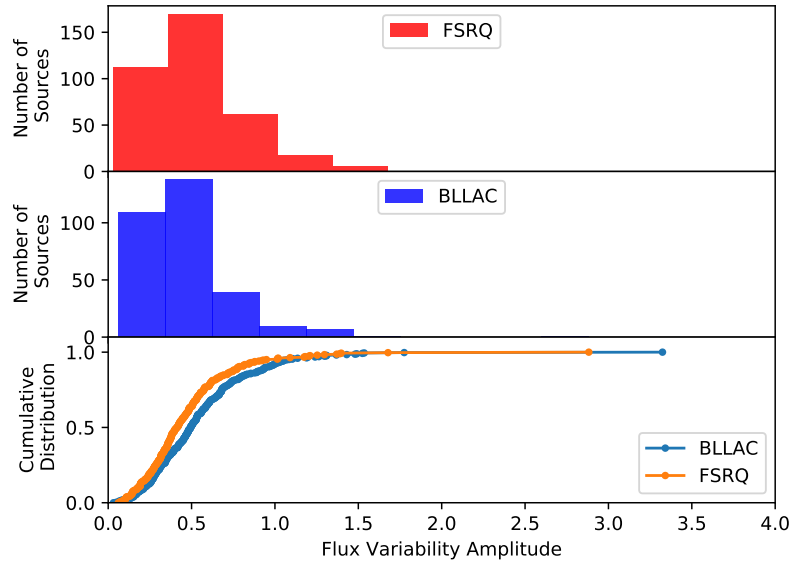
FIGURE 5.3: Histogram and cumulative distribution of F_{var} for variable FSRQs and BL Lacs.
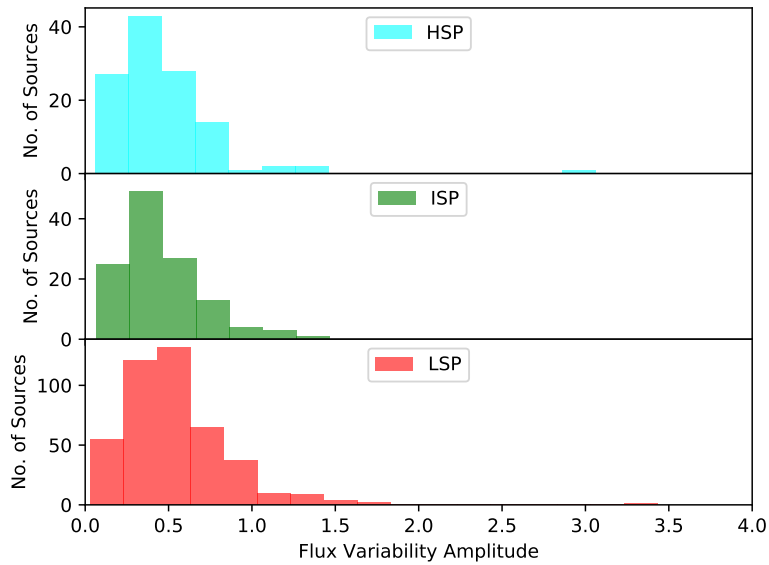
FIGURE 5.4: Distribution of F_{var} values for variable LSP, ISP and HSP blazars.
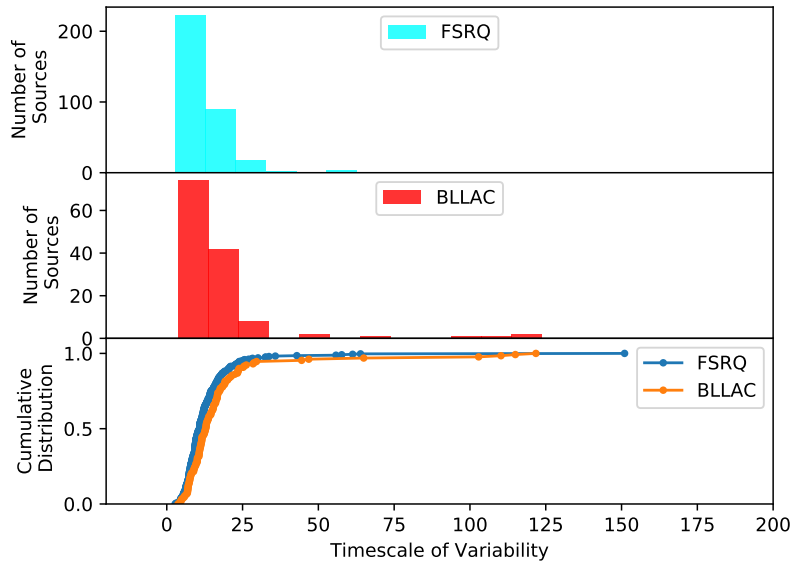
FIGURE 5.5: Histogram and cumulative distribution of the time scale of variability (days) for FSRQs and BL Lacs. The time scales of variability are corrected for the redshift of the sources.
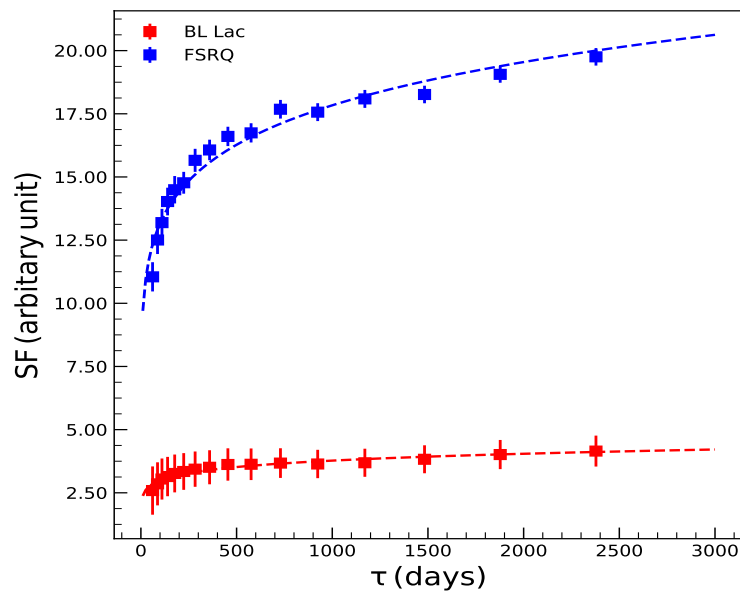
FIGURE 5.6: Structure function (SF) against observed frame time lag for BL Lacs (red dots) and FSRQs (blue dots). The dashed lines are the best fits to the SF using Equation 5.9.
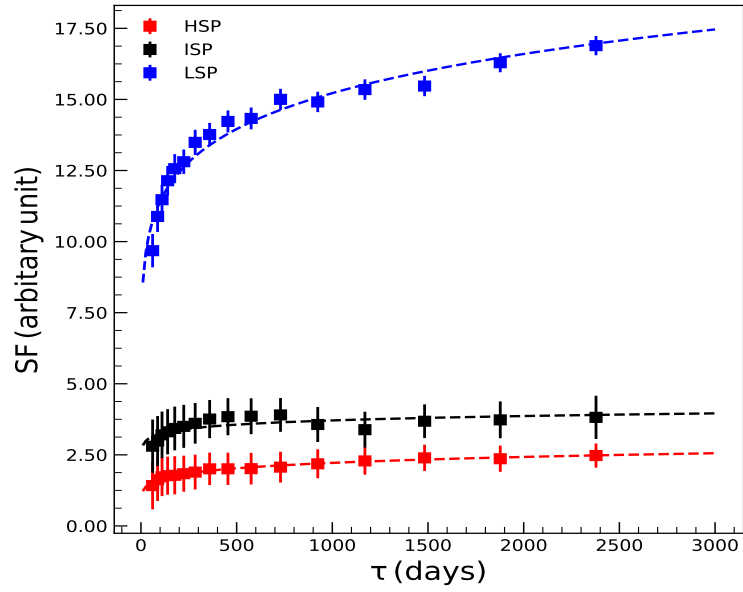
FIGURE 5.7: Structure functions for HSP (red), ISP (black) and LSP (blue) blazars. The dashed lines are the best fits to the SF using Equation 5.9.

.
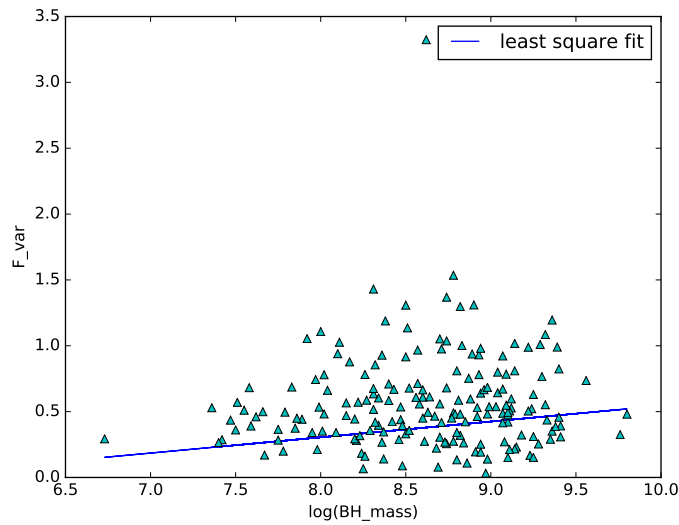
FIGURE 5.8: Correlation between F_{var} and M_{BH} values for FSRQs. The solid line is the unweighted linear least squares fit to the data
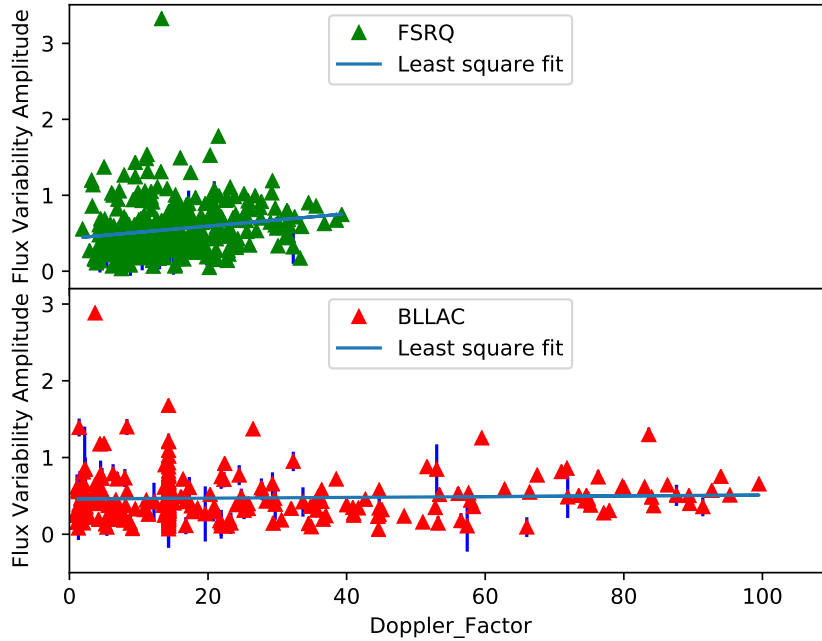
FIGURE 5.9: Relation between F_{var} and Doppler factor for FSRQs (top panel) and BL Lacs (bottom panel). Unweighted linear least squares fit to the data are shown as solid lines.
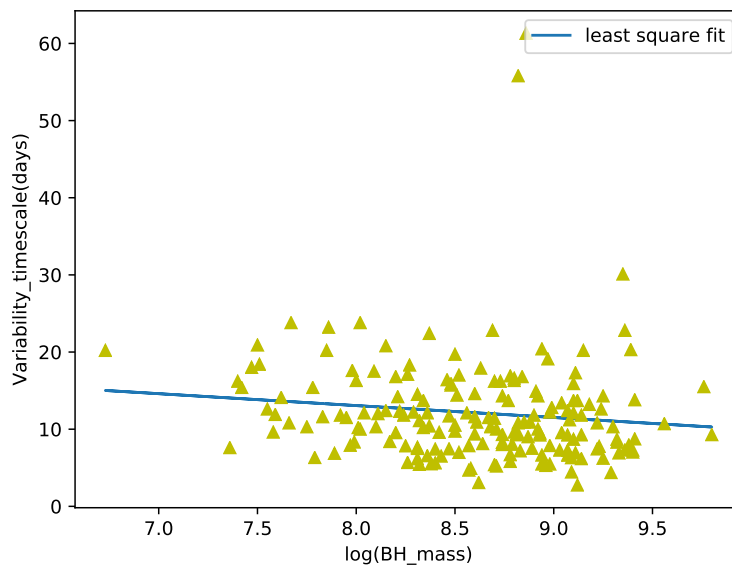
FIGURE 5.10: Correlation between time scale of variability and M_{BH} for blazars. The solid line is the unweighted linear least squares fit to the data points.
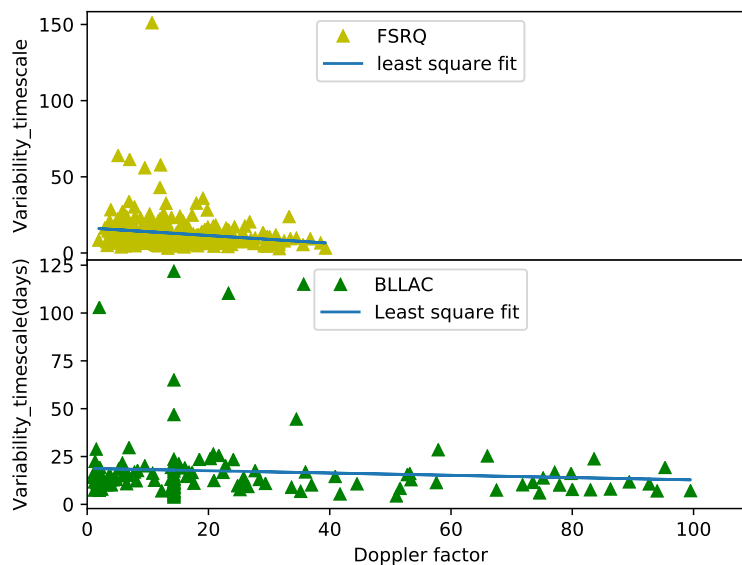
FIGURE 5.11: Correlation between time scale of variability and Doppler factor for FSRQs(top panel) and BL Lacs (bottom panel). Linear least squares fit to the data are shown as solid lines.

In Figure 5.3, the distribution and cumulative distribution of F_{var} for FSRQs and BL Lacs are shown. I found mean F_{var} values of 0.47 ± 0.29 and 0.55 ± 0.33 for BL Lacs and FSRQs, respectively. A two sample Kolmogorov Smirnov (KS) test shows that the two distributions are indeed different at the 95% level with statistics of 0.15 and a p value of 0.001. I also sub-divided the sample into different spectral energy distribution classes based on the peak frequency of the low energy synchrotron component in their broad-band SED. The mean F_{var} values for the different sub-classes are 0.54 ± 0.33 for LSPs, 0.45 ± 0.25 for ISPs, and 0.47 ± 0.33 for HSPs. The distribution of F_{var} values for the different sub-classes are shown in Figure 5.4 Ackermann *et al.* (2011) also find a similar trend of flux variations in the γ-ray band for different classes of blazars.

5.3 Duty cycle of variability

I calculated the duty cycle (DC) of variability, including only those sources that have a redshift measurement, in order to determine the fraction of time a particular class of sources shows flux variations. The DC was estimated following Romero *et al.* (1999) and is given as

$$DC = 100\frac{\Sigma_{i=1}^{N}Q_i(1/\Delta t_i)}{\Sigma_{i=1}^{N}(1/\Delta t_i)} \tag{5.6}$$

where $\Delta t_i = \Delta t_i(1 + z)^{-1}$ is the time in the rest frame of the source, $N_i = 1$ if a particular source is variable, or else $N_i = 0$. For FSRQs, I found a DC of 66%, while for BL Lacs, I found a DC of 36%. For the sub-classes of blazars I found DCs of 65%, 43%, and 36% for LSP, ISP, and HSP blazars, respectively. Thus, LSP sources show a larger DC of γ-ray variability on month-like time scales related to the other classes of blazars.

5.4 Variability timescale

The variability time scale (τ) is a very important parameter that can be deduced from the light curves, which in turn can provide constraints on the physical processes that cause γ-ray flux variations. Since I analysed monthly binned light curves in this work, I was able to probe time scales of the order of months. I calculated τ of γ-ray flux variability for the sources in the sample that showed γ-ray flux variability following Jorstad *et al.* (2013)

$$\tau \equiv \triangle t/ln(S_2/S_1) \tag{5.7}$$

Here S_2 and S_1 are the flux values at times of t_2 and t_1, respectively, and $\Delta t = |t_2\text{-}t_1|$. In order to estimate τ, I considered all possible pairs of flux values that satisfy the conditions (i) $S_2 > S_1$ and (ii) $S_2 - S_1 > 3(\sigma_{S_1} + \sigma_{S_2})/2$, where σ_{S_2} and σ_{S_1} are the uncertainties corresponding to the flux measurements S_1 and S_2, respectively. Among all of the calculated values of τ for a particular source, I considered the minimum τ value as the timescale of variability of the source with the γ-ray flux changing by a factor greater than 2. The histogram and cumulative distribution of τ for FSRQs and BL Lacs are shown in Figure 5.5.

5.5 Ensemble structure function

The variability of AGN can also be described by the structure function (SF), which shows the dependency of variability as a function of time lag (Simonetti *et al.* 1985). The SF can be calculated for individual AGN that have a light curve with multiple epochs of observations, which takes the magnitude difference for each pair of time lags in a light curve. It can also be calculated for a group of AGN, known as the ensemble structure function, allowing us to obtain the mean variability behaviour of the population that is similar to what has been obtained from the flux variability amplitude. I studied the mean variability of different classes of AGN by using the ensemble structure function following di Clemente *et al.* (1996)

$$\text{SF} = \sqrt{\frac{\pi}{2} < |\Delta m| >^2 - < \sigma^2_n >}, \tag{5.8}$$

where $|\Delta m| = m_i - m_j$, is the magnitude difference between any two epochs (i, j) that are separated by time $\Delta \tau = t_i - t_j$. $\sigma^2_n = \sigma^2_i + \sigma^2_j$, which is the square of the uncertainty of the magnitude differences. As majority of our sources do not have redshift measurements in the literature, thus, the SF was calculated in the observed frame. In Figure 5.6, is shown the SF against the observed frame time lag

for BL Lacs (red) and FSRQs (blue). The error bar in the SF was calculated via error propagation following Vanden Berk *et al.* (2004). Figure 5.6 clearly shows that FSRQs are more variable than BL Lacs, which is consistent with the result obtained by F_{var} analysis. The SF increases gradually from time lags ranging from one to ∼400 days and becomes flatter at higher time lags. Such a trend has been noted previously by various authors (Vanden Berk *et al.* 2004; Welsh *et al.* 2011; Kozłowski 2016). To characterise the structure function, I fitted the following simple power-law model:

$$ \text{SF} = S_0 \times \left(\frac{\Delta \tau}{\tau_0} \right)^{\gamma} . \tag{5.9} $$

By adopting τ_0=4 years in the observed frame (Kozłowski 2016) I estimated S_0 and γ. The fitting results are given in Table 5.1. S_0 is higher in FSRQs than in BL Lacs, suggesting that the former has higher variability than the latter. This is also confirmed from the higher flux variability of the FSRQs compared to BL Lacs. In Figure 5.7, the SFs of HSP, ISP, and LSP are shown. I found that LSPs have stronger variability followed by ISP and HSP blazars. This is also in agreement with that was obtained from the F_{var} analysis.

Based on the analysis of 106 γ-ray light curves using 11 months of data from *Fermi*, Abdo *et al.* (2010c) find FSRQs to show a higher amplitude of γ-ray variability than other AGN classes. Similarly, from an analysis of the sources in the second LAT AGN catalogue, Ackermann *et al.* (2011) find FSRQs to have more flux variability than BL Lacs. According to Ackermann *et al.* (2011), the higher variability seen in FSRQs relative to BL Lacs could be attributed to the location of the high-energy peak (in the broad-band SED of blazars) with respect to the *Fermi* band. In the *Fermi* band, FSRQs are observed at energies greater than the inverse Compton peak in the SED; the observed emission is therefore produced by high-energy electrons with shorter cooling time scales and thereby shows more variations. Alternatively, in the *Fermi* band, BL Lacs are observed at frequencies

TABLE 5.1: Results of model fits to the structure function using power-law model.

Object class	S_0 (10^{-8} ph cm^2 s^{-1})	γ
BL Lac	3.92 ± 0.04	0.100 ± 0.007
FSRQ	18.70 ± 0.20	0.132 ± 0.007
HSP	2.33 ± 0.02	0.129 ± 0.006
ISP	3.79 ± 0.08	0.058 ± 0.014
LSP	15.95 ± 0.16	0.124 ± 0.007

much lower than the inverse Compton peak, the low-energy electrons have longer cooling time scales, and therefore show low variations. The results obtained in this work on a large sample of blazars having data spanning about nine years is in agreement with the earlier results that obtained on a smaller sample of blazars with less time coverage (Ackermann *et al.* 2011; Abdo *et al.* 2010c).

5.6 F_{var}, M$_{BH}$, and Doppler factor

I searched in the literature for the availability of M_{BH} values for the sources analysed for variability here. I could gather M_{BH} values (Chen 2018) for a total of 184 FSRQs. In Figure 5.8, is shown the plot of F_{var} as a function of M_{BH} for FSRQs. There is a weak indication of larger γ-ray flux variations in sources with large M_{BH} values. However, linear least squares fit to the data showed an insignificant correlation between F_{var} and M_{BH} with a linear correlation coefficient of 0.07. Lu and Yu (2001) carried out an analysis of the X-ray flux variations on a composite sample of Seyfert 1 galaxies, quasars and narrow line Seyfert 1 galaxies and found a significant anti-correlation between X-ray variability and M_{BH}. Upon the analysis of the long term optical variability characteristics of a large sample of quasars, Zuo *et al.* (2012) could not find any correlation between M_{BH} and

variability amplitude, however, other studies have found a correlation between quasar variability and M_{BH} (Wold *et al.* 2007; Bauer *et al.* 2009), while Kelly *et al.* (2009) found a negative correlation between M_{BH} and quasar variability. Ai *et al.* (2010) note that the correlation between optical variability and M_{BH} vanishes when the Eddington ratio is controlled.

The correlation between F_{var} and δ for FSRQs and BL Lacs is shown in Figure 5.9. The values of δ was also collected from Chen (2018). The figure is suggestive of a positive correlation between F_{var} and δ. However, from the linear least squares fit to the data points, I found no correlation between F_{var} and δ in both FSRQs and BL Lacs. Any small changes in the jet emission in blazars would get Doppler boosted, leading to the large amplitude of flux variations by the observer. Even though our data sets are indicative of such a correlation, no clear trend could be established.

5.7 Time scale of variability, M_{BH}, and Doppler factor

Knowledge on the time scale of flux variations in blazar light curves is very important as it can provide us important clues as to the physical processes responsible for γ-ray flux variations in blazars. The power spectral density (PSD) is generally used to quantify the time scale of flux variations in blazars, however, I followed the approach given in Equation 5.7 to determine the time scale of variability in the monthly binned blazar light curves. From a homogeneous analysis of the blazar light curves, I found that most of the sources analysed in this work have a time scale of variability that is less than 50 days, while few sources have time scales larger than 100 days. From a PSD analysis of the weekly and daily binned γ-ray light curves of 13 blazars spanning about ten years, Ryan *et al.* (2019) observed

two time scales of variability, the longer time scale having a duration of the order of years and the shorter time scale spanning of the order of days. According to them, the longer time scales might represent the thermal time scale of the accretion disc, while the shorter time scales may be related to processes in the jet. For most of the sources analysed here, the estimated time scales are of the order of days, and such time scales could be related to emission processes in the jet (Ryan *et al.* 2019).

Even though, historically, blazars are separated into FSRQs and BL Lacs based on the width of the emission lines present in their optical spectrum, Ghisellini *et al.* (2009) postulated a physical distinction between FSRQs and BL Lacs. The PSDs associated with EC, which produces γ-ray emission in FSRQs, and SSC, producing γ-ray emission in BL Lacs, show different break frequencies (Ryan *et al.* 2019) . In such a scenario, different time scales of variability in the γ-ray band are expected. The distribution of τ for both FSRQs and BL Lacs are shown in Figure 5.5. A KS test indicates that the distribution for each of them is marginally different, with a statistic of 0.18 and p values of 0.004. I thus noticed a difference in the distribution of the time scales of variability between FSRQs and BL Lacs.

The correlation between τ and M_{BH} in blazars were found in the X-ray (Chatterjee *et al.* 2018) and optical (Kelly *et al.* 2009; MacLeod *et al.* 2010). In Figure 5.10, I show the correlation between τ in the γ-ray band against M_{BH}. The linear least squares fit to the data yields a low correlation coefficient of -0.12. I therefore do not find a significant correlation between τ and M_{BH}. I also do not find any correlation between τ and δ for both FSRQs and BL Lacs (Figure 5.11). Doppler boosting shortens the observed time scale by δ^{-1}, and the observed hint (though insignificant) of a negative correlation is a consequence of the effect of δ on the time scale of flux variations.

5.8 Summary

In this work I generated one month binned γ-ray light curves for a total of 1120 blazars, comprising 481 FSRQs and 639 BL Lacs to characterise their γ-ray variability with the data collected from *Fermi* for over approximately nine years. The main motivation of this is to characterise the long term (on month-like time scales) γ-ray variability nature of blazars, which includes characterising the flux variability amplitude and flux variability time scale that could put constraints on blazar emission models, in principle. In addition to characterising variability, I also looked for a correlation in variability with other physical properties of the sources such as the mass of the black hole (M_{BH}) and Doppler factor (δ). The results are summarizes below.

1. More than 50% of the blazars studied in this work are found to be variable. Out of the total 639 BL Lacs analysed for variability, 304 sources showed variability. Similarly, out of the 481 FSRQs studied for flux variability, 371 are found to be variable. Thus, about 80% of FSRQs are variable, while only about 50% of BL Lacs are variable. I found mean F_{var} values of 0.55 $\pm$ 0.33 and 0.47 $\pm$ 0.29 for FSRQs and BL Lacs, respectively. Thus FSRQs are more variable than BL Lacs in the γ-ray band. This difference in the γ-ray flux variations between FSRQs and BL Lacs can be explained by the location of the inverse Compton peak in their broad-band SED with respect to the *Fermi* observing band. Among different sub-classes of blazars, LSPs are more variable followed by ISP and HSP blazars. The ensemble structure function analysis also shows that FSRQs are more variable than BL Lacs.

2. FSRQs show the highest DC of variability of 66% relative to BL Lacs that show a DC of 36%.

3. The majority of FSRQs and BL Lacs in the sample analysed here show time scales of variability of about 20 days. This time scale could be related to

processes in the jets of these sources. The distribution of timescales between FSRQs and BL Lacs are different.

4. Statistically F_{var} is not found to be not correlated with either M_{BH} and δ. Additionally, the time scale of the γ-ray flux variability does not show statistically significant correlation between M_{BH} and δ.

Chapter 6

Optical flux and polarization variations in the flat spectrum radio quasar 3C 279 *

The radio to optical emission of blazars is observed to be highly polarized due to the synchrotron emission process from blazar jets and also highly variable in both polarization degree and position angle. A systematic study has been performed using the first and second RoboPol observing seasons on the samples of γ-ray-loud and γ-ray-quiet blazars by (Angelakis *et al.* 2016). In this study the γ-ray-loud class found to be exhibit higher polarization fraction than γ-ray-quiet blazars. This result is likely due to the fact that γ-ray-loud class of blazars are more synchrotron dominated in optical band because of high Doppler boosting and thus accelerate the particles more around the synchrotron peak. With the increasing degree of polarization the synchrotron peak frequency decreases because of the efficient acceleration of the electrons around the peak and increase in the helical

---

B-field component downstream the shock. In this thesis I aim for a systematic analysis of the optical flux and polarization variations in the flat spectrum radio quasar 3C 279. 3C 279 is a very bright FSRQ at a redshift of $z = 0.538$ (Burbidge and Rosenberg 1965). Powered by a massive black hole with a mass of 2.7×10^8 $M_\odot$ (Woo and Urry 2002), it has kilo-parsec scale jets with apparent velocities of 4 to 20c (Lister *et al.* 2013). It was among the sources to be discovered in the γ-rays (30 MeV to over 5 GeV) by the EGRET (Hartman *et al.* 1992)). It has been regularly detected in the 100 MeV to 300 GeV range by *Fermi* and on several occasions high intensity flares were recorded. It has also been detected at energies beyond 100 GeV by the ground based Cherenkov telescope MAGIC (MAGIC Collaboration *et al.* 2008). 3C 279 has also been studied for optical polarization variations (Rani *et al.* 2018). It showed a significant change in the position angle, which coincided with the γ-ray flare during 18 February 2009 to 10 March 2009 (Abdo *et al.* 2010f). During the period $2008-2012$ 3C 279 revealed different polarization behaviours at low optical flux and flaring states. According to Kiehlmann *et al.* (2016) the polarization behaviour of the source at two optical flux states could be due to two different processes, a stochastic process during low optical flux state and a deterministic process during flaring. In this work I present analysis of the relation between optical flux and polarization variations in 3C 279 on day like timescales as well as year like timescale using data for a period of 10 years between August 2008 and 2018. The total flux and polarization data in the optical V-band were taken from the archives of the Steward Observatory.

TABLE 6.1: Details of the epochs studied for correlation between flux and polarization. Here, R is the Spearman rank correlation coefficient and P is the null hypothesis probability of no correlation between flux and PD variations. NC indicates PD and total flux are anti-correlated, while PC indicates PD and total flux are positively correlated.

Time-period	Epoch	F_γ v/s time		F_{opt} v/s time		PD v/s time			F_{opt} v/s PD	
		R	P	R	P	R	P	Remark	R	P
54790 - 54810	A	−0.42	0.08	−0.91	0.01	0.73	0.02	NC	−0.75	0.05
55920 - 55930	B	−0.43	0.29	1.00	0.00	1.00	0.00	PC	1.00	0.00
55948 - 55958	C	−0.12	0.78	−1.00	0.00	0.81	0.01	NC	−0.77	0.07
56038 - 56048	D	−0.77	0.07	0.99	0.00	0.98	0.00	PC	0.99	0.00
56740 - 56751	E	0.25	0.49	0.93	0.00	−0.84	0.00	NC	−0.42	0.00
57010 - 57021	F	0.10	0.78	0.90	0.04	−0.86	0.01	NC	−0.99	0.00
57041 - 57052	G	−0.30	0.62	0.75	0.08	−1.00	0.00	NC	−0.75	0.08
57065 - 57075	H	0.03	0.96	−0.90	0.04	0.86	0.01	NC	−0.90	0.04
57124 - 57135	I	-	-	−0.94	0.00	−0.83	0.01	PC	0.73	0.03
57159 - 57169	J	0.43	0.24	0.86	0.01	0.81	0.01	PC	0.72	0.07
57913 - 57923	K	0.28	0.46	−0.97	0.00	−0.90	0.04	PC	0.82	0.09

TABLE 6.2: Statistics of the observed flux and polarization properties. F_γ is in units of 10^{-6} ph cm^{-2} s^{-1} and F_{opt} is in units of 10^{-11} erg cm^{-2} s^{-1}. The polarization degree PD is in %, while the position angle PA is in degrees.

Epoch	F_{opt}			F_γ			PD			PA		
	Min	Max	Average	Min	Max	Average	Min	Max	Average	Min	Max	Average
A	1.36	1.49	1.43±0.05	0.93	2.05	1.57±0.26	21.02	30.54	26.78±3.61	43	66	51±8
B	1.71	1.98	1.83±0.10	0.03	0.57	0.22±0.17	7.71	11.09	9.61±1.23	−353	−349	−349 ±2
C	1.36	1.74	1.54±0.14	0.14	0.45	0.29±0.01	10.68	12.79	11.79±0.77	−325	−321	−322 ±1
D	0.96	1.15	1.06±0.08	0.16	0.29	0.22±0.05	10.91	16.29	13.08±1.89	−202	−188	−196 ±6
E	1.72	2.21	2.05±0.13	0.49	6.13	2.43±1.75	9.8	13.42	10.70±0.98	−140	−123	−129 ±5
F	0.52	0.64	0.58±0.04	0.21	0.60	0.38±0.13	20.8	26.57	23.77±2.14	−143	−137	−141 ±2
G	0.88	1.04	0.96±0.06	0.19	0.29	0.22±0.04	18.09	24.01	21.14±2.14	−141	−132	−135 ±3
H	1.06	1.27	1.15±0.10	0.26	0.55	0.40±0.11	12.64	17.59	14.98±1.80	−137	−120	−127 ±6
I	0.66	0.77	0.72±0.04	—	—	—	17.70	22.29	20.45±1.85	−140	−132	−135 ±3
J	0.62	0.77	0.68±0.05	0.26	0.71	0.44±0.18	14.15	20.06	16.72±2.12	−147	−135	−143 ±4
K	0.64	0.74	0.68±0.04	0.39	1.00	0.61±0.20	6.97	14.92	10.23±3.47	−138	−133	−135 ±2

TABLE 6.3: Analysis of optical variability characteristics. The observed timescale of variability τ_{obs} is in days and the magnetic field B is in Gauss.

Epoch	F_{var}	spectral index min	max	diff	τ_{obs}	δ	B
A	0.03±0.006	0.44	0.48	0.04	0.33±0.74	1.22	1.67
B	0.06±0.004	0.48	0.58	0.10	21.94±6.73	0.67	0.13
C	0.09±0.008	0.48	0.48	0.00	17.91±4.58	0.74	0.14
D	0.08±0.004	0.39	0.44	0.05	21.96±3.37	0.60	0.13
E	0.06±0.002	0.04	0.44	0.39	3.63±5.57	1.11	0.35
F	0.08±0.004	0.44	0.53	0.09	10.90±1.67	0.65	0.20
G	0.07±0.004	0.39	0.48	0.09	9.79±1.37	0.68	0.22
H	0.09±0.008	0.44	0.53	0.09	14.89±3.05	0.66	0.17
I	0.06±0.008	0.04	0.39	0.34	21.15±6.50	0.53	0.14
J	0.08±0.004	0.34	0.48	0.14	11.40±1.75	0.63	0.20
K	0.06±0.01	0.24	0.48	0.24	16.41±9.17	0.50	0.17

6.1 Analysis

6.1.1 Optical and γ-ray lightcurves

The optical and γ-ray light curves during the time interval $2008-2018$ (MJD $54500-58400$) are shown in Figure 6.1. In addition to optical and γ-ray fluxes, optical V-band PD and electric vector position angle (PA) are also plotted. I adopted the standard procedure to overcome the 180° ambiguity in the PA measurements (Abdo *et al.* 2010f; Ikejiri *et al.* 2011; Blinov *et al.* 2015), wherein changes in the PA between consecutive measurements should be minimum i.e. $-90° \leq \Delta\theta \leq 90°$. Here, $\Delta\theta$ is defined as $|\theta_n - \theta_{n-1}| - \sqrt{\sigma(\theta_n)^2 + \sigma(\theta_{n-1})^2}$, where θ_{n-1} and θ_n are the $(n-1)^{th}$ and nth measurement of PA and $\sigma(\theta_{n-1})$, $\sigma(\theta_n)$ are the corresponding errors of the PA measurements. For $\Delta\theta > 90°$, θ_n is shifted to $\theta_n - 180°$ and for
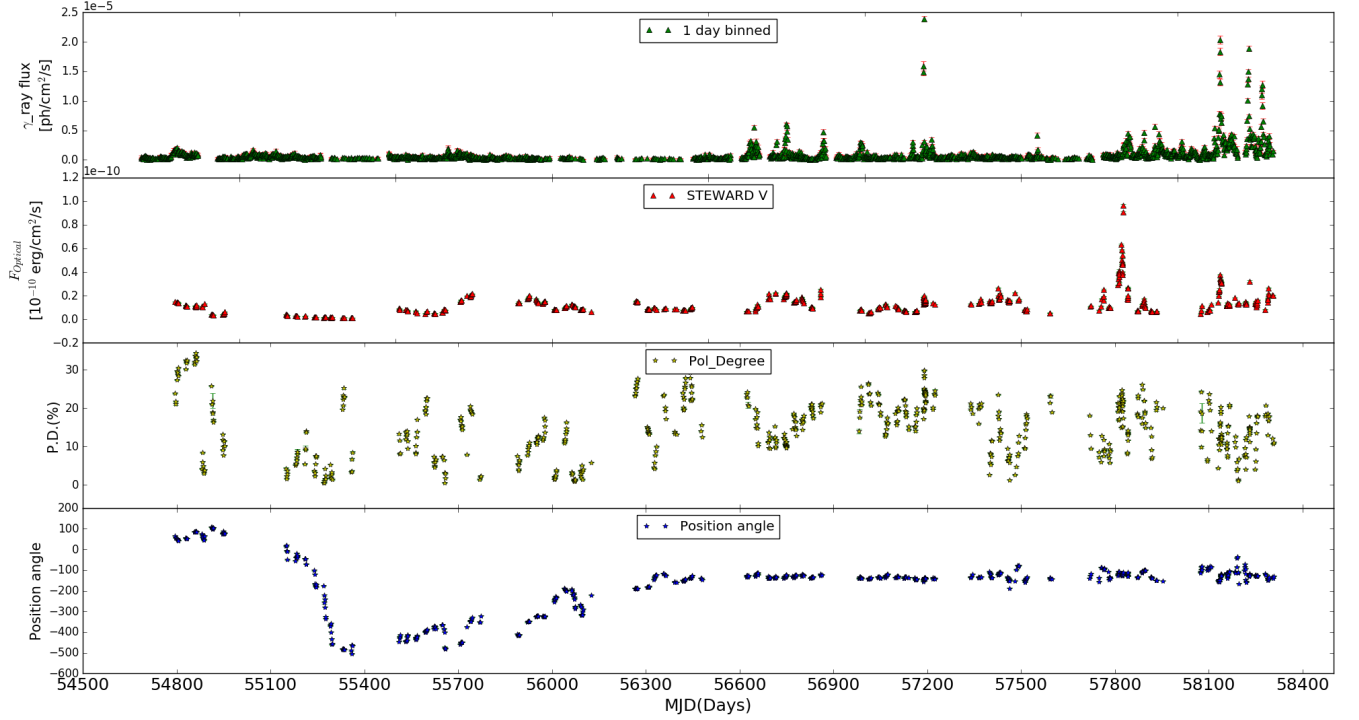
FIGURE 6.1: Multi-wavelength light curve for the source 3C 279. From the top, the first panel shows the 1 day binned γ-ray light curve for the time range MJD 54500-58400; the second panel shows the optical light curve in V-band, the third panel shows the variation of the degree of polarization and the fourth panel shows the variation of PA (corrected for the 180° ambiguity.)

$\Delta\theta < -90°$, θ_n is shifted to $\theta_n + 180°$.

6.1.2 Relation between optical flux and polarization

During the whole period the source showed a maximum V-band brightness of 13.28 ± 0.01 mag and a minimum V-band brightness of 17.99 ± 0.04 mag. During the same period, the PD showed minimum and maximum values of 0.63 ± 0.15% and 34.5 ± 0.06% respectively. I examined the correlation between total flux and PD on both day like timescales and year like timescales. Firstly, I divided the 10 year period into 10 segments based on the seasonal gaps over this 10-year period. These
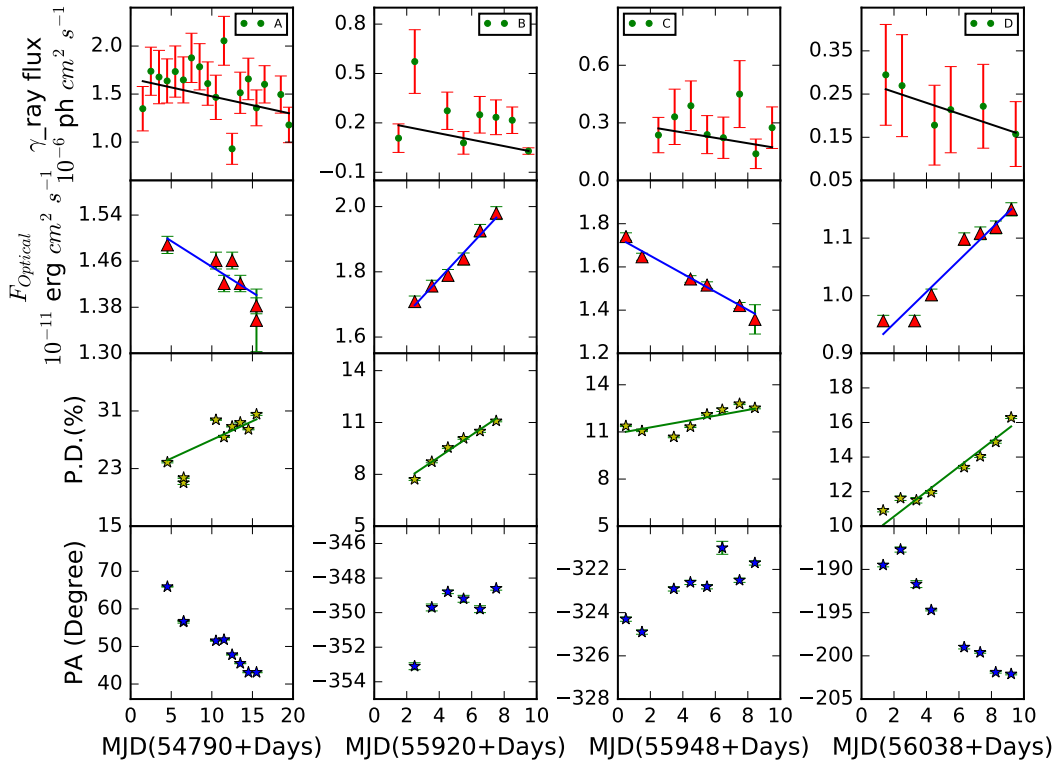
FIGURE 6.2: Multi-wavelength light curves along with polarization measurements for epochs A,B,C and D. The names of the epochs are given in each panel. In each panel, from the top, the first panel shows the one day binned γ-ray light curve, the second panel shows the light curve in the optical V-band, the third and fourth panels show the variation the degree of optical polarization and position angle respectively. The solid lines are the linear least squares fit to the data.

10 epochs were used for studying the relation between flux and PD on year like timescales. To explore the correlation between flux and PD on day like timescale, I inspected each of these 10 sub light curves. Each sub light curves were then divided into segments. For each segment I imposed a criteria of having a minimum of 5 measurements in PD, PA, and V-band total flux. By this approach I selected a total of 55 segments with each segment having observations that span about 10 days. This period matches with the Steward Observatory's monitoring program that carries out observations in cycles, and each observing cycle corresponds to observing runs of ~10 days every month (Patiño-Álvarez *et al.* 2018). I carried
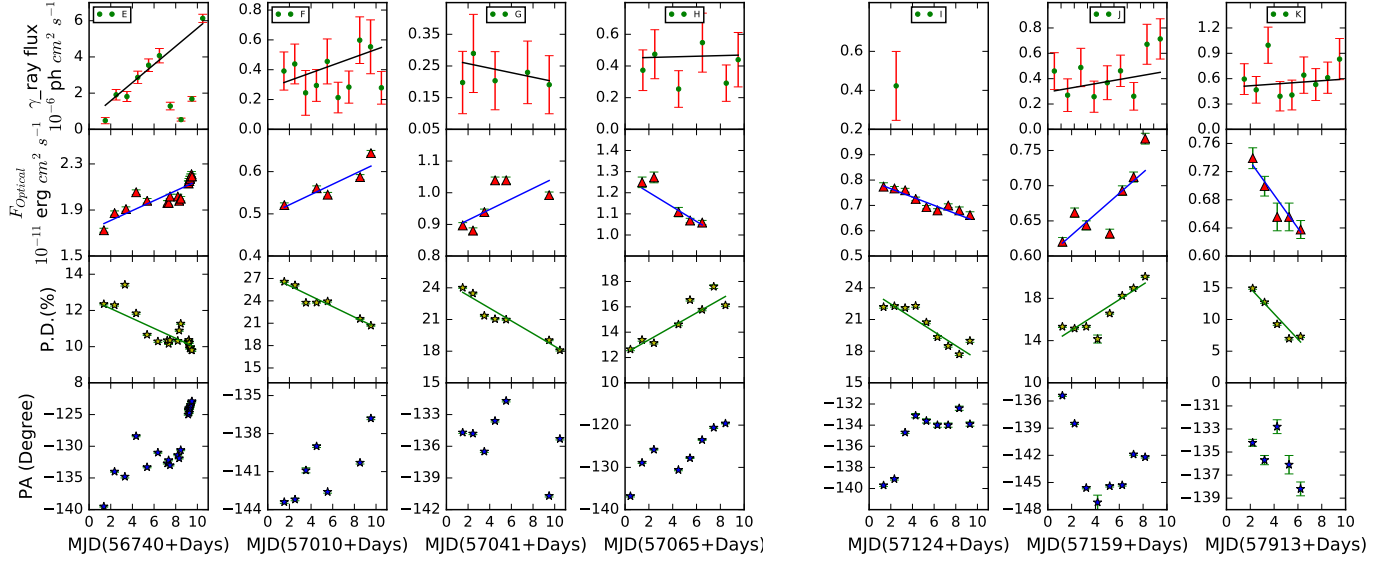
FIGURE 6.3: Multi-wavelength light curves along with polarization measurements for epochs E to K. The panels have the same meaning as in Figure 6.2.

out linear least squares fit to the data points in the PD v/s total flux variation plane for each of the 55 segments by taking into account the errors in both PD and total flux. For detailed analysis I considered only those segments that satisfy the following criteria (i) the Spearman rank correlation coefficient between PD and total flux must be either > 0.5 or < -0.5 and (ii) the null hypothesis probability for no-correlation between PD and flux is < 0.05. By applying the above two criteria I arrived at a total of 11 epochs for further correlation analysis. A summary of these eleven epochs is given in Table 6.1. The optical and γ-ray light curves along with PD and PA for those 11 epochs are given in Figs. 6.2 and 6.3. The statistics of the flux and polarization variations are given in Table 6.2. Further details on these 11 epochs are given below

1. Epoch A: During this epoch the γ-ray flux remained nearly stable. While the optical flux decreased by a factor of about 1.2, the PD increased by a factor of 1.5 and the PA decreased by about 25 deg. During this period, PD significantly anti-correlates with the total flux.
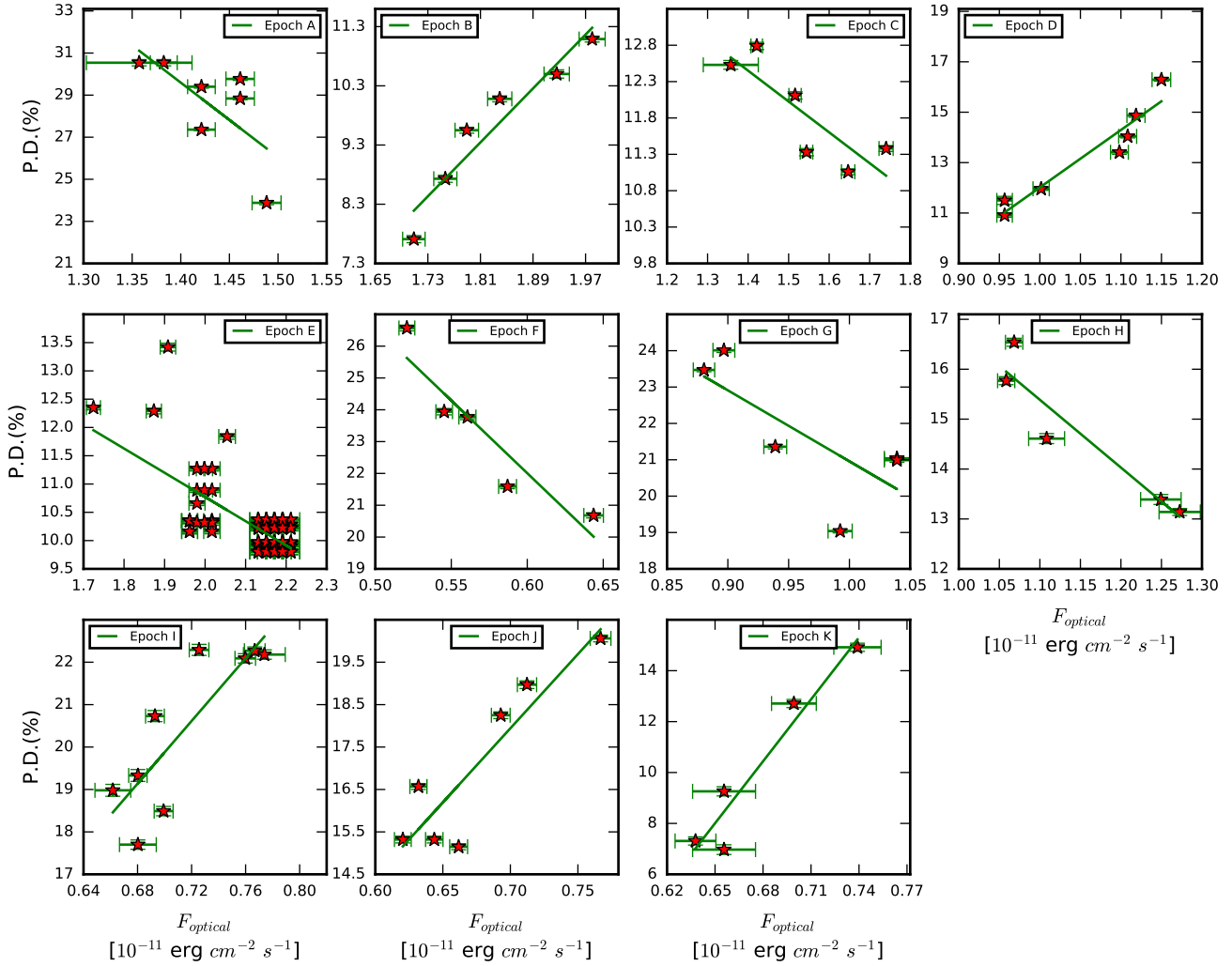
FIGURE 6.4: Relation between total flux and degree of polarization in the optical V-band. The names of the epochs are given in each panel. The solid line is the linear least squares fit to the data.

2. Epoch B: The γ-ray flux during this epoch tend to show a gradual decline. This is not statistically significant and therefore consistent of being constant. The optical flux and PD increased by factors of 1.2 and 1.5 respectively. The PA too gradually increased by about 6 deg during this period. The total flux and polarization is tightly correlated with a Spearman rank correlation coefficient of unity and a probability of no correlation close to zero (see Table. 6.1).

3. Epoch C: The γ-ray flux is consistent with constant during this epoch. Optical flux decreased with time, while PD increased with time. PA gradually increased by $\sim$4 deg. The PD is anti-correlated with total flux at the 90% confidence level with a Spearman rank correlation coefficient of -0.77.

4. Epoch D: Both optical flux and PD increased with time during this epoch, while γ-ray flux decreased with time, which is statistically significant at greater than the 90% level. PA gradually decreased by $\sim$15 deg. There is thus a tight positive correlation between optical flux and polarization with a Spearman rank correlation coefficient of 0.99 and a probability of no correlation close to zero.

5. Epoch E: There is a hint for the γ-ray flux to increase with time. However, this is statistically insignificant and consistent with a constant. There is increase in the optical flux, while the PD decreased by a factor of 1.2. PA was nearly constant except for a sudden increase by about 10 deg in the last two days. The optical flux was thus found to be anti-correlated with PD.

6. Epoch F: During this epoch the source did not show variation in γ-rays statistically consistent to have a constant flux. Optical flux increased with time, while PD decreased with time. PA decreased by $\sim$ 6 deg, returned to the original in the next two days and again increased by $\sim$ 8 deg. There is strong anti-correlation between optical flux and PD with a Spearman rank correlation coefficient of -0.99 and a probability of no correlation close to zero.

7. Epoch G: The γ-rays during is epoch is non-variable. Optical brightness increased with time, while PD decreased with time. PA was constant for $\sim$5 days, increased by about 2 deg in the next two days, further decreased by about 8 deg and again increased by 8 deg during the next two days. In this epoch PD is anti-correlated with the total flux significant to better than 90%.

8. Epoch H: The γ-ray emission from the source has not shown any variation during this epoch. During this period, optical flux decreased with time while PD increased with time. PA increased by about 20 deg in 10 days time. The PD is found to be anti-correlated with flux with a Speraman rank correlation coefficient of -0.90 and a probability of no correlation of 0.04.

9. Epoch I: The source was undetected by *Fermi* during most of the time during this epoch. Both optical flux and PD decreased with time. PA increased by about 8 deg in the beginning 3 days, remained steady at 135 deg during the next one week. Thus in this epoch PD is positively correlated with flux with a Spearman rank correlation coefficient and probability of no-correlation of 0.73 and 0.03 respectively.

10. Epoch J: Variation in the γ-ray flux during this epoch was found to be statistically consistent with a constant flux. Both optical flux and PD were nearly constant for about 3 days in the beginning and then both increased with time. Both PD and flux are positively correlated with a Spearman correlation coefficient of 0.73 and a probability of no correlation of 0.07. PA decreased by about 12 deg in the beginning and then gradually increased by about 6 deg.

11. Epoch K: The γ-ray flux from the source did not show variations. Both flux and PD increased with time. PA decreased by about 10 deg during the initial four days and remained steady during the remaining time.

Thus, among the 11 epochs analysed for correlation between PD and flux on day like timescales, on five epochs, I noticed positive correlation, while on six epochs, PD was found to be negatively correlated with total flux. The linear least squares fit to the points in the PD against total flux plane for all the eleven epochs are given in Figure 6.4. On year like timescales, I found the observations to be randomly distributed in the PD v/s flux plane with no significant correlation between the two.
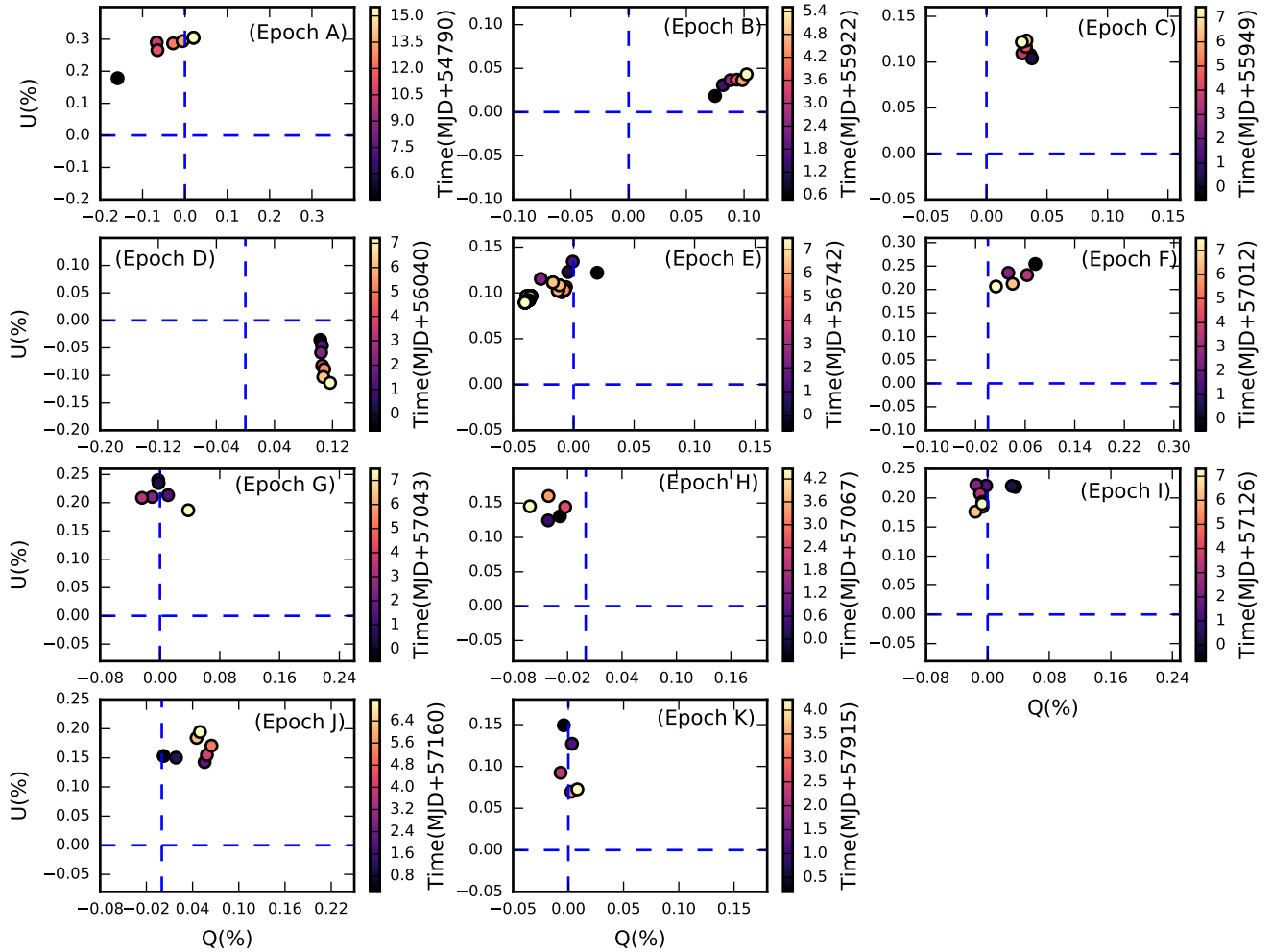
FIGURE 6.5: Plot of Stokes U against Stokes Q for the 11 epochs. The Q=0 and U=0 are shown as blue dashed lines.

6.2   Results and Discussion

6.2.1   Optical flux variability

During the whole 10 year period the source varied in V-band brightness by about 100 times having the brightest and faintest brightness of 13.28 ± 0.01 mag and
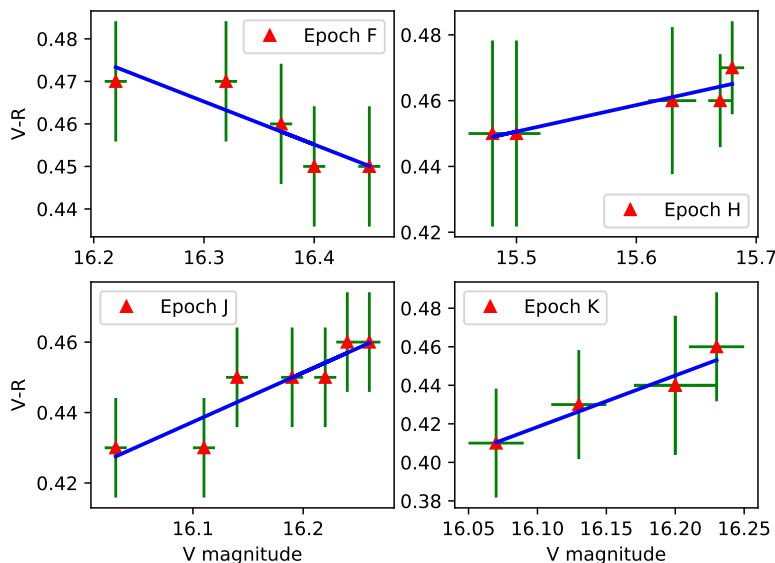
FIGURE 6.6: The (V-R) v/s V colour-magnitude diagram. The blue solid line is the linear least squares fit to the data.

17.99 ± 0.04 mag respectively. For the light curves analysed in this work, I calculated the optical variability amplitude using the fractional root mean square variability (F_{var}) given by (Vaughan *et al.* 2003)

$$F_{var} = \sqrt{\frac{S^2 - \overline{\sigma_{err}^2}}{\bar{x}^2}} \qquad (6.1)$$

where S^2 is the sample variance of the light curve and $\overline{\sigma_{err}^2}$ is mean square error defined as $\overline{\sigma_{err}^2} = \frac{1}{N}\sum_{i=1}^{N}\sigma_{err,i}^2$ I also calculated the minimum variability timescale. Following Burbidge *et al.* (1974), I used $\tau_{obs} = dt/ln(F_1/F_2)$, where dt is the difference in time between any two flux measurements F_1 and F_2. For each of the 11 epochs I calculated all possible time differences τ_{ij} that satisfy the condition $|F_i - F_j| > \sigma_{F_i} + \sigma_{F_j}$. The minimum from the ensemble of τ_{ij} values was taken as the minimum variability timescale τ_{obs}. The errors in τ_{ij} were obtained by error propagation (Bevington and Robinson 1992). The τ_{obs} values for all the epochs are given in Table 6.3. The values range between about 0.33 and 22 days . Due to relativistic beaming the observed timescale is shortened from the intrinsic

timescale τ_{int} by

$$\tau_{obs} = \tau_{int}(1+z)/\delta \tag{6.2}$$

This sets an upper limit on the size of the emission region as $R < 1.69 \times 10^{16} \tau_{obs}(\delta/10)$ cm, where δ is the Doppler factor and τ_{obs} is in days. From the observed smallest and largest timescales of variability (see Table 6.3), I obtained values of the size of the emission region R as $5.6 \times 10^{15}(\delta/10)$ cm and $3.7 \times 10^{17}(\delta/10)$ cm. Broad band SED modelling of 3C 279 at different epochs gave values of the bulk Lorentz factor (Γ) of around 10 (Rajput et al. 2020) and assuming $\Gamma = \delta$, as the jets of blazars are aligned close to the line of sight to the observer, I found the size of the emission region to range between 5.6×10^{15} cm to 3.7×10^{17} cm. Considering relativistic beaming, I also estimated the observed Doppler factor δ_{obs}. From the observed flux in the V-band and R-band I estimated the monochromatic luminosity (Rakshit *et al.* 2017) in the V-band in the source frame using

$$L_V = 4\pi D_L^2 f_R \left(\frac{\lambda_R}{\lambda_V(1+z)} \right)^\alpha (1+z)^{-1} \tag{6.3}$$

where D_L is the luminosity distance, f_R is the R-band flux, which is calculated from the R-band magnitude (m_R) using the formula $f_R = 3.08 \times 10^{-23} \, 10^{-0.4m_R}$ W m^{-2} Hz^{-1}. λ_R and λ_V are effective wavelength in R and V-band. For the spectral index α, I used the average α for each epoch. I calculated the observed bolometric luminosity as $L_{Bol} = 13.2\nu_V L_V$ (Elvis *et al.* 1994), where ν_V is the frequency of V-band. Using the fact that any observed variation with energy $\Delta L = |L_i - L_j|$ must occur on timescales larger than $\tau_{min} = \tau_{obs}/(1+z)$, I calculated the inferred efficiency of accretion as $\eta_{obs} > 5 \times 10^{-43} \Delta L/\tau_{min}$. Relativistic beaming amplifies the observed flux relative to the intrinsic flux as $\Delta L_{obs} = \delta^{3+\alpha} \Delta L_{int}$ and shortens the observed timescale as $\tau_{obs} = \delta^{-1}\tau_{int}$. Using this and the relations $\eta_{obs} \geq 5 \times 10^{-43} \Delta L_{obs}/\tau_{obs}$ and $\eta_{int} \geq 5 \times 10^{-43} \Delta L_{int}/\tau_{int}$ I calculated the observed Doppler factor as

$$\delta_{obs} = \left(\frac{\eta_{obs}}{\eta_{int}} \right)^{1/(4+\alpha)} \tag{6.4}$$

Using the above equation and adopting $\eta_{int} = 0.05$ which is the geometric mean value between $\eta_{int} = 0.007$ (nuclear fusion) and $\eta_{int} = 0.32$ (accretion) I calculated δ_{obs} for all the epochs. They are given in Table 6.3. I also calculated the magnetic field considering the observed variability timescale to be lesser than the synchrotron lifetime of the relativistic electrons in the jet of 3C 279 as

$$t_{syn} \propto 4.75 \times 10^2 \left(\frac{1+z}{\delta \nu_{GHz} B^3} \right)^{1/2} days \tag{6.5}$$

Using τ_{obs} and δ_{obs} calculated using Equations 6.2 and 6.4, the calculated magnetic fields during the different epochs are given in Table 6.3 . In the leptonic scenario of emission from blazars jets, the typical magnetic field strength in FSRQs is of the order of ~1 to 10 G (Petropoulou and Mastichiadis 2012). From SED modelling of 3C 279 using one zone leptonic emission model Rajput et al. (2020) found magnetic field strengths around 1 Gauss. The estimated magnetic fields from variability analysis are therefore similar to the magnetic fields expected in FSRQs.

6.2.2   Relation between flux and polarization variations

Using 10 years of data accumulated between $2008-2018$ August, I carried out an analysis of the correlation between PD and total flux variations on both year like timescale and day like timescale. During the same period the maximum change in PD is about 30% with minimum and maximum PD of $0.63 \pm 0.15\%$ and $34.5 \pm 0.06\%$ respectively. On year like timescales I noticed no significant correlation between flux and PD variations (the variations between flux and PD are random), however, on day like timescales, I noticed close correlations between PD and flux variations. Among the eleven epochs that I analysed, on five epochs I found positive correlation between PD and flux, while on six occasions I found negative correlation between PD and flux (see Table 6.1).

Flux variations in blazars are explained by models as being caused by extrinsic as well as intrinsic mechanisms. If the observed flux variations in 3C 279 are caused by extrinsic effects, the observed correlation and anti-correlation between total flux and PD can be explained due to changes in the trajectories of the jet as postulated by Gopal-Krishna and Wiita (1992) in their "swinging jet model". The observed flux variations in blazars if intrinsic to the source can be well explained by the shock-in-jet model (Marscher and Gear 1985). In this model the observed positive correlation between total flux and PD can be understood due to shock alignment of the magnetic field and thereby creation of an ordered magnetic field. Changes in the PD can also be explained by changes in the spectral index of the electrons in their relativistic jet (Rani *et al.* 2018). The maximum degree of polarization from synchrotron emission from a power law distribution of relativistic electrons with $dN/dE \propto E^{-p}$, where $p = 2\alpha + 1$ is given by

$$PD = \frac{(\alpha + 1)}{\alpha + 5/3} \tag{6.6}$$

where α is the spectral index and the PA is perpendicular to the magnetic field direction as projected on the sky (Marscher 2014). For each of the 11 epochs, in addition to the V-band data used in this work, data is also available in other optical and infrared bands from SMARTS data base[†]. Considering that the optical-infrared spectrum is well described by a power law of the form $S_\nu \propto \nu^{-\alpha}$, I estimated the spectral indices for each of the observations in the 11 epochs. The maximum change in the spectral indices observed during any of these epochs is lesser than 0.4 (see Table 6.3). Change of of the spectral index by 0.4, produces a maximum change in the PD of about 1% from Equation 6.6. The observed variation in PD in all epochs is larger than 1%. Therefore, the changes in PD cannot be caused by changes in the power law index of the distribution of electrons in the jet.

[†]http://www.astro.yale.edu/smarts/glast/home.php

On the other hand, if the enhanced flux variations coincide with the emergence of a new VLBI knot (a new emission region), the observed increased flux can be due to this new emission region. If the magnetic field in this new blob of emission is aligned with the large scale magnetic field a correlation between flux and PD is expected. Alternatively, if the new blob of emission is either chaotic or if it is misaligned with the large scale magnetic field, an anti-correlation between flux and PD can be expected. Also, such anti-correlation between flux and PD can be explained by the Turbulent, Extreme Multi-zone (TEMZ, Marscher 2014) model. According to this model, there can be more turbulent cells (smallest scale emission regions) during outburst compared to other times. These multiple cells can have different polarizations leading to low polarization with increase in flux. To test the hypothesis of the presence of more than one emission components, for example, a stable polarized component plus other multiple components, I plot the observed Q and U Stokes parameters for all the eleven epochs in Figure 6.5. In this Figure, the Q and U measurements deviate from $(Q,U) = (0,0)$ implying the presence of a stable polarized component (Jones *et al.* 1985) with the PA aligned along the jet direction. This steady polarized component with a higher degree of polarization can also gives rise to anti-correlation between PD and total flux (Blinov and Hagen-Thorn 2009). Furthermore, multi-wavelength of observations of 3C 379 have found instances of X-ray flares without corresponding optical and/or γ-ray flares (Abdo *et al.* 2010f). This challenges the one-zone emission models generally used to explain the broad band emission from 3C 279. The broad band SEDs of 3C 279 are fit with one-zone leptonic model (Paliya *et al.* 2015) as well as lepto-hadronic models (Paliya *et al.* 2016). I found overlapping VLBI observations at 15 GHz (Lister *et al.* 2018) on four of the eleven epochs studied in this work. The PA found from VLBI observations that could provide parsec scale resolution are in agreement with the polarization PA (see Table 6.4). This indicates that the optical PA is similar to the jet direction, provided the direction of the jet at sub parsec scales is similar to that of the direction of jet at parsec scales resolvable by VLBI. This indicates that the direction of the magnetic field at the optical

emission region is perpendicular to the jet axis. However, the PD from VLBI during those four epochs are different from that of the PD in the optical. This suggests that the radio emission (from low energy electrons) could be produced in a emission region at a much larger distance from the black hole compared to the optical and γ-ray emission region containing high energy electron population. Among these four epochs, too, on two epochs (A and G) I found the total flux to be anti-correlated with the PD, while on the other two epochs (D and K) I found tight positive correlation between flux and PD. Therefore, the varied correlations between total flux and PD (both correlation and anti-correlation) observed on day like timescales in 3C 279 could be due to the presence of multiple emission components in the jet of 3C 279.

6.2.3   Optical spectral variations

I also investigated spectral variations on all the 11 epochs. I constructed colour (V-R) magnitude (V-band) diagram and fitted the points in the (V-R) v/s V plane with a straight line by taking into account the errors in both colour and brightness. I considered the source to show spectral variations if the Spearman rank correlation coefficient is greater than 0.5 or lesser -0.5 and the probability (p) of no correlation is lesser than 0.05. With this criteria I found prominent variations in colour on four epochs as can be seen in Figure 6.6. During epoch F, the spectrum gets redder as the source brightness (RWB), while during epochs H, J and K the source showed a bluer when brighter (BWB) trend. A RWB spectral variability is predominantly seen in FSRQs (Bonning *et al.* 2012; Sarkar *et al.* 2019), however, both BWB and RWB trends are also seen in FSRQs (Rajput *et al.* 2019; Wu *et al.* 2011, Safna et al. 2020). Here, too I found BWB trend on one epoch and RWB trend on three epochs. FSRQs generally have prominent accretion disk component in their broad band SED and RWB trend is expected if the red non-thermal synchrotron emission dominates the blue thermal emission from the accretion disk (Sarkar *et al.* 2019).

A BWB trend can happen because of geometric effects such as changes in the viewing angle of the jet (Villata *et al.* 2004; Papadakis *et al.* 2007). Alternatively, in the one zone synchrotron emission model, BWB trend can also be caused due the injection of fresh electrons with a harder energy distribution (Kirk *et al.* 1998; Mastichiadis and Kirk 2002). BWB trend is also expected in the TEMZ model (Marscher 2014). According to this model, turbulence driven by instabilities in the jet that also varies with time can (i) influence the number of cells in a given emission region and (ii) influence particle acceleration. Particle acceleration and the increase in the number of cells with each cells having a preferred magnetic field direction can lead to BWB trend and low PD (Rani *et al.* 2018). During epochs H,J and K I found BWB trend and the average PD are $14.98 \pm 1.80\%$, $16.72 \pm 2.12\%$ and $10.23 \pm 3.47\%$ respectively. This is lesser than the average PD of $21.14 \pm 2.14\%$ at epoch F, during which time a RWB trend is observed. It is likely that during this epoch, the contribution of the stable polarized component with increased polarization dominates. The presence of a stable polarized component is evident in the offset of average Q and U vectors from (0,0) in Figure 6.5.

Analysis of the correlation between flux and polarization variations as well as spectral variability in conjunction with polarization observations point to the presence of multiple emission regions in the jet of 3C 279. Rani *et al.* (2018) too noticed anticorrelation between PD and optical flux on an analysis of the multi-wavelength data of 3C 279 during the period $2013-2014$, which they explained as due to the presence of more active cells during the outburst phase. Our knowledge on the flux and polarization variability characteristics of 3C 279 are drawn from the analysis of different modes of multi-wavelength data that are scanty and with poor time resolution. Near simultaneous observations over several wavelengths and covering different timescales (with good time sampling) on a large sample of blazars are needed to pinpoint the exact causes for different correlations between flux and polarization in blazars.

TABLE 6.4: Comparison between the polarization PA (in %) and the PA (in degrees, after accounting for the 180 deg. ambiguity) of the innermost jet from VLBI observations.

	optical			VLBI		
Epoch	Period	PD	PA	Epoch	PD	PA
A	54790 - 54810	26.8±3.6	51.3±7.5	54796	3.9	48
D	56038 - 56048	13.1±1.9	164.0±5.7	56046	5.8	140
G	57041 - 57052	21.1±2.1	44.7±2.8	57040	7.8	26
K	57913 - 57923	10.2±3.3	44.6±2.0	57921	9.7	27

6.3 Summary

Using optical V-band flux and polarization data from the observations of Steward Observatory for a 10 year period between $2008-2018$, I probed (i) the correlation between optical flux and polarization, (ii) optical flux variability on day like timescales and (iii) optical spectral variability on day like timescales. I summarize the findings of this work below.

1. One year like timescales the source showed variations in optical and γ-rays. On such timescales I found the relation between total flux and polarization to be random with no significant correlation or anti-correlation between the two.

2. On day like timescales, I found significant variations in the optical band on eleven epochs. Of these eleven epochs, on only one epoch I found the γ-ray flux to change with time at the 90% confidence level. The γ-ray flux was found to be consistent with a constant flux on the remaining 10 epochs. Thus there is no correspondence between optical and γ-ray flux variations on day like timescales analysed here.

3. On day like timescales, during six epochs I detected anti-correlation between PD and optical total flux, while positive correlation between PD and total flux was seen on five epochs. The diverse correlations observed between optical flux and polarization variations can be well explained by the multi-zone emission model of Marscher (2014).

4. From the plots of Stokes Q and U parameters for all the epochs, I noticed that they are shifted from the origin, suggesting the presence of a stable polarized component.

5. Spectral variations were noticed on four of the 11 epochs. On one epoch (F) I observed a redder when brighter trend, while on three epochs (H, J and K) I found a bluer when brighter trend. The PD during epochs H, J and K is lower than that of epoch F. The observed spectral variations in conjunction with polarization observation also point to the presence of multiple emission regions in the jet of 3C 279.

Chapter 7

Summary and Future Work

Blazars (that comprise FSRQs and BL Lacs) are a class of AGN with their relativistic jets pointed close (within a few degree) to the observer. Their radiation output is dominated by non thermal emission procedure and span the entire accessible electromagnetic spectrum. They show flux variations on a wide range of timescales from minutes to days to months. In the high energy γ-ray band flux variations as short as minutes have been observed in few sources (Shukla *et al.* 2018; Meyer *et al.* 2019; Arlen *et al.* 2013; Aleksić *et al.* 2011; Albert *et al.* 2007; Aharonian *et al.* 2007). In spite of that, the band of the electromagnetic spectrum where flux variability is less characterized is the γ-ray band. This is due to the lack of monitoring observation for a large number of sources. But the high energy γ-ray band needs to be explored as this is the region where the peak of the high energy hump of the broad-band SED of blazars lie. The launch of *Fermi* in the year 2008 and its capacity to scan the sky once in 3 hrs has now made possible the study of the high energy γ-ray variability characteristics of blazars.

The SED of blazars in the log νF_ν v/s log ν representation has two dominant humps. The low energy hump that peaks in the UV/optical range is well understood, as due to synchrotron emission. The origin of the high energy hump that

peaks in the MeV−GeV is still debated. A likely process is the inverse Compton scattering of the low energy photons by relativistic electrons in the jet (leptonic process). An alternative mechanism for the high energy emission in blazars is via hadronic processes that includes proton synchrotron process (Aharonian 2000) or photo pion process (Mannheim 1993). But, often the observed SED of blazars can be modelled satisfactorily by leptonic (Paliya *et al.* 2015) and hadronic (Böttcher *et al.* 2013) or lepto-hadronic models (Paliya *et al.* 2016). A way to understand the high energy emission in blazars is via correlated studies of flux variation between the optical and γ-ray bands. To probe the high energy emission in blazars, in this thesis I carried out

1. A systematic analysis of the γ-ray flux variability characteristics (on month like timescales) of a large sample of blazars.

2. An analysis of the correlation between optical and γ-ray flux variations on a sample of 8 blazars that comprises 5 FSRQs and 3 BL Lacs.

3. An investigation of the correlation between optical flux and polarization variation in the FSRQ 3C 279, and its relation to γ-ray flux variations.

The outcome of the investigations carried out in the thesis are summarized below.

1. On month like timescales, in the γ-ray band (100 MeV − 300 GeV) FSRQs are more variable than BL Lacs. The difference in the γ-ray flux variations between FSRQs and BL Lacs can be explained by the location of the inverse Compton peak in the broad band SED with respect to the *Fermi* observing band. Majority of the objects in my sample showed timescale of variability of about 20 days, which could be related to processes in the jets of these sources.

2. Varied correlations between optical and GeV flux variations were observed in FSRQs, I found instances when (a) optical and GeV fluxes are correlated (b) optical fluxes without γ-ray counterparts and (c) γ-ray fluxes without optical counterparts. Analysis of these epochs through broad band SED fits indicate that the region giving rise to optical and γ-ray flux variations are co-spatial. SED model fits also indicate (i) correlated optical and γ-ray flux variations are caused by increase in the bulk Lorentz factor (ii) γ-ray fluxes with no counterparts are due to an increase in the bulk Lorentz factor and/or increase in the electron number density and (iii) optical fluxes with no γ-ray counterparts is due to an increase in the magnetic field.

3. In all the three BL Lacs studied in this work, optical and γ-ray fluxes are found to be correlated, which can be explained predominantly due to changes in the bulk Lorentz factor.

4. In the FSRQ 3C 279, on day like timescales, at certain epochs the degree of optical polarization is found to be correlated with optical flux, while at certain epochs, the degree of optical polarization is found to be anticorrelated with optical flux. Such diverse correlation observed between optical flux and polarization variations could be explained by multizone emission models.

The flux variations seen in the blazars studied in the thesis are thus complex. In the leptonic scenario of high energy emission in blazars a correlation between optical and GeV flux variations is expected, while in the hadronic scenario of high energy emission from blazar jets a close correlation between optical and GeV flux variations is not expected. However, in this thesis observations of the varied variability behaviours in the same source suggest that " *Variability studies might not be definitive in constraining leptonic v/s hadronic models of high energy emission in blazars jets.*"

7.1   Outline of the future work

The code used in this thesis work to fit the observed SED is a static one. To carry-out a more realistic modelling of the SED, I intend to work towards development of a time dependent SED fitting code. Secondly, the optical flux and polarization analysis carried out on 3C 279 in this thesis has displayed varied correlation between optical flux and polarization variations. This needs to be checked on other blazars too. Therefore, I plan to examine the correlation between optical flux and polarization variations in a large sample of blazars, the data for which is available in the archives of the Steward Observatory. A search in the archives of Steward Observatory shows the availability of quality optical flux and polarization data for about two dozen AGN.

Bibliography

Abdalla, M, Li, Hai-Jun, Bi, Xiao-Jun, Lin, Su-Jie and Yin, Peng-Fei, 2020, "The implications of the axion like particle from the Fermi-LAT and H.E.S.S. observations of PG 1553+113 and PKS 2155-304", *arXiv e-prints*, arXiv:2002.07571. [ADS], [arXiv:2002.07571 [astro-ph.HE]]

Abdo, A. A., and et al., 2009, "Bright Active Galactic Nuclei Source List from the First Three Months of the Fermi Large Area Telescope All-Sky Survey", *Astrophys. J.*, **700**, 597–622. [DOI], [ADS], [arXiv:0902.1559 [astro-ph.HE]]

Abdo, A. A., and et al., 2010a, "Spectral Properties of Bright Fermi-Detected Blazars in the Gamma-Ray Band", *Astrophys. J.*, **710**, 1271–1285. [DOI], [ADS], [arXiv:1001.4097 [astro-ph.HE]]

Abdo, A. A., and et al., 2010b, "Fermi-Large Area Telescope Observations of the Exceptional Gamma-ray Outbursts of 3C 273 in 2009 September", *Astrophys. J. Lett.*, **714**(1), L73–L78. [DOI], [ADS], [arXiv:1012.2980 [astro-ph.HE]]

Abdo, A. A., and et al., 2010c, "The Spectral Energy Distribution of Fermi Bright Blazars", *Astrophys. J.*, **716**(1), 30–70. [DOI], [ADS], [arXiv:0912.2040 [astro-ph.CO]]

Abdo, A. A., and et al., 2010d, "Fermi Large Area Telescope and Multi-wavelength Observations of the Flaring Activity of PKS 1510-089 between 2008 September and 2009 June", *Astrophys. J.*, **721**, 1425–1447. [DOI], [ADS], [arXiv:1007.1237]

Abdo, A. A., and et al., 2010e, "Gamma-ray Light Curves and Variability of Bright Fermi-detected Blazars", *Astrophys. J.*, **722**, 520–542. [DOI], [ADS], [arXiv:1004.0348 [astro-ph.HE]]

Abdo, A. A., and et al., 2010f, "A change in the optical polarization associated with a γ-ray flare in the blazar 3C279", *Nature*, **463**(7283), 919–923. [DOI], [ADS], [arXiv:1004.3828 [astro-ph.CO]]

Abdo, A. A., and et al., 2011, "Fermi Gamma-ray Space Telescope Observations of the Gamma-ray Outburst from 3C454.3 in November 2010", *Astrophys. J. Lett.*, **733**, L26. [DOI], [ADS], [arXiv:1102.0277 [astro-ph.HE]]

Abdollahi, S., and et al., 2020, "Fermi Large Area Telescope Fourth Source Catalog", *Astrophys. J. Suppl.*, **247**(1), 33. [DOI], [ADS], [arXiv:1902.10045 [astro-ph.HE]]

Acero, F., and et al., 2015, "Fermi Large Area Telescope Third Source Catalog", *Astrophys. J. Suppl.*, **218**(2), 23. [DOI], [ADS], [arXiv:1501.02003 [astro-ph.HE]]

Ackermann, M., and et al., 2010, "Fermi Gamma-ray Space Telescope Observations of Gamma-ray Outbursts from 3C 454.3 in 2009 December and 2010 April", *Astrophys. J.*, **721**, 1383–1396. [DOI], [ADS], [arXiv:1007.0483 [astro-ph.HE]]

Ackermann, M., and et al., 2011, "The Second Catalog of Active Galactic Nuclei Detected by the Fermi Large Area Telescope", *Astrophys. J.*, **743**(2), 171. [DOI], [ADS], [arXiv:1108.1420 [astro-ph.HE]]

Ackermann, M., and et al., 2012, "Multi-wavelength Observations of Blazar AO 0235+164 in the 2008-2009 Flaring State", *Astrophys. J.*, **751**(2), 159. [DOI], [ADS], [arXiv:1207.2932 [astro-ph.HE]]

Ackermann, M., and et al., 2015a, "The Third Catalog of Active Galactic Nuclei Detected by the Fermi Large Area Telescope", *Astrophys. J.*, **810**, 14. [DOI], [ADS], [arXiv:1501.06054 [astro-ph.HE]]

Ackermann, M., and et al., 2015b, "Multiwavelength Evidence for Quasi-periodic Modulation in the Gamma-Ray Blazar PG 1553+113", *Astrophys. J. Lett.*, **813**(2), L41. [DOI], [ADS], [arXiv:1509.02063 [astro-ph.HE]]

Agudo, Iván, and et al., 2011, "Location of γ-ray Flare Emission in the Jet of the BL Lacertae Object OJ287 More than 14 pc from the Central Engine", *Astrophys. J. Lett.*, **726**(1), L13. [DOI], [ADS], [arXiv:1011.6454 [astro-ph.CO]]

Aharonian, F., and et al., 2007, "An Exceptional Very High Energy Gamma-Ray Flare of PKS 2155-304", *Astrophys. J. Lett.*, **664**(2), L71–L74. [DOI], [ADS], [arXiv:0706.0797 [astro-ph]]

Aharonian, F., and et al., 2009, "Simultaneous Observations of PKS 2155-304 with HESS, Fermi, RXTE, and Atom: Spectral Energy Distributions and Variability in a Low State", *Astrophys. J. Lett.*, **696**(2), L150–L155. [DOI], [ADS], [arXiv:0903.2924 [astro-ph.HE]]

Aharonian, F. A., 2000, "TeV gamma rays from BL Lac objects due to synchrotron radiation of extremely high energy protons", *New Astronomy*, **5**, 377–395. [DOI], [ADS], [astro-ph/0003159]

Ai, Y. L., Yuan, W., Zhou, H. Y., Wang, T. G., Dong, X.-B., Wang, J. G. and Lu, H. L., 2010, "Dependence of the Optical/Ultraviolet Variability on the Emission-line Properties and Eddington Ratio in Active Galactic Nuclei", *Astrophys. J. Lett.*, **716**, L31–L35. [DOI], [ADS], [arXiv:1005.0901]

Albert, J., and et al., 2007, "Variable Very High Energy γ-Ray Emission from Markarian 501", *Astrophys. J.*, **669**, 862–883. [DOI], [ADS], [astro-ph/0702008]

Aleksić, J., and et al., 2011, "MAGIC Discovery of Very High Energy Emission from the FSRQ PKS 1222+21", *Astrophys. J. Lett.*, **730**, L8. [DOI], [ADS], [arXiv:1101.4645 [astro-ph.HE]]

Aleksić, J., and et al., 2014, "MAGIC gamma-ray and multi-frequency observations of flat spectrum radio quasar PKS 1510-089 in early 2012", *Astron. Astrophys.*, **569**, A46. [DOI], [ADS], [arXiv:1401.5646 [astro-ph.HE]]

Angel, J. R. P. and Stockman, H. S., 1980, "Optical and infrared polarization of active extragalactic objects", *Ann. Rev. Astron. Astrophys.*, **18**, 321–361. [DOI], [ADS]

Angelakis, E., Hovatta, T., Blinov, D., Pavlidou, V., Kiehlmann, S., Myserlis, I., Böttcher, M., Mao, P., Panopoulou, G. V., Liodakis, I., King, O. G., Baloković, M., Kus, A., Kylafis, N., Mahabal, A., Marecki, A., Paleologou, E., Papadakis, I., Papamastorakis, I., Pazderski, E., Pearson, T. J., Prabhudesai, S., Ramaprakash, A. N., Readhead, A. C. S., Reig, P., Tassis, K., Urry, M. and Zensus, J. A., 2016, "RoboPol: the optical polarization of gamma-ray-loud and gamma-ray-quiet blazars", *Mon. Not. Roy. Astron. Soc.*, **463**(3), 3365–3380. [DOI], [ADS], [arXiv:1609.00640 [astro-ph.HE]]

Antonucci, R., 1993, "Unified models for active galactic nuclei and quasars.", *Ann. Rev. Astron. Astrophys.*, **31**, 473–521. [DOI], [ADS]

Arlen, T., and et al., 2013, "Rapid TeV Gamma-Ray Flaring of BL Lacertae", *Astrophys. J.*, **762**, 92. [DOI], [ADS], [arXiv:1211.3073 [astro-ph.HE]]

Arnaud, K. A., 1996, "XSPEC: The First Ten Years", in *Astronomical Data Analysis Software and Systems V*, (Eds.) Jacoby, G. H., Barnes, J., Astronomical Society of the Pacific Conference Series, 101, [ADS]

Atwood, W. B., Abdo, A. A., Ackermann, M., Althouse, W., Anderson, B., Axelsson, M., Baldini, L., Ballet, J., Band, D. L., Barbiellini, G. and et al., 2009, "The Large Area Telescope on the Fermi Gamma-Ray Space Telescope Mission", *Astrophys. J.*, **697**, 1071–1102. [DOI], [ADS], [arXiv:0902.1089 [astro-ph.IM]]

Baring, Matthew G., Böttcher, Markus and Summerlin, Errol J., 2017, "Probing acceleration and turbulence at relativistic shocks in blazar jets", *Mon. Not. Roy. Astron. Soc.*, **464**(4), 4875–4894. [DOI], [ADS], [arXiv:1609.03899 [astro-ph.HE]]

Barkov, M. V., Aharonian, F. A., Bogovalov, S. V., Kelner, S. R. and Khangulyan, D., 2012, "Rapid TeV Variability in Blazars as a Result of Jet-Star Interaction", *Astrophys. J.*, **749**(2), 119. [DOI], [ADS], [arXiv:1012.1787 [astro-ph.HE]]

Bastieri, D., 2009, "Fermi LAT detection of a GeV flare from 3C 273", *The Astronomer's Telegram*, **2168**, 1. [ADS]

Bauer, A., Baltay, C., Coppi, P., Ellman, N., Jerke, J., Rabinowitz, D. and Scalzo, R., 2009, "Quasar Optical Variability in the Palomar-QUEST Survey", *Astrophys. J.*, **696**, 1241–1256. [DOI], [ADS], [arXiv:0902.4103 [astro-ph.CO]]

Begelman, M. C., Sikora, M., Giommi, P., Barr, P., Garilli, B., Gioia, I. M., Maccacaro, T., Maccagni, D. and Schild, R. E., 1987, "Inverse Compton scattering of ambient radiation by a cold relativistic jet - A source of beamed, polarized continuum in blazars?", *Astrophys. J.*, **322**, 650–661. [DOI], [ADS]

Begelman, Mitchell C., Blandford, Roger D. and Rees, Martin J., 1984, "Theory of extragalactic radio sources", *Rev. Mod. Phys.*, **56**, 255–351. [DOI]URL: `https://link.aps.org/doi/10.1103/RevModPhys.56.255`

Bell, A. R., Araudo, A. T., Matthews, J. H. and Blundell, K. M., 2018, "Cosmic-ray acceleration by relativistic shocks: limits and estimates", *Mon. Not. Roy. Astron. Soc.*, **473**(2), 2364–2371. [DOI], [ADS], [arXiv:1709.07793 [astro-ph.HE]]

Bevington, Philip R. and Robinson, D. Keith, 1992, *Data reduction and error analysis for the physical sciences*. [ADS]

Bhatta, Gopal, 2019, "Blazar Mrk 501 shows rhythmic oscillations in its γ-ray emission", *Mon. Not. Roy. Astron. Soc.*, **487**(3), 3990–3997. [DOI], [ADS], [arXiv:1808.06067 [astro-ph.HE]]

Blandford, Roger and Eichler, David, 1987, "Particle acceleration at astrophysical shocks: A theory of cosmic ray origin", , **154**(1), 1–75. [DOI], [ADS]

Błażejowski, M., Sikora, M., Moderski, R. and Madejski, G. M., 2000, "Comptonization of Infrared Radiation from Hot Dust by Relativistic Jets in Quasars", *Astrophys. J.*, **545**, 107–116. [DOI], [ADS], [astro-ph/0008154]

Blinov, D., and et al., 2015, "RoboPol: first season rotations of optical polarization plane in blazars", *Mon. Not. Roy. Astron. Soc.*, **453**(2), 1669–1683. [DOI], [ADS], [arXiv:1505.07467 [astro-ph.HE]]

Blinov, D. A. and Hagen-Thorn, V. A., 2009, "Stochastic model of optical variability of BL Lacertae", *Astron. Astrophys.*, **503**(1), 103–106. [DOI], [ADS], [arXiv:0906.5127 [astro-ph.CO]]

Boettcher, M., Mause, H. and Schlickeiser, R., 1997, "γ-ray emission and spectral evolution of pair plasmas in AGN jets. I. General theory and a prediction for the GeV - TeV emission from ultrarelativistic jets.", *Astron. Astrophys.*, **324**, 395–409. [ADS], [astro-ph/9604003]

Bolton, J. G. and Ekers, J., 1966, "Identification of strong extragalactic radio sources in the declination zone 0deg to − 20deg″, $AustralianJournalofPhysics$, **19**, 559. $[DOI], [ADS]$

Bonning, E., Urry, C. M., Bailyn, C., Buxton, M., Chatterjee, R., Coppi, P., Fossati, G., Isler, J. and Maraschi, L., 2012, "SMARTS Optical and Infrared Monitoring of 12 Gamma-Ray Bright Blazars", *Astrophys. J.*, **756**, 13. [DOI], [ADS], [arXiv:1201.4380 [astro-ph.HE]]

Bonning, E. W., Bailyn, C., Urry, C. M., Buxton, M., Fossati, G., Maraschi, L., Coppi, P., Scalzo, R., Isler, J. and Kaptur, A., 2009, "Correlated Variability in the Blazar 3C 454.3", *Astrophys. J. Lett.*, **697**, L81–L85. [DOI], [ADS], [arXiv:0812.4582]

Böttcher, M., 2007, "Modeling the emission processes in blazars", *Astrophys. Space Sci.*, **309**, 95–104. [DOI], [ADS], [astro-ph/0608713]

Böttcher, M. and Dermer, C. D., 2010, "Timing Signatures of the Internal-Shock Model for Blazars", *Astrophys. J.*, **711**(1), 445–460. [DOI], [ADS], [arXiv:1001.1606 [astro-ph.CO]]

Böttcher, M., Reimer, A., Sweeney, K. and Prakash, A., 2013, "Leptonic and Hadronic Modeling of Fermi-detected Blazars", *Astrophys. J.*, **768**, 54. [DOI], [ADS], [arXiv:1304.0605 [astro-ph.HE]]

Bowyer, S., Brodie, J., Clarke, J. T. and Henry, J. P., 1984, "Optical observations of the BL Lacertae object PKS 2155-304 and implications regarding the X-ray absorption feature at 600-700 eV.", *Astrophys. J. Lett.*, **278**, L103–L107. [DOI], [ADS]

Breeveld, A. A., Landsman, W., Holland, S. T., Roming, P., Kuin, N. P. M. and Page, M. J., 2011, "An Updated Ultraviolet Calibration for the Swift/UVOT", in *American Institute of Physics Conference Series*, (Eds.) McEnery, J. E., Racusin, J. L., Gehrels, N., American Institute of Physics Conference Series, 1358, [DOI], [ADS], [arXiv:1102.4717 [astro-ph.IM]]

Burbidge, E. Margaret and Rosenberg, Fred D., 1965, "The Redshift of the Quasi-Stellar Radio Source 3c 279.", *Astrophys. J.*, **142**, 1673. [DOI], [ADS]

Burbidge, G. R., Jones, T. W. and Odell, S. L., 1974, "Physics of compact nonthermal sources. III. Energetic considerations.", *Astrophys. J.*, **193**, 43–54. [DOI], [ADS]

Burrows, D.N., and et al., 2005, "The Swift X-Ray Telescope", *Space Sci. Rev.*, **120**, 165–195. [DOI], [ADS], [astro-ph/0508071]

Cardelli, Jason A., Clayton, Geoffrey C. and Mathis, John S., 1988, "The Determination of Ultraviolet Extinction from the Optical and Near-Infrared", *Astrophys. J. Lett.*, **329**, L33. [DOI], [ADS]

Carnerero, M. I., and et al., 2015, "Multiwavelength behaviour of the blazar OJ 248 from radio to γ-rays", *Mon. Not. Roy. Astron. Soc.*, **450**, 2677–2691. [DOI], [ADS], [arXiv:1505.00916 [astro-ph.HE]]

Castignani, G., and et al., 2017, "Multiwavelength variability study and search for periodicity of PKS 1510-089", *Astron. Astrophys.*, **601**, A30. [DOI], [ADS], [arXiv:1612.05281 [astro-ph.HE]]

Cerruti, Matteo, Dermer, Charles D., Lott, Benoît, Boisson, Catherine and Zech, Andreas, 2013, "Gamma-Ray Blazars near Equipartition and the Origin of the GeV Spectral Break in 3C 454.3", *Astrophys. J. Lett.*, **771**(1), L4. [DOI], [ADS], [arXiv:1305.4159 [astro-ph.HE]]

Chatterjee, R., and et al., 2008, "Correlated Multi-Wave Band Variability in the Blazar 3C 279 from 1996 to 2007", *Astrophys. J.*, **689**, 79–94. [DOI], [ADS], [arXiv:0808.2194]

Chatterjee, R., Bailyn, C. D., Bonning, E. W., Buxton, M., Coppi, P., Fossati, G., Isler, J., Maraschi, L. and Urry, C. M., 2012, "Similarity of the Optical-Infrared and γ-Ray Time Variability of Fermi Blazars", *Astrophys. J.*, **749**, 191. [DOI], [ADS], [arXiv:1101.3815 [astro-ph.HE]]

Chatterjee, R., Fossati, G., Urry, C. M., Bailyn, C. D., Maraschi, L., Buxton, M., Bonning, E. W., Isler, J. and Coppi, P., 2013, "An Optical-Near-infrared Outburst with no Accompanying γ-Rays in the Blazar PKS 0208-512", *Astrophys. J. Lett.*, **763**, L11. [DOI], [ADS], [arXiv:1212.2629 [astro-ph.HE]]

Chatterjee, Ritaban, Roychowdhury, Agniva, Chandra, Sunil and Sinha, Atreyee, 2018, "Possible Accretion Disk Origin of the Emission Variability of a Blazar Jet", *Astrophys. J. Lett.*, **859**(2), L21. [DOI], [ADS], [arXiv:1805.06222 [astro-ph.HE]]

Chen, L., 2018, "On the Jet Properties of γ-Ray-loud Active Galactic Nuclei", *Astrophys. J. Suppl.*, **235**, 39. [DOI], [ADS], [arXiv:1803.05715 [astro-ph.HE]]

Christie, I. M., Petropoulou, M., Sironi, L. and Giannios, D., 2019, "Radiative signatures of plasmoid-dominated reconnection in blazar jets", *Mon. Not. Roy. Astron. Soc.*, **482**(1), 65–82. [DOI], [ADS], [arXiv:1807.08041 [astro-ph.HE]]

Ciprini, S., 2016, "Fermi LAT observation of renewed and strong GeV gamma-ray activity from blazar CTA 102", *The Astronomer's Telegram*, **9869**. [ADS]

Cohen, D. P., Romani, R. W., Filippenko, A. V., Cenko, S. B., Lott, B., Zheng, W. and Li, W., 2014, "Temporal Correlations between Optical and Gamma-Ray Activity in Blazars", *Astrophys. J.*, **797**, 137. [DOI], [ADS], [arXiv:1404.5967 [astro-ph.HE]]

Cohen, Ross D., Smith, Harding E., Junkkarinen, Vesa T. and Burbidge, E. Margaret, 1987, "The Nature of the BL Lacertae Object AO 0235+164", *Astrophys. J.*, **318**, 577. [DOI], [ADS]

Coogan, R. T., Brown, A. M. and Chadwick, P. M., 2016, "Localizing the γ-ray emission region during the 2014 June outburst of 3C 454.3", *Mon. Not. Roy. Astron. Soc.*, **458**, 354–365. [DOI], [ADS], [arXiv:1601.07180 [astro-ph.HE]]

Costamante, L., Cutini, S., Tosti, G., Antolini, E. and Tramacere, A., 2018, "On the origin of gamma-rays in Fermi blazars: beyondthe broad-line region", *Mon. Not. Roy. Astron. Soc.*, **477**(4), 4749–4767. [DOI], [ADS], [arXiv:1804.02408 [astro-ph.HE]]

Covino, S., Sandrinelli, A. and Treves, A., 2019, "Gamma-ray quasi-periodicities of blazars. A cautious approach", *Mon. Not. Roy. Astron. Soc.*, **482**(1), 1270–1274. [DOI], [ADS], [arXiv:1810.02409 [astro-ph.HE]]

Dermer, C. D. and Schlickeiser, R., 1993, "Model for the High-Energy Emission from Blazars", *Astrophys. J.*, **416**, 458. [DOI], [ADS]

Dermer, Charles D., Cerruti, Matteo, Lott, Benoit, Boisson, Catherine and Zech, Andreas, 2014, "Equipartition Gamma-Ray Blazars and the Location of the

Gamma-Ray Emission Site in 3C 279", *Astrophys. J.*, **782**(2), 82. [DOI], [ADS], [arXiv:1304.6680 [astro-ph.HE]]

di Clemente, A., Giallongo, E., Natali, G., Trevese, D. and Vagnetti, F., 1996, "The Variability of Quasars. II. Frequency Dependence", *Astrophys. J.*, **463**, 466. [DOI], [ADS], [astro-ph/9512159]

Dickel, J. R., Yang, K. S., McVittie, G. C. and Swenson, G. W., Jr., 1967, "A survey of the sky at 610.5 MHz. II. The region between declinations +15 and +22 degrees.", *Astron. J.*, **72**, 757–768. [DOI], [ADS]

Diltz, C. and Böttcher, M., 2016, "Leptonic and Lepto-Hadronic Modeling of the 2010 November Flare from 3C 454.3", *Astrophys. J.*, **826**, 54. [DOI], [ADS], [arXiv:1605.06923 [astro-ph.HE]]

Dutka, Michael S., and et al., 2013, "Multi-wavelength Observations of PKS 2142-75 during Active and Quiescent Gamma-Ray States", *Astrophys. J.*, **779**(2), 174. [DOI], [ADS], [arXiv:1311.0383 [astro-ph.HE]]

Edelson, R. A. and Krolik, J. H., 1988, "The discrete correlation function - A new method for analyzing unevenly sampled variability data", *Astrophys. J.*, **333**, 646–659. [DOI], [ADS]

Elvis, M., Wilkes, B. J., McDowell, J. C., Green, R. F., Bechtold, J., Willner, S. P., Oey, M. S., Polomski, E. and Cutri, R., 1994, "Atlas of quasar energy distributions", *Astrophys. J. Suppl.*, **95**, 1–68. [DOI], [ADS]

Fabian, A. C., 1999, "The obscured growth of massive black holes", *Mon. Not. Roy. Astron. Soc.*, **308**, L39–L43. [DOI], [ADS], [astro-ph/9908064]

Fanaroff, B. L. and Riley, J. M., 1974, "The morphology of extragalactic radio sources of high and low luminosity", *Mon. Not. Roy. Astron. Soc.*, **167**, 31P–36P. [DOI], [ADS]

Fichtel, C. E., and et al., 1994, "The First Energetic Gamma-Ray Experiment Telescope (EGRET) Source Catalog", *Astrophys. J. Suppl.*, **94**, 551. [DOI], [ADS]

Fossati, G., Maraschi, L., Celotti, A., Comastri, A. and Ghisellini, G., 1998, "A unifying view of the spectral energy distributions of blazars", *Mon. Not. Roy. Astron. Soc.*, **299**, 433–448. [DOI], [ADS], [astro-ph/9804103]

Gao, Shan, Fedynitch, Anatoli, Winter, Walter and Pohl, Martin, 2019, "Modelling the coincident observation of a high-energy neutrino and a bright blazar flare", *Nature Astronomy*, **3**, 88–92. [DOI], [ADS], [arXiv:1807.04275 [astro-ph.HE]]

Gaskell, C. M. and Peterson, B. M., 1987, "The accuracy of cross-correlation estimates of quasar emission-line region sizes", *Astrophys. J. Suppl.*, **65**, 1–11. [DOI], [ADS]

Gaskell, C. M. and Sparke, L. S., 1986, "Line variations in quasars and Seyfert galaxies", *Astrophys. J.*, **305**, 175–186. [DOI], [ADS]

Gaur, H., Gupta, A. C. and Wiita, P. J., 2012a, "Multiwavelength Variability of the Blazars Mrk 421 and 3C 454.3 in the High State", *Astron. J.*, **143**, 23. [DOI], [ADS], [arXiv:1112.3126 [astro-ph.CO]]

Gaur, H., Gupta, A. C., Wiita, P. J., Uemura, M., Itoh, R. and Sasada, M., 2014, "Anti-correlated Optical Flux and Polarization Variability in BL Lac", *Astrophys. J. Lett.*, **781**, L4. [DOI], [ADS], [arXiv:1312.0939 [astro-ph.HE]]

Gaur, Haritma, Gupta, Alok C., Strigachev, A., Bachev, R., Semkov, E., Wiita, Paul J., Peneva, S., Boeva, S., Slavcheva-Mihova, L., Mihov, B., Latev, G. and Pandey, U. S., 2012b, "Optical flux and spectral variability of blazars", *Mon. Not. Roy. Astron. Soc.*, **425**(4), 3002–3023. [DOI], [ADS], [arXiv:1207.5943 [astro-ph.HE]]

Gehrels, N., and et al., 2004, "The Swift Gamma-Ray Burst Mission", *Astrophys. J.*, **611**, 1005–1020. [DOI], [ADS]

Ghisellini, G. and Madau, P., 1996, "On the origin of the gamma-ray emission in blazars", *Mon. Not. Roy. Astron. Soc.*, **280**, 67–76. [DOI], [ADS]

Ghisellini, G. and Maraschi, L., 1989, "Bulk acceleration in relativistic jets and the spectral properties of blazars", *Astrophys. J.*, **340**, 181–189. [DOI], [ADS]

Ghisellini, G. and Tavecchio, F., 2008, "The blazar sequence: a new perspective", *Mon. Not. Roy. Astron. Soc.*, **387**, 1669–1680. [DOI], [ADS], [arXiv:0802.1918]

Ghisellini, G. and Tavecchio, F., 2009, "Canonical high-power blazars", *Mon. Not. Roy. Astron. Soc.*, **397**(2), 985–1002. [DOI], [ADS], [arXiv:0902.0793 [astro-ph.CO]]

Ghisellini, G., Maraschi, L. and Tavecchio, F., 2009, "The Fermi blazars' divide", *Mon. Not. Roy. Astron. Soc.*, **396**(1), L105–L109. [DOI], [ADS], [arXiv:0903.2043 [astro-ph.CO]]

Ghisellini, G., Tavecchio, F., Foschini, L. and Ghirlanda, G., 2011, "The transition between BL Lac objects and flat spectrum radio quasars", *Mon. Not. Roy. Astron. Soc.*, **414**, 2674–2689. [DOI], [ADS], [arXiv:1012.0308]

Ghosh, K. K., Ramsey, B. D., Sadun, A. C. and Soundararajaperumal, S., 2000, "Optical Variability of Blazars", *Astrophys. J. Suppl.*, **127**(1), 11–26. [DOI], [ADS]

Giannios, D. and Spruit, H. C., 2006, "The role of kink instability in Poynting-flux dominated jets", *Astron. Astrophys.*, **450**(3), 887–898. [DOI], [ADS], [arXiv:astro-ph/0601172 [astro-ph]]

Giannios, Dimitrios, 2013, "Reconnection-driven plasmoids in blazars: fast flares on a slow envelope", *Mon. Not. Roy. Astron. Soc.*, **431**(1), 355–363. [DOI], [ADS], [arXiv:1211.0296 [astro-ph.HE]]

Gopal-Krishna and Wiita, Paul J., 1992, "Swinging jets and the variability of active nuclei.", *Astron. Astrophys.*, **259**, 109–117. [ADS]

Guo, Fan, Li, Xiaocan, Li, Hui, Daughton, William, Zhang, Bing, Lloyd-Ronning, Nicole, Liu, Yi-Hsin, Zhang, Haocheng and Deng, Wei, 2016, "Efficient Production of High-energy Nonthermal Particles during Magnetic Reconnection in a Magnetically Dominated Ion-Electron Plasma", *Astrophys. J. Lett.*, **818**(1), L9. [DOI], [ADS], [arXiv:1511.01434 [astro-ph.HE]]

Gupta, A. C., and et al., 2017, "A peculiar multiwavelength flare in the blazar 3C 454.3", *Mon. Not. Roy. Astron. Soc.*, **472**, 788–798. [DOI], [ADS], [arXiv:1708.03504 [astro-ph.HE]]

Gupta, Alok C., Tripathi, Ashutosh, Wiita, Paul J., Kushwaha, Pankaj, Zhang, Zhongli and Bambi, Cosimo, 2019, "Detection of a quasi-periodic oscillation in γ-ray light curve of the high-redshift blazar B2 1520+31", *Mon. Not. Roy. Astron. Soc.*, **484**(4), 5785–5790. [DOI], [ADS], [arXiv:1810.12607 [astro-ph.HE]]

H. E. S. S. Collaboration, and et al., 2013, "H.E.S.S. discovery of VHE γ-rays from the quasar PKS 1510-089", *Astron. Astrophys.*, **554**, A107. [DOI], [ADS], [arXiv:1304.8071 [astro-ph.HE]]

H. E. S. S. Collaboration, and et al., 2014, "Long-term monitoring of PKS 2155-304 with ATOM and H.E.S.S.: investigation of optical/γ-ray correlations in different spectral states", *Astron. Astrophys.*, **571**, A39. [DOI], [ADS], [arXiv:1409.0253 [astro-ph.HE]]

Hagen-Thorn, V. A., Larionov, V. M., Jorstad, S. G., Arkharov, A. A., Hagen-Thorn, E. I., Efimova, N. V., Larionova, L. V. and Marscher, A. P., 2008, "The Outburst of the Blazar AO 0235+164 in 2006 December: Shock-in-Jet Interpretation", *Astrophys. J.*, **672**(1), 40–47. [DOI], [ADS], [arXiv:0709.3550 [astro-ph]]

Harris, D. E. and Krawczynski, Henric, 2006, "X-Ray Emission from Extragalactic Jets", *Ann. Rev. Astron. Astrophys.*, **44**(1), 463–506. [DOI], [ADS], [arXiv:astro-ph/0607228 [astro-ph]]

Harris, J., Daniel, M. K. and Chadwick, P. M., 2012, "Identifying Breaks and Curvature in the Fermi Spectra of Bright Flat Spectrum Radio Quasars", *Astrophys. J.*, **761**(1), 2. [DOI], [ADS], [arXiv:1210.6047 [astro-ph.HE]]

Harris, J., Chadwick, P. M. and Daniel, M. K., 2014, "An investigation into the spectral properties of bright Fermi blazars", *Mon. Not. Roy. Astron. Soc.*, **441**(4), 3591–3599. [DOI], [ADS], [arXiv:1405.2699 [astro-ph.HE]]

Hartman, R. C., and et al., 1992, "Detection of high-energy gamma radiation from quasar 3C 279 by the EGRET telescope on the Compton Gamma Ray Observatory", *Astrophys. J. Lett.*, **385**, L1–L4. [DOI], [ADS]

Hartman, R. C., and et al., 1993, "EGRET Detection of High-Energy Gamma Radiation from the OVV Quasar 3C 454.3", *Astrophys. J. Lett.*, **407**, L41. [DOI], [ADS]

Hartman, R. C., and et al., 1999, "The Third EGRET Catalog of High-Energy Gamma-Ray Sources", *Astrophys. J. Suppl.*, **123**, 79–202. [DOI], [ADS]

Hayashida, Masaaki, Madejski, Greg, Blandford, Roger, Asano, Katsuaki, Larsson, Stefan, Fermi-LAT Collaboration, Nalewajko, Krzysztof and Sikora, Marek, 2017, "First minute-scale variability in Fermi-LAT blazar observations during the giant outburst of 3C279 in 2015 June", in *6th International Symposium on High Energy Gamma-Ray Astronomy*, American Institute of Physics Conference Series, 1792, [DOI], [ADS]

Hewitt, A. and Burbidge, G., 1980, "A revised optical catalogue of quasi-stellar objects .", *Astrophys. J. Suppl.*, **43**, 57–158. [DOI], [ADS]

Hovatta, T., and et al., 2014, "Connection between optical and γ-ray variability in blazars", *Mon. Not. Roy. Astron. Soc.*, **439**(1), 690–702. [DOI], [ADS], [arXiv:1401.0538 [astro-ph.HE]]

IceCube Collaboration, and et al., 2018a, "Neutrino emission from the direction of the blazar TXS 0506+056 prior to the IceCube-170922A alert", *Science*, **361**(6398), 147–151. [DOI], [ADS], [arXiv:1807.08794 [astro-ph.HE]]

IceCube Collaboration, and et al., 2018b, "Multimessenger observations of a flaring blazar coincident with high-energy neutrino IceCube-170922A", *Science*, **361**(6398), eaat1378. [DOI], [ADS], [arXiv:1807.08816 [astro-ph.HE]]

Ikejiri, Yuki, and et al., 2011, "Photopolarimetric Monitoring of Blazars in the Optical and Near-Infrared Bands with the Kanata Telescope. I. Correlations between Flux, Color, and Polarization", *Pub. Astron. Soc. Japan*, **63**, 639. [DOI], [ADS], [arXiv:1105.0255 [astro-ph.HE]]

Impey, C. D., Lawrence, C. R. and Tapia, S., 1991, "Optical Polarization of a Complete Sample of Radio Sources", *Astrophys. J.*, **375**, 46. [DOI], [ADS]

Jolley, Erin J. D. and Kuncic, Zdenka, 2008, "Constraints on Jet-driven Disk Accretion in Sagittarius A*", *Astrophys. J.*, **676**(1), 351–360. [DOI], [ADS], [arXiv:0711.4626 [astro-ph]]

Jones, Frank C. and Ellison, Donald C., 1991, "The plasma physics of shock acceleration", *Space Sci. Rev.*, **58**(1), 259–346. [DOI], [ADS]

Jones, T. W., Rudnick, L., Aller, H. D., Aller, M. F., Hodge, P. E. and Fiedler, R. L., 1985, "Magnetic field structures in active compact radio sources.", *Astrophys. J.*, **290**, 627–636. [DOI], [ADS]

Jorstad, S., Marscher, A., Stevens, J., Smith, P., Forster, J., Lister, M., Stirling, A., Gómez, J., Cawthorne, T., Gear, W. and Robson, I., 2006, "Multifrequency Polarization Properties of Blazars", *Chinese Journal of Astronomy and Astrophysics Supplement*, **6**(S1), 247–252. [DOI], [ADS]

Jorstad, S. G., and et al., 2013, "A Tight Connection between Gamma-Ray Outbursts and Parsec-scale Jet Activity in the Quasar 3C 454.3", *Astrophys. J.*, **773**, 147. [DOI], [ADS], [arXiv:1307.2522 [astro-ph.HE]]

Kalberla, P. M. W., Burton, W. B., Hartmann, D., Arnal, E. M., Bajaja, E., Morras, R. and Pöppel, W. G. L., 2005, "The Leiden/Argentine/Bonn (LAB) Survey of Galactic HI. Final data release of the combined LDS and IAR surveys with improved stray-radiation corrections", *Astron. Astrophys.*, **440**, 775–782. [DOI], [ADS], [astro-ph/0504140]

Kaur, N. and Baliyan, K. S., 2018, "CTA 102 in exceptionally high state during 2016-2017", *Astron. Astrophys.*, **617**, A59. [DOI], [ADS], [arXiv:1805.04692]

Kellermann, K. I., Sramek, R., Schmidt, M., Shaffer, D. B. and Green, R., 1989, "VLA observations of objects in the Palomar Bright Quasar Survey", *Astron. J.*, **98**, 1195–1207. [DOI], [ADS]

Kelly, B. C., Bechtold, J. and Siemiginowska, A., 2009, "Are the Variations in Quasar Optical Flux Driven by Thermal Fluctuations?", *Astrophys. J.*, **698**, 895-910. [DOI], [ADS], [arXiv:0903.5315 [astro-ph.CO]]

Kiehlmann, S., and et al., 2016, "Polarization angle swings in blazars: The case of ¡ASTROBJ¿3C 279¡/ASTROBJ¿", *Astron. Astrophys.*, **590**, A10. [DOI], [ADS], [arXiv:1603.00249 [astro-ph.HE]]

Kinman, T. D., Lamla, E. and Wirtanen, C. A., 1966, "The Optical Brightness Variations and Polarization of the Quasi-Stellar Radio Source 3c 446", *Astrophys. J.*, **146**, 964. [DOI], [ADS]

Kirk, J. G., Rieger, F. M. and Mastichiadis, A., 1998, "Particle acceleration and synchrotron emission in blazar jets", *Astron. Astrophys.*, **333**, 452–458. [ADS], [arXiv:astro-ph/9801265 [astro-ph]]

Konigl, A., 1981, "Relativistic jets as X-ray and gamma-ray sources", *Astrophys. J.*, **243**, 700–709. [DOI], [ADS]

Kozłowski, S., 2016, "Revisiting Stochastic Variability of AGNs with Structure Functions", *Astrophys. J.*, **826**, 118. [DOI], [ADS], [arXiv:1604.05858]

Kushwaha, P., Gupta, A. C., Misra, R. and Singh, K. P., 2017, "Multiwavelength temporal variability of the blazar 3C 454.3 during 2014 activity phase", *Mon. Not. Roy. Astron. Soc.*, **464**, 2046–2052. [DOI], [ADS], [arXiv:1609.06952 [astro-ph.HE]]

Kushwaha, Pankaj, Sahayanathan, S. and Singh, K. P., 2013, "High energy emission processes in OJ 287 during 2009 flare", *Mon. Not. Roy. Astron. Soc.*, **433**(3), 2380–2388. [DOI], [ADS], [arXiv:1305.5065 [astro-ph.HE]]

Kushwaha, Pankaj, and et al., 2018, "Multiwavelength temporal and spectral variability of the blazar OJ 287 during and after the 2015 December flare: a major accretion disc contribution", *Mon. Not. Roy. Astron. Soc.*, **473**(1), 1145–1156. [DOI], [ADS], [arXiv:1709.04957 [astro-ph.HE]]

Larionov, V. M., and et al., 2020, "Multiwavelength behaviour of the blazar 3C 279: decade-long study from γ-ray to radio", *Mon. Not. Roy. Astron. Soc.*, **492**(3), 3829–3848. [DOI], [ADS], [arXiv:2001.06512 [astro-ph.HE]]

Li, S., Xia, Z.-Q., Liang, Y.-F., Liao, N.-H. and Fan, Y.-Z., 2018, "Fast γ-Ray Variability in Blazars beyond Redshift 3", *Astrophys. J.*, **853**, 159. [DOI], [ADS], [arXiv:1710.02904 [astro-ph.HE]]

Liao, N. H., Bai, J. M., Liu, H. T., Weng, S. S., Chen, Liang and Li, F., 2014, "Multiwavelength Variability Properties of Fermi Blazar S5 0716+714", *Astrophys. J.*, **783**(2), 83. [DOI], [ADS], [arXiv:1401.4937 [astro-ph.HE]]

Lin, Chao, Fan, Jun-Hui and Xiao, Hu-Bing, 2017, "The intrinsic γ-ray emissions of Fermi blazars", *Research in Astronomy and Astrophysics*, **17**(7), 066. [DOI], [ADS], [arXiv:1703.06566 [astro-ph.HE]]

Liodakis, Ioannis, Romani, Roger W., Filippenko, Alexei V., Kocevski, Daniel and Zheng, WeiKang, 2019, "Probing Blazar Emission Processes with Optical/Gamma-Ray Flare Correlations", *Astrophys. J.*, **880**(1), 32. [DOI], [ADS], [arXiv:1905.11418 [astro-ph.HE]]

Lister, M. L., Aller, M. F., Aller, H. D., Homan, D. C., Kellermann, K. I., Kovalev, Y. Y., Pushkarev, A. B., Richards, J. L., Ros, E. and Savolainen, T., 2013, "MOJAVE. X. Parsec-scale Jet Orientation Variations and Superluminal Motion in Active Galactic Nuclei", *Astron. J.*, **146**(5), 120. [DOI], [ADS], [arXiv:1308.2713 [astro-ph.CO]]

Lister, M. L., Aller, M. F., Aller, H. D., Hodge, M. A., Homan, D. C., Kovalev, Y. Y., Pushkarev, A. B. and Savolainen, T., 2018, "MOJAVE. XV. VLBA 15 GHz Total Intensity and Polarization Maps of 437 Parsec-scale AGN Jets from 1996 to 2017", *Astrophys. J. Suppl.*, **234**(1), 12. [DOI], [ADS], [arXiv:1711.07802 [astro-ph.GA]]

Lister, Matthew L., 2001, "Parsec-Scale Jet Polarization Properties of a Complete Sample of Active Galactic Nuclei at 43 GHz", *Astrophys. J.*, **562**(1), 208–232. [DOI], [ADS], [arXiv:astro-ph/0107594 [astro-ph]]

Lu, Youjun and Yu, Qingjuan, 2001, "The relationship between X-ray variability and the central black hole mass", *Mon. Not. Roy. Astron. Soc.*, **324**(3), 653–658. [DOI], [ADS], [arXiv:astro-ph/0106292 [astro-ph]]

Lynden-Bell, D., 1969, "Galactic Nuclei as Collapsed Old Quasars", *Nature*, **223**, 690–694. [DOI], [ADS]

Lynds, C. R., Stockton, A. N. and Livingston, W. C., 1965, "New Spectroscope Observations of Quasi-Stellar Sources.", *Astrophys. J.*, **142**, 1667. [DOI], [ADS]

MacDonald, N. R., Marscher, A. P., Jorstad, S. G. and Joshi, M., 2015, "Through the Ring of Fire: Gamma-Ray Variability in Blazars by a Moving Plasmoid Passing a Local Source of Seed Photons", *Astrophys. J.*, **804**, 111. [DOI], [ADS], [arXiv:1505.01239 [astro-ph.HE]]

MacLeod, C. L., Ivezić, Ž., Kochanek, C. S., Kozłowski, S., Kelly, B., Bullock, E., Kimball, A., Sesar, B., Westman, D., Brooks, K., Gibson, R., Becker, A. C. and de Vries, W. H., 2010, "Modeling the Time Variability of SDSS Stripe 82

Quasars as a Damped Random Walk", *Astrophys. J.*, **721**, 1014–1033. [DOI], [ADS], [arXiv:1004.0276 [astro-ph.CO]]

MAGIC Collaboration, Albert, J. and et al., 2008, "Very-High-Energy gamma rays from a Distant Quasar: How Transparent Is the Universe?", *Science*, **320**, 1752. [DOI], [ADS], [arXiv:0807.2822]

Mannheim, K., 1993, "The proton blazar", *Astron. Astrophys.*, **269**, 67–76. [ADS], [astro-ph/9302006]

Mao, P., Urry, C. M., Massaro, F., Paggi, A., Cauteruccio, J. and Künzel, S. R., 2016, "A Comprehensive Statistical Description of Radio-through-Gamma-Ray Spectral Energy Distributions of All Known Blazars", *Astrophys. J. Suppl.*, **224**, 26. [DOI], [ADS], [arXiv:1604.03856]

Maraschi, L., Ghisellini, G., Tanzi, E. G. and Treves, A., 1986, "Spectral Properties of Blazars. II. an X-Ray Observed Sample", *Astrophys. J.*, **310**, 325. [DOI], [ADS]

Marscher, A. P. and Gear, W. K., 1985, "Models for high-frequency radio outbursts in extragalactic sources, with application to the early 1983 millimeter-to-infrared flare of 3C 273", *Astrophys. J.*, **298**, 114–127. [DOI], [ADS]

Marscher, Alan P., 2014, "Turbulent, Extreme Multi-zone Model for Simulating Flux and Polarization Variability in Blazars", *Astrophys. J.*, **780**(1), 87. [DOI], [ADS], [arXiv:1311.7665 [astro-ph.HE]]

Marscher, Alan P., Jorstad, Svetlana G., Mattox, John R. and Wehrle, Ann E., 2002, "High-Frequency VLBA Total and Polarized Intensity Images of Gamma-Ray Bright Blazars", *Astrophys. J.*, **577**(1), 85–97. [DOI], [ADS]

Marscher, Alan P., and et al., 2008, "The inner jet of an active galactic nucleus as revealed by a radio-to-γ-ray outburst", *Nature*, **452**(7190), 966–969. [DOI], [ADS]

Marscher, Alan P., and et al., 2010, "Probing the Inner Jet of the Quasar PKS 1510-089 with Multi-Waveband Monitoring During Strong Gamma-Ray Activity", *Astrophys. J. Lett.*, **710**(2), L126–L131. [DOI], [ADS], [arXiv:1001.2574 [astro-ph.CO]]

Massardi, Marcella, and et al., 2011, "The Australia Telescope 20 GHz (AT20G) Survey: analysis of the extragalactic source sample", *Mon. Not. Roy. Astron. Soc.*, **412**(1), 318–330. [DOI], [ADS], [arXiv:1010.5942 [astro-ph.CO]]

Mastichiadis, Apostolos and Kirk, John G., 2002, "Models of Variability in Blazar Jets", , **19**(1), 138–142. [DOI], [ADS]

Mattox, J. R., and et al., 1996, "The Likelihood Analysis of EGRET Data", *Astrophys. J.*, **461**, 396. [DOI], [ADS]

McEnery, Julie, and et al., 2019, "All-sky Medium Energy Gamma-ray Observatory: Exploring the Extreme Multimessenger Universe", *arXiv e-prints*, arXiv:1907.07558. [ADS], [arXiv:1907.07558 [astro-ph.IM]]

Mead, A. R. G., Ballard, K. R., Brand, P. W. J. L., Hough, J. H., Brindle, C. and Bailey, J. A., 1990, "Optical and infrared polarimetry and photometry of blazars.", *Astron. Astrophys. Suppl.*, **83**, 183–204. [ADS]

Meyer, M., Scargle, J. D. and Blandford, R. D., 2019, "Characterizing the Gamma-Ray Variability of the Brightest Flat Spectrum Radio Quasars Observed with the Fermi LAT", *arXiv e-prints*. [ADS], [arXiv:1902.02291 [astro-ph.HE]]

Miller, H. R., Carini, M. T. and Goodrich, B. D., 1989, "Detection of microvariability for BL Lacertae objects", *Nature*, **337**(6208), 627–629. [DOI], [ADS]

Moore, R. L. and Stockman, H. S., 1981, "The class of highly polarized quasars : observations and description.", *Astrophys. J.*, **243**, 60–75. [DOI], [ADS]

Mücke, A. and Protheroe, R. J., 2001, "A proton synchrotron blazar model for flaring in Markarian 501", *Astroparticle Physics*, **15**, 121–136. [DOI], [ADS], [astro-ph/0004052]

Mücke, A., Protheroe, R. J., Engel, R., Rachen, J. P. and Stanev, T., 2003, "BL Lac objects in the synchrotron proton blazar model", *Astroparticle Physics*, **18**, 593–613. [DOI], [ADS], [astro-ph/0206164]

Nalewajko, Krzysztof, 2013, "The brightest gamma-ray flares of blazars", *Mon. Not. Roy. Astron. Soc.*, **430**(2), 1324–1333. [DOI], [ADS], [arXiv:1211.0274 [astro-ph.HE]]

Nalewajko, Krzysztof, Sikora, Marek, Madejski, Greg M., Exter, Katrina, Szostek, Anna, Szczerba, Ryszard, Kidger, Mark R. and Lorente, Rosario, 2012, "Herschel PACS and SPIRE Observations of Blazar PKS 1510-089: A Case for Two Blazar Zones", *Astrophys. J.*, **760**(1), 69. [DOI], [ADS], [arXiv:1210.4552 [astro-ph.HE]]

Nolan, P. L., Abdo, A. A., Ackermann, M., Ajello, M., Allafort, A., Antolini, E., Atwood, W. B., Axelsson, M., Baldini, L., Ballet, J. and et al., 2012, "Fermi Large Area Telescope Second Source Catalog", *Astrophys. J. Suppl.*, **199**, 31. [DOI], [ADS], [arXiv:1108.1435 [astro-ph.HE]]

Oke, J. B., 1967, "Spectrophotometric Observations of Rapid Variability in 3c 279 and 3c 446", *Astrophys. J.*, **147**, 901. [DOI], [ADS]

Osterman Meyer, Angela, Miller, H. Richard, Marshall, Kevin, Ryle, Wesley T., Aller, Hugh, Aller, Margo and Balonek, Tom, 2009, "Simultaneous Multiwavelength and Optical Microvariability Observations of CTA 102 (PKS J2232+1143)", *Astron. J.*, **138**(6), 1902–1910. [DOI], [ADS], [arXiv:0911.1481 [astro-ph.CO]]

Paliya, V. S., Sahayanathan, S. and Stalin, C. S., 2015, "Multi-Wavelength Observations of 3C 279 During the Extremely Bright Gamma-Ray Flare in 2014 March-April", *Astrophys. J.*, **803**, 15. [DOI], [ADS], [arXiv:1501.07363 [astro-ph.HE]]

Paliya, V. S., Diltz, C., Böttcher, M., Stalin, C. S. and Buckley, D., 2016, "A Hard Gamma-Ray Flare from 3C 279 in 2013 December", *Astrophys. J.*, **817**, 61. [DOI], [ADS], [arXiv:1512.00203 [astro-ph.HE]]

Paliya, V. S., Zhang, H., Böttcher, M., Ajello, M., Domínguez, A., Joshi, M., Hartmann, D. and Stalin, C. S., 2018, "Leptonic and Hadronic Modeling of Fermi-LAT Hard Spectrum Quasars and Predictions for High-energy Polarization", *Astrophys. J.*, **863**, 98. [DOI], [ADS], [arXiv:1807.02085 [astro-ph.HE]]

Paliya, Vaidehi S., Marcotulli, L., Ajello, M., Joshi, M., Sahayanathan, S., Rao, A. R. and Hartmann, D., 2017a, "General Physical Properties of CGRaBS Blazars", *Astrophys. J.*, **851**(1), 33. [DOI], [ADS], [arXiv:1711.01292 [astro-ph.HE]]

Paliya, Vaidehi S., Stalin, C. S., Ajello, M. and Kaur, A., 2017b, "Intra-night Optical Variability Monitoring of Fermi Blazars: First Results from 1.3 m J. C. Bhattacharya Telescope", *Astrophys. J.*, **844**(1), 32. [DOI], [ADS], [arXiv:1812.10614 [astro-ph.HE]]

Paliya, Vaidehi S., Böttcher, M., María Del Olmo García, A., Domínguez, A., Gil de Paz, A., Franckowiak, A., Garrappa, S. and Stein, R., 2020, "Multi-Frequency Observations of the Candidate Neutrino Emitting Blazar BZB J0955+3551", *arXiv e-prints*, arXiv:2003.06012. [ADS], [arXiv:2003.06012 [astro-ph.HE]]

Pandey, Ashwani, Gupta, Alok C. and Wiita, Paul J., 2017, "X-Ray Intraday Variability of Five TeV Blazars with NuSTAR", *Astrophys. J.*, **841**(2), 123. [DOI], [ADS], [arXiv:1705.02719 [astro-ph.HE]]

Papadakis, I. E., Villata, M. and Raiteri, C. M., 2007, "The long-term optical spectral variability of BL Lacertae", *Astron. Astrophys.*, **470**(3), 857–863. [DOI], [ADS], [arXiv:0705.2094 [astro-ph]]

Patiño-Álvarez, V. M., Fernandes, S., Chavushyan, V., López-Rodríguez, E., León-Tavares, J., Schlegel, E. M., Carrasco, L., Valdés, J. and Carramiñana, A., 2018, "Multiwavelength photometric and spectropolarimetric analysis of the

FSRQ 3C 279", *Mon. Not. Roy. Astron. Soc.*, **479**, 2037–2064. [DOI], [ADS], [arXiv:1806.01693 [astro-ph.HE]]

Pauliny-Toth, I. I. K. and Kellermann, K. I., 1966, "Variations in the Radio-Frequency Spectra of 3c 84, 3c 273, 3c 279, and Other Radio Sources", *Astrophys. J.*, **146**, 634. [DOI], [ADS]

Peterson, B. M., Ferrarese, L., Gilbert, K. M., Kaspi, S., Malkan, M. A., Maoz, D., Merritt, D., Netzer, H., Onken, C. A., Pogge, R. W., Vestergaard, M. and Wandel, A., 2004, "Central Masses and Broad-Line Region Sizes of Active Galactic Nuclei. II. A Homogeneous Analysis of a Large Reverberation-Mapping Database", *Astrophys. J.*, **613**, 682–699. [DOI], [ADS], [astro-ph/0407299]

Petropoulou, M. and Mastichiadis, A., 2012, "On proton synchrotron blazar models: the case of quasar 3C 279", *Mon. Not. Roy. Astron. Soc.*, **426**(1), 462–472. [DOI], [ADS], [arXiv:1207.5227 [astro-ph.HE]]

Petropoulou, M., Nalewajko, K., Hayashida, M. and Mastichiadis, A., 2017, "A hadronic minute-scale GeV flare from quasar 3C 279?", *Mon. Not. Roy. Astron. Soc.*, **467**(1), L16–L20. [DOI], [ADS], [arXiv:1612.05699 [astro-ph.HE]]

Petropoulou, Maria, Giannios, Dimitrios and Sironi, Lorenzo, 2016, "Blazar flares powered by plasmoids in relativistic reconnection", *Mon. Not. Roy. Astron. Soc.*, **462**(3), 3325–3343. [DOI], [ADS], [arXiv:1606.07447 [astro-ph.HE]]

Poutanen, Juri and Stern, Boris, 2010, "GeV Breaks in Blazars as a Result of Gamma-ray Absorption Within the Broad-line Region", *Astrophys. J. Lett.*, **717**(2), L118–L121. [DOI], [ADS], [arXiv:1005.3792 [astro-ph.HE]]

Prince, Raj, Majumdar, Pratik and Gupta, Nayantara, 2017, "Long-term Study of the Light Curve of PKS 1510-089 in GeV Energies", *Astrophys. J.*, **844**(1), 62. [DOI], [ADS], [arXiv:1706.02133 [astro-ph.HE]]

Prince, Raj, Gupta, Nayantara and Nalewajko, Krzysztof, 2019, "Two-zone Emission Modeling of PKS 1510-089 during the High State of 2015", *Astrophys. J.*, **883**(2), 137. [DOI], [ADS], [arXiv:1908.04803 [astro-ph.HE]]

Qian, S. J., Britzen, S., Krichbaum, T. P. and Witzel, A., 2019, "Possible evidence of a supermassive black hole binary with two radio jets in blazar 3C279", *Astron. Astrophys.*, **621**, A11. [DOI], [ADS]

Raiteri, C. M., and et al., 2001, "Optical and radio variability of the BL Lacertae object ¡ASTROBJ¿AO 0235+16¡/ASTROBJ¿: A possible 5-6 year periodicity", *Astron. Astrophys.*, **377**, 396–412. [DOI], [ADS], [astro-ph/0108165]

Raiteri, C. M., and et al., 2009, "WEBT multiwavelength monitoring and XMM-Newton observations of ¡ASTROBJ¿BL Lacertae¡/ASTROBJ¿ in 2007-2008. Unveiling different emission components", *Astron. Astrophys.*, **507**, 769–779. [DOI], [ADS], [arXiv:0909.1701 [astro-ph.HE]]

Rajput, Bhoomika, Stalin, C. S., Sahayanathan, S., Rakshit, Suvendu and Mandal, Amit Kumar, 2019, "Temporal correlation between the optical and γ-ray flux variations in the blazar 3C 454.3", *Mon. Not. Roy. Astron. Soc.*, **486**(2), 1781–1795. [DOI], [ADS], [arXiv:1903.12637 [astro-ph.HE]]

Rakshit, Suvendu, Stalin, C. S., Muneer, S., Neha, S. and Paliya, Vaidehi S., 2017, "Flux and Polarization Variability of OJ 287 during the Early 2016 Outburst", *Astrophys. J.*, **835**(2), 275. [DOI], [ADS], [arXiv:1612.07464 [astro-ph.GA]]

Rani, B., and et al., 2018, "Exploring the Connection between Parsec-scale Jet Activity and Broadband Outbursts in 3C 279", *Astrophys. J.*, **858**(2), 80. [DOI], [ADS], [arXiv:1805.04723 [astro-ph.HE]]

Rani, P., Stalin, C. S. and Rakshit, S., 2017, "X-ray flux variability of active galactic nuclei observed using NuSTAR", *Mon. Not. Roy. Astron. Soc.*, **466**, 3309–3322. [DOI], [ADS], [arXiv:1612.02768]

Romero, G. E., Cellone, S. A. and Combi, J. A., 1999, "Optical microvariability of southern AGNs", *Astron. Astrophys. Suppl.*, **135**, 477–486. [DOI], [ADS]

Ryan, James L., Siemiginowska, Aneta, Sobolewska, Malgosia and Grindlay, Jonathan, 2019, "Characteristic Variability Timescales in the Gamma-ray Power Spectra of Blazars", *arXiv e-prints*, arXiv:1909.04227. [ADS], [arXiv:1909.04227 [astro-ph.HE]]

Rybicki, George B. and Lightman, Alan P., 1986, *Radiative Processes in Astrophysics*. [ADS]

Sahakyan, N., 2020, "Investigation of the γ-ray spectrum of CTA 102 during the exceptional flaring state in 2016-2017", *Astron. Astrophys.*, **635**, A25. [DOI], [ADS], [arXiv:1911.12087 [astro-ph.HE]]

Sahayanathan, S., 2008, "A two-zone synchrotron model for the knots in the M87 jet", *Mon. Not. Roy. Astron. Soc.*, **388**(1), L49–L53. [DOI], [ADS], [arXiv:0805.2842 [astro-ph]]

Sahayanathan, S. and Godambe, S., 2012, "Modelling the very high energy flare of 3C 279 using one-zone leptonic model", *Mon. Not. Roy. Astron. Soc.*, **419**, 1660–1666. [DOI], [ADS], [arXiv:1109.2442 [astro-ph.HE]]

Sahayanathan, S., Sinha, A. and Misra, R., 2018, "Broadband spectral fitting of blazars using XSPEC", *Research in Astronomy and Astrophysics*, **18**, 035. [DOI], [ADS], [arXiv:1801.00685 [astro-ph.HE]]

Sarkar, A., and et al., 2019, "Long-term Variability and Correlation Study of the Blazar 3C 454.3 in the Radio, NIR, and Optical Wavebands", *Astrophys. J.*, **887**(2), 185. [DOI], [ADS]

Schmidt, M., 1963, "3C 273 : A Star-Like Object with Large Red-Shift", *Nature*, **197**, 1040. [DOI], [ADS]

Schmidt, Maarten, 1965, "Large Redshifts of Five Quasi-Stellar Sources.", *Astrophys. J.*, **141**, 1295. [DOI], [ADS]

Shah, Z., Sahayanathan, S., Mankuzhiyil, N., Kushwaha, P., Misra, R. and Iqbal, N., 2017, "Clues on high-energy emission mechanism from blazar 3C 454.3 during 2015 August flare", *Mon. Not. Roy. Astron. Soc.*, **470**, 3283–3299. [DOI], [ADS], [arXiv:1705.06185 [astro-ph.HE]]

Shah, Zahir, Jithesh, V., Sahayanathan, S., Misra, Ranjeev and Iqbal, Naseer, 2019, "Study on temporal and spectral behaviour of 3C 279 during 2018 January flare", *Mon. Not. Roy. Astron. Soc.*, **484**(3), 3168–3179. [DOI], [ADS], [arXiv:1901.04184 [astro-ph.HE]]

Shakura, N. I. and Sunyaev, R. A., 1973, "Black holes in binary systems. Observational appearance.", *Astron. Astrophys.*, **24**, 337–355. [ADS]

Shimmins, A. J. and Bolton, J. G., 1974, "The Parkes 2700 MHz Survey (Sixth Part): Catalogue for the Declination zone -30° to -35°", *Australian Journal of Physics Astrophysical Supplement*, **32**, 1. [ADS]

Shukla, A. and Mannheim, K., 2020, "Gamma-ray flares from relativistic magnetic reconnection in the jet of the quasar 3C 279", *Nature Communications*, **11**, 4176. [DOI], [ADS]

Shukla, A., Mannheim, K., Patel, S. R., Roy, J., Chitnis, V. R., Dorner, D., Rao, A. R., Anupama, G. C. and Wendel, C., 2018, "Short-timescale γ-Ray Variability in CTA 102", *Astrophys. J. Lett.*, **854**, L26. [DOI], [ADS]

Sikora, M., Begelman, M. C. and Rees, M. J., 1994, "Comptonization of diffuse ambient radiation by a relativistic jet: The source of gamma rays from blazars?", *Astrophys. J.*, **421**, 153–162. [DOI], [ADS]

Sillanpaa, A., Haarala, S., Valtonen, M. J., Sundelius, B. and Byrd, G. G., 1988, "OJ 287: Binary Pair of Supermassive Black Holes", *Astrophys. J.*, **325**, 628. [DOI], [ADS]

Simonetti, J. H., Cordes, J. M. and Heeschen, D. S., 1985, "Flicker of extragalactic radio sources at two frequencies.", *Astrophys. J.*, **296**, 46–59. [DOI], [ADS]

Singal, J., Ko, A. and Petrosian, V., 2014, "Gamma-Ray Luminosity and Photon Index Evolution of FSRQ Blazars and Contribution to the Gamma-Ray Background", *Astrophys. J.*, **786**(2), 109. [DOI], [ADS], [arXiv:1403.4961 [astro-ph.HE]]

Sironi, Lorenzo, Petropoulou, Maria and Giannios, Dimitrios, 2015, "Relativistic jets shine through shocks or magnetic reconnection?", *Mon. Not. Roy. Astron. Soc.*, **450**(1), 183–191. [DOI], [ADS], [arXiv:1502.01021 [astro-ph.HE]]

Smith, P. S., Montiel, E., Rightley, S., Turner, J., Schmidt, G. D. and Jannuzi, B. T., 2009, "Coordinated Fermi/Optical Monitoring of Blazars and the Great 2009 September Gamma-ray Flare of 3C 454.3", *ArXiv e-prints*. [ADS], [arXiv:0912.3621 [astro-ph.HE]]

Sorcia, Marco, Benítez, Erika, Hiriart, David, López, José M., Cabrera, José I., Mújica, Raúl, Heidt, Jochen, Agudo, Iván, Nilsson, Kari and Mommert, Michael, 2013, "Long-term Optical Polarization Variability of the TeV Blazar 1ES 1959+650", *Astrophys. J. Suppl.*, **206**(2), 11. [DOI], [ADS], [arXiv:1304.2819 [astro-ph.HE]]

Spinrad, H. and Smith, H. E., 1975, "AO 0235+164 a red BL Lacertae object.", *Astrophys. J.*, **201**, 275–276. [DOI], [ADS]

Stockman, H. S. and Angel, J. R. P., 1978, "A linear polarization survey of bright QSOs.", *Astrophys. J. Lett.*, **220**, L67–L71. [DOI], [ADS]

Swanenburg, B. N., Bennett, K., Bignami, G. F., Caraveo, P., Hermsen, W., Kanbach, G., Masnou, J. L., Mayer-Hasselwander, H. A., Paul, J. A., Sacco, B., Scarsi, L. and Wills, R. D., 1978, "COS B observation of high-energy gamma radiation from 3C273", *Nature*, **275**, 298. [DOI], [ADS]

Tanner, A. M., Bechtold, Jill, Walker, C. E., Black, John H. and Cutri, R. M., 1996, "A Study of Quasar Absorption-Line Systems With IRAS", *Astron. J.*, **112**, 62. [DOI], [ADS]

Urry, C. M. and Padovani, P., 1995, "Unified Schemes for Radio-Loud Active Galactic Nuclei", *Pub. Astron. Soc. Pac.*, **107**, 803. [DOI], [ADS], [astro-ph/9506063]

Vanden Berk, D. E., and et al., 2004, "The Ensemble Photometric Variability of ˜25,000 Quasars in the Sloan Digital Sky Survey", *Astrophys. J.*, **601**, 692–714. [DOI], [ADS], [astro-ph/0310336]

Vaughan, S., Edelson, R., Warwick, R. S. and Uttley, P., 2003, "On characterizing the variability properties of X-ray light curves from active galaxies", *Mon. Not. Roy. Astron. Soc.*, **345**, 1271–1284. [DOI], [ADS], [astro-ph/0307420]

Vercellone, S., and et al., 2009, "Multiwavelength Observations of 3C 454.3. I. The AGILE 2007 November campaign on the "Crazy Diamond"", *Astrophys. J.*, **690**, 1018–1030. [DOI], [ADS], [arXiv:0809.1737]

Vercellone, S., and et al., 2010, "Multiwavelength Observations of 3C 454.3. III. Eighteen Months of Agile Monitoring of the "Crazy Diamond"", *Astrophys. J.*, **712**, 405–420. [DOI], [ADS], [arXiv:1002.1020 [astro-ph.HE]]

Vercellone, S., and et al., 2011, "The Brightest Gamma-Ray Flaring Blazar in the Sky: AGILE and Multi-wavelength Observations of 3C 454.3 During 2010 November", *Astrophys. J. Lett.*, **736**(2), L38. [DOI], [ADS], [arXiv:1106.5162 [astro-ph.HE]]

Villata, M., and et al., 2004, "The WEBT ¡ASTROBJ¿BL Lacertae¡/ASTROBJ¿ Campaign 2001 and its extension. Optical light curves and colour analysis 1994-2002", *Astron. Astrophys.*, **421**, 103–114. [DOI], [ADS], [arXiv:astro-ph/0404155 [astro-ph]]

Wagner, S. J. and Witzel, A., 1995, "Intraday Variability In Quasars and BL Lac Objects", *Ann. Rev. Astron. Astrophys.*, **33**, 163–198. [DOI], [ADS]

Weisskopf, Martin C., Ramsey, Brian, O'Dell, Stephen, Tennant, Allyn, Elsner, Ronald, Soffitta, Paolo, Bellazzini, Ronaldo, Costa, Enrico, Kolodziejczak, Jeffrey, Kaspi, Victoria, Muleri, Fabio, Marshall, Herman, Matt, Giorgio and Romani, Roger, 2016, "The Imaging X-ray Polarimetry Explorer (IXPE)", in *Proceedings of the SPIE, Volume 9905, id. 990517 10 pp. (2016).*, Society of Photo-Optical Instrumentation Engineers (SPIE) Conference Series, 9905, [DOI], [ADS]

Welsh, B. Y., Wheatley, J. M. and Neil, J. D., 2011, "GALEX observations of quasar variability in the ultraviolet", *Astron. Astrophys.*, **527**, A15. [DOI], [ADS], [arXiv:1101.2191]

Wierzcholska, Alicja, Zacharias, Michael, Jankowsky, Felix, Wagner, Stefan and H. E. S. S. Collaboration, 2019a, "H.E.S.S. Monitoring of PKS 2155-304 in 2015 and 2016", *Galaxies*, **7**(1), 21. [DOI], [ADS], [arXiv:1908.01232 [astro-ph.HE]]

Wierzcholska, Alicja, Zacharias, Michael, Jankowsky, Felix, Wagner, Stefan and H. E. S. S. Collaboration, 2019b, "Unraveling The Complex Nature Of The Very High-Energy γ-Ray Blazar PKS 2155-304", *arXiv e-prints*, arXiv:1912.01880. [ADS], [arXiv:1912.01880 [astro-ph.HE]]

Wold, M., Brotherton, M. S. and Shang, Z., 2007, "The dependence of quasar variability on black hole mass", *Mon. Not. Roy. Astron. Soc.*, **375**, 989–999. [DOI], [ADS], [astro-ph/0612042]

Woo, J.-H. and Urry, C. M., 2002, "Active Galactic Nucleus Black Hole Masses and Bolometric Luminosities", *Astrophys. J.*, **579**, 530–544. [DOI], [ADS], [astro-ph/0207249]

Wu, J., Zhou, X., Peng, B., Ma, J., Jiang, Z. and Chen, J., 2005, "Optical monitoring of PKS 1510-089: a binary black hole system?", *Mon. Not. Roy. Astron. Soc.*, **361**(1), 155–159. [DOI], [ADS], [arXiv:astro-ph/0504587 [astro-ph]]

Wu, Jianghua, Zhou, Xu, Ma, Jun and Jiang, Zhaoji, 2011, "Optical variability and colour behaviour of 3C 345", *Mon. Not. Roy. Astron. Soc.*, **418**(3), 1640–1648. [DOI], [ADS], [arXiv:1108.1020 [astro-ph.CO]]

Xiong, Dingrong, Bai, Jinming, Zhang, Haojing, Fan, Junhui, Gu, Minfeng, Yi, Tingfeng and Zhang, Xiong, 2017, "Multicolor Optical Monitoring of the Quasar 3C 273 from 2005 to 2016", *Astrophys. J. Suppl.*, **229**(2), 21. [DOI], [ADS], [arXiv:1703.01645 [astro-ph.HE]]

Zhang, Bing-Kai, Zhao, Xiao-Yun, Wang, Chun-Xiao and Dai, Ben-Zhong, 2014, "Optical quasi-periodic oscillation and color behavior of blazar PKS 2155-304", *Research in Astronomy and Astrophysics*, **14**(8), 933-941. [DOI], [ADS], [arXiv:1405.6858 [astro-ph.HE]]

Zhang, Peng-fei, Yan, Da-hai, Liao, Neng-hui and Wang, Jian-cheng, 2017, "Revisiting Quasi-periodic Modulation in γ-Ray Blazar PKS 2155-304 with Fermi Pass 8 Data", *Astrophys. J.*, **835**(2), 260. [DOI], [ADS], [arXiv:1611.04354 [astro-ph.HE]]

Zheng, Y. G., Zhang, L., Huang, B. R. and Kang, S. J., 2013, "Modelling the γ-ray variability of 3C 273", *Mon. Not. Roy. Astron. Soc.*, **431**(3), 2356–2361. [DOI], [ADS], [arXiv:1608.00288 [astro-ph.HE]]

Zuo, W., Wu, X.-B., Liu, Y.-Q. and Jiao, C.-L., 2012, "The Correlations between Optical Variability and Physical Parameters of Quasars in SDSS Stripe 82", *Astrophys. J.*, **758**, 104. [DOI], [ADS], [arXiv:1209.0524 [astro-ph.HE]]